MECHANICS BASED APPROACH FOR DUCTILITY OF REINFORCED CONCRETE BEAMS UNDER CYCLIC LOADING

AHMAD AZIM BIN SHUKRI

FACULTY OF ENGINEERING
UNIVERSITY OF MALAYA
KUALA LUMPUR

2015

MECHANICS BASED APPROACH FOR DUCTILITY OF REINFORCED CONCRETE BEAMS UNDER CYCLIC LOADING

AHMAD AZIM BIN SHUKRI

DESSERTATION SUBMITTED IN FULFILMENT OF THE REQUIREMENTS FOR THE DEGREE OF MASTER OF ENGINEERING SCIENCE

FACULTY OF ENGINEERING
UNIVERSITY OF MALAYA
KUALA LUMPUR

2015

UNIVERSITY OF MALAYA

ORIGINAL LITERARY WORK DECLARATION

Name of Candidate: Ahmad Azim Bin Shukri

Registration/Matric No: KGA120098

Name of Degree: Master of Engineering Science

Title of Project Paper/Research Report/Dissertation/Thesis ("this Work"):

Mechanics Based Approach for Ductility of Reinforced Concrete Beams under Cyclic Loading

Field of Study: Civil Engineering

I do solemnly and sincerely declare that:

(1) I am the sole author/writer of this Work;
(2) This Work is original;
(3) Any use of any work in which copyright exists was done by way of fair dealing and for permitted purposes and any excerpt or extract from, or reference to or reproduction of any copyright work has been disclosed expressly and sufficiently and the title of the Work and its authorship have been acknowledged in this Work;
(4) I do not have any actual knowledge nor do I ought reasonably to know that the making of this work constitutes an infringement of any copyright work;
(5) I hereby assign all and every rights in the copyright to this Work to the University of Malaya ("UM"), who henceforth shall be owner of the copyright in this Work and that any reproduction or use in any form or by any means whatsoever is prohibited without the written consent of UM having been first had and obtained;
(6) I am fully aware that if in the course of making this Work I have infringed any copyright whether intentionally or otherwise, I may be subject to legal action or any other action as may be determined by UM.

Candidate's Signature Date:

Subscribed and solemnly declared before,

Witness's Signature Date:

Name:

Designation:

ABSTRACT

The ductility of reinforced concrete refers to the ability to absorb energy such as that from seismic loading and normal traffic loads. It is an important parameter in reinforced concrete design process, particularly in situations where major cyclic loads are a concern. However, the process of quantifying ductility in reinforced concrete structures is made complex by the interface displacements that dominates the behaviour of reinforced concrete members when cracks appear. Current methods used to quantify ductility are strain-based, therefore they cannot be used to directly simulate interface displacement. Indirect simulation is possible using empirically determined values, but being empirically derived means it cannot be applied outside the testing regime from which it is derived. In recent years a mechanics-based moment-rotation approach was developed to overcome this problem. The approach is primarily displacement-based, which allows it to simulate the interface displacement mechanisms and thus remove the dependency on empirical values. In this research, the mechanics based approach is extended to allow for cyclic loading and also include the use of size-dependent stress-strain relationship for concrete for better simulation of concrete softening. From comparisons with experimental results, it was found that the method was able to simulate the moment-rotation curves of cyclically loaded beam with acceptable accuracy. The maximum moments were simulated with an accuracy between -7.23% and 1.51% while the minimum moments were simulated with an accuracy between -16.55% and -5.83%. From this, it can be seen that the moment-rotation approach give conservative estimations for the strength of RC beams.

ABSTRAK

Kemuluran konkrit bertetulang merujuk kepada kebolehan untuk menyerap tenaga seperti daripada gempa bumi dan juga beban trafik biasa. Kemuluran adalah satu parameter penting dalam proses reka bentuk struktur konkrit bertetulang, terutamanya dalam situasi di mana beban berkitar adalah masalah utama. Namun, proses pengukuran kemuluran dalam struktur konkrit bertetulang menjadi kompleks akibat daripada anjakan antaramuka yang mendominasikan sifat konkrit bertetulang apabila retakan mula muncul. Kaedah semasa untuk mengukur kemuluran adalah bergantung kepada keterikan, maka ianya tidak dapat digunakan untuk mensimulasi anjakan antaramuka secara langsung. Simulasi tidak langsung dapat dilakukan menggunakan nilai empirik yang diperolehi, tetapi nilai empirik tidak dapat digunakan diluar daripada regim ujikaji yang menghasilkannya. Beberapa tahun kebelakangan ini, satu kaedah putaran momen berunsurkan mekanik telah dihasilkan untuk mengatasi masalah ini. Kaedah ini adalah berasaskan anjakan yang membolehkannya untuk mensimulasi mekanisma anjakan antaramuka dan tidak perlu bergantung kepada nilai empirik. Dalam kajian ini, kaedah berunsur mekanik ini dimajukan lagi dengan membolehkannya digunakan untuk beban berkitar dan juga menggunakan satu hubungan tegasan-keterikan yang bergantung kepada saiz specimen untuk simulasi pelembutan konkrit yang lebih baik. Daripada perbandingan dengan keputusan ujikaji, didapati bahawa kaedah ini boleh digunakan untuk mensimulasi putaran momen untuk rasuk konkrit yang dikenakan beban berkitar dengan ketepatan yang memuaskan. Momen maksimum telah disimulasikan dengan ketepatan antara -7.23% dan 1.51% manakala momen minimum pula telah disimulasikan dengan ketepatan antara -16.55% dan -5.83%. Daripada ini, dapat dilihat bahawa kaedah momen putaran memberikan anggaran yang konservatif untuk kekuatan rasuk konkrit bertetulang.

ACKNOWLEDGEMENT

I express my sincere gratitude to my supervisor Professor Ir. Dr. Mohd Zamin Bin Jumaat from University of Malaya and Dr. Philip Visintin from University of Adelaide for their guidance and support throughout the whole period of this research.

Many thanks as well to my parents and my sisters, who supported me throughout my study, especially when things are looking down.

Special thanks go to the University of Malaya, High Impact Research Grant (HIRG) No. UM.C/625/1/HIR/MOHE/ENG/36 (16001-00-D000036) - "Strengthening Structural Elements for Load and Fatigue", for the financial support towards this research.

TABLE OF CONTENTS

LIST OF TABLES

LIST OF FIGURES

CHAPTER 1: INTRODUCTION

1.1 General

An earthquake is the most devastating type of natural hazard that can affect a structure. The seismic force that an earthquake brings is transferred to buildings through its foundations, causing strong cyclic loads that can affect the entirety of the buildings. Structural damage is usually unavoidable in cases of strong earthquakes, and the focus of earthquake designs are usually in limiting the damage and prevent the total collapse of buildings.

Structures that are in danger of being exposed to earthquake or any other source of high strength cyclic loads are designed to dissipate energy through inelastic deformation of structural members. As columns are usually integral to preventing the collapse of building, some design guidelines suggest a strong column-weak beam theory, where the beam is designed to be weaker than the column and thus the bulk of energy dissipation is done through deformation of beams instead of the columns. Due to this, it is important to quantify the ductility of the beams. In the case of reinforced concrete beams, ductility can be referred to as the ability of the beam to rotate when under load. The rotations are concentrated in locations of flexural cracks, which are called hinges. Due to this ductility is usually defined in terms of a beam's moment-curvature relationship, where the curvature = (rotation / hinge length) represents how much the beam can rotate.

Based on the moment-curvature approach, many research works have been done on attempting to predict and capture the cyclic behaviour of reinforced concrete beams and this led to the proposal of several moment–curvature models. According to Sivaselvan and Reinhorn (2000), these moment-curvature models can generally be divided into two types, which are the polygonal hysteretic model (PHM) and the smooth hysteretic model (SHM).

SHMs are based on continuous change of stiffness due to yielding but sharp changes due to unloading and deteriorating behavior. Examples of important SHM include the model by Bouc (1967), the model by Mostaghel (1999) and the model by Sivaselvan and Reinhorn (2000). Most of the currently available SHM models are variations of the model by Bouc (1967).

PHMs on the other hand are based on piecewise linear behaviour. These models are most often motivated by actual behavioural stages of a reinforced concrete beam as seen in practice. These include concrete cracking, yielding of steel reinforcement, loss of stiffness and strength, and crack opening and closing. Examples of earlier PHM include the model by Clough (1966), the model by Takeda et al. (1970), and the model by Park et al. (1987). Most, if not all of PHM models are based on the works of Clough (1966).

While the approach taken by SHM and PHM can be different, there are some similarities between them. The models use the Euler-Bernoulli theorem, which states that plane sections remain plane during bending of beam. The models are also strain based, which refers to the fact that strain of materials in beam is first determined, which is then used to determine the force acting on the beam section through material stress-strain relationship. This allows models based on the moment-curvature approach to simulate the behaviour of materials under cyclic loading, which is important to capture the degradation of cyclically loaded materials as seen in practice.

1.2 Problem Statement

The moment-curvature models work well in normal construction practices and the research community as well is largely content in applying older models, sometimes with variations added into them in order to achieve a perceived better result. But more and more advances are made in terms of construction materials, such as the use of fiber reinforced concrete, fiber reinforced polymers (FRP), palm oil fuel ash concrete and many more. These new materials presents a large problem in using the moment-curvature

models. This is due to the fact that the models are largely dependent on empirical based factors, which would usually be formed based on normal concrete only. Ignoring this fact and continuing to use the empirical factors anyway would be disastrous as it has been shown that when the empirical factors are applied to situations outside of the testing regime that formed them, the correlation is very poor (Haskett et al. 2009, Haskett et al. 2010a; Haskett et al. 2010b).

There are two ways to solve this problem with the moment-curvature models. Firstly lots of tests must be made to create new empirical factors that can then be used with the moment-curvature models. However it should be noted that the current empirical factors are based on hundreds of full-size specimens before being established, and the research itself spans decades. The budget and time needed is prohibitive, especially considering that these tests would have to be repeated every time a new material is to be introduced to the industry. Due to this a second way to solve the problem is proposed, which is to create another cyclic model that is mechanics-based, which allows it to perform analysis without the need of any empirical factors.

First of all let us consider what causes the moment-curvature models to turn to empirical factors in their analyses. There exist a certain complexity in quantifying ductility of reinforced concrete beams at all load levels following flexural cracking. This is due to the fact that the post cracking behaviour of reinforced concrete beams is heavily dependent of localised behaviours. These are: (1) the interface slip between the reinforcement and the concrete which result in crack opening as well as tension stiffening which is particularly important pre yield and (2) the interface slip between concrete to concrete sliding planes which allow for the formation of concrete softening wedges. Current models using the moment-rotation approach the Euler Bernoulli plane sections remain plane theorem cannot directly incorporate the effect of interface slips as they are strain based. Hence the moment-curvature models must resort to some empiricisms such

as effective flexural rigidities (Bischoff 2005) and hinge lengths (Coleman and Spacone 2001; Panagotakos and Fardis 2001) to allow for the localised behaviours of concrete cracking and softening.

In response to the limitations of applying empiricisms a mechanics-based moment rotation approach has recently been developed for monotonic loading (Haskett et al. 2009, 2010a, 2010b, 2011; Chen et al. 2014.; Muhammad et al. 2011a, 2011b; Lucas et al. 2011; Visintin et al. 2012a, 2012b). This approach directly applies established partial interaction theory (Haskett et al. 2009; Muhamad et al. 2011b; Visintin et al. 2012b; Oehlers et al. 2013) to simulate the slip of the reinforcement relative to the concrete which surrounds it and shear friction theory (Walraven et al. 1987; Haskett et al. 2011; Chen et al. 2014) to simulate the formation of concrete softening wedges.

The main advantage of the moment-rotation approach is that it is mechanics-based, as it does not require empiricism in the component of the model, although it should be noted that empiricism is still present in material models used in conjunction with the model. This makes the approach generic, allowing it to be used to simulate the behaviour of any structure with irregular building materials, such as the ones mentioned earlier.

1.3 Objectives

The focus of this research is to further extend the existing moment-rotation approach to allow for the analysis of cyclically loaded beams, hence creating a cyclic moment-rotation model. The work done will be as follows:

- To simulate a cyclic partial-interaction numerical simulation model for tension stiffening behaviour of beams.
- To simulate a cyclic size-dependent stress-strain numerical simulation model for concrete that can be used to determine the force acting on concrete in the compression region of the beams.

- To propose a cyclic moment-rotation numerical simulation model, which uses the partial-interaction model and size-dependent stress-strain model for concrete to determine the forces acting on the beam section during beam rotation when under cyclic load.

CHAPTER 2: LITERATURE REVIEW

A brief literature review on matters related to the research will now be presented. The literature review will focus on:

- Current research works on moment-rotation approach that has been done by other researchers.
- The interface displacements mechanisms that is to be simulated in the moment-rotation model.
- The cyclic material models that will be used in conjunction with the moment-rotation model.

2.1 Previous Works by Other Researchers

This section will discuss the contribution of past researchers to the moment-rotation approach. Note however that only the works that are most relevant in terms of simulating beam behaviour is mentioned here.

The earlier works on moment-rotation include the work of Daniell et al. (2008), which was prompt by the problem in identifying the hinge length. Numerical models, such as the finite element models, have shown difficulty in terms of directly quantifying the length of the concrete softening region. Concrete softening refers to the behaviour of concrete when under compression, where after reaching the peak stress the concrete slowly loses its strength. More on this will be discussed later in the literature review. Daniell et al. (2008) states that empirical models also have a problem in this regard, as the models do not identify what exactly causes and governs the rotation of beams, instead relying on empirically derived factors that as we have discussed in the section 1.2, is highly inaccurate when applied in situations outside of their testing regime. The assumption of a fixed hinge length was also questioned, as this does not tally with what

is seen in practice. Hence Daniel et al. (2008) proposed a mathematical model that forms the basis of the moment-rotation approach.

Haskett et al. (2008) explored the possibility of predicting intermediate crack debonding, which is a type of premature failure that occurs in beams strengthened with fibre reinforced polymers (FRP). While it is not directly related to the moment-rotation approach, he proposed a numerical model for simulating the load-slip relationship of steel-concrete interface which has been adopted in many other research works on moment-rotation as it has been found to simulate the tension stiffening behaviour of reinforced concrete beams. Tension stiffening refers to the increase in rigidity of cracked beams in comparison of bare steel reinforcement. More details on this behaviour will be discussed later. It should be noted that this research also uses the numerical model proposed by Haskett et al. (2008) to determine the load-slip relationship.

The moment-rotation approach has since then been applied in many ways. Muhamad et al. (2011a) used the moment-rotation approach to determine the discrete rotation of reinforced concrete beams at serviceability limit. Lucas et al. (2011) used the moment-rotation approach to quantify shear failure. Visintin et al. (2012b) proposed an extension to the moment-rotation approach to simulate beam behavior when multiple cracks are present within a single hinge length. Moment-rotation approach has also been used to simulate the behavior of reinforced concrete beams strengthened with mechanically fastened FRP stripes in Knight et al. (2014). Finally the moment-rotation approach was used to simulate reinforced concrete beams strengthened with unbonded FRP and steel prestressing tendons present in the beam.

2.2 Interface Displacements Mechanisms

There are two mechanisms caused by interface displacements in reinforced concrete, and simulating these mechanisms is the primary focus of the moment-rotation approach. The first mechanism is tension stiffening, which is associated with the interface slip

between reinforcement and the adjacent concrete (Massicotte et al. 1990; Muhammad et al. 2011b) The tension stiffening occurs in the tensile region if the beam and affects the concrete surrounding the tensile reinforcement, as shown in the B-B to C-C section in Figure 2.1. The second is the concrete softening mechanism associated with the sliding of concrete-concrete interface during the formation of concrete wedges at reinforced concrete hinges (Fields et al. 2004).

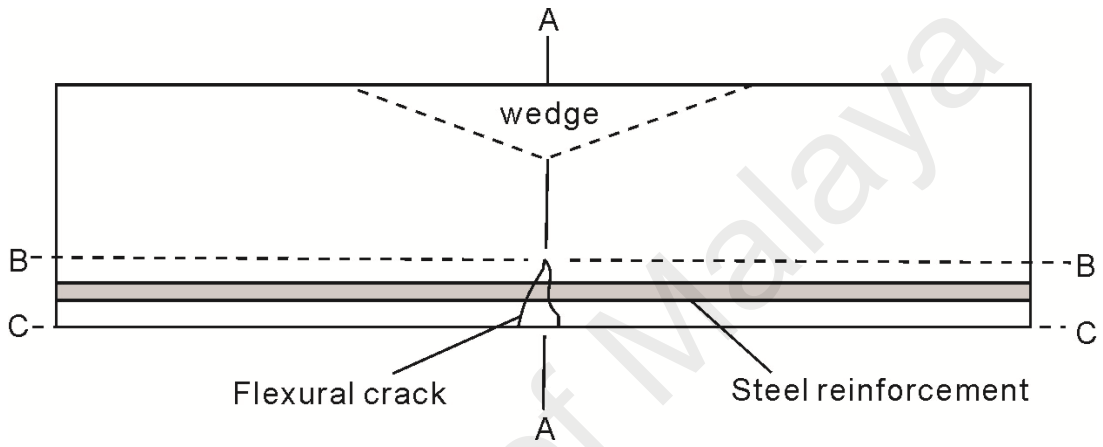

Figure 2.1: Interface Displacements in Hinge Segments of Beams.

2.2.1 Tension Stiffening Mechanism

Tension stiffening is a fundamental characteristic of reinforced concrete. The basic reinforced concrete element in which tension stiffening develops is composed of a reinforced concrete prism as illustrated in Figure 2.2 which is made up of a single reinforcement of cross-section area A_r and modulus E_r and concrete prism of area A_c and modulus E_c, which is extracted from section B-B and C-C in Figure 2.1. In its initial uncracked state, the axial rigidity of the prism is equal to $A_rE_r+A_cE_c$. Once flexural crack has formed the axial rigidity of the prism is thus reduced since concrete can no longer resist load. However despite the reduction, the new axial rigidity is actually higher than the rigidity of only steel reinforcement, A_rE_r, and this increase in stiffness is called as tension stiffening.

The tension stiffening mechanism allows for the transfer of stress from the reinforcement to the surrounding concrete through the interface bond stress-slip relationship. The bond stress acts against the force pulling out the reinforcement, causing slip in reinforcement to gradually decrease the further it gets from the crack face. Slip-strain, which refers to the step change in slip caused by the tension stiffening effect also decreases along with slip, until a point where both slip and slip-strain becomes zero. This point is referred to as the point of full-interaction, which refers to the fact that partial-interaction due to slip of reinforcement no longer occur beyond that point.

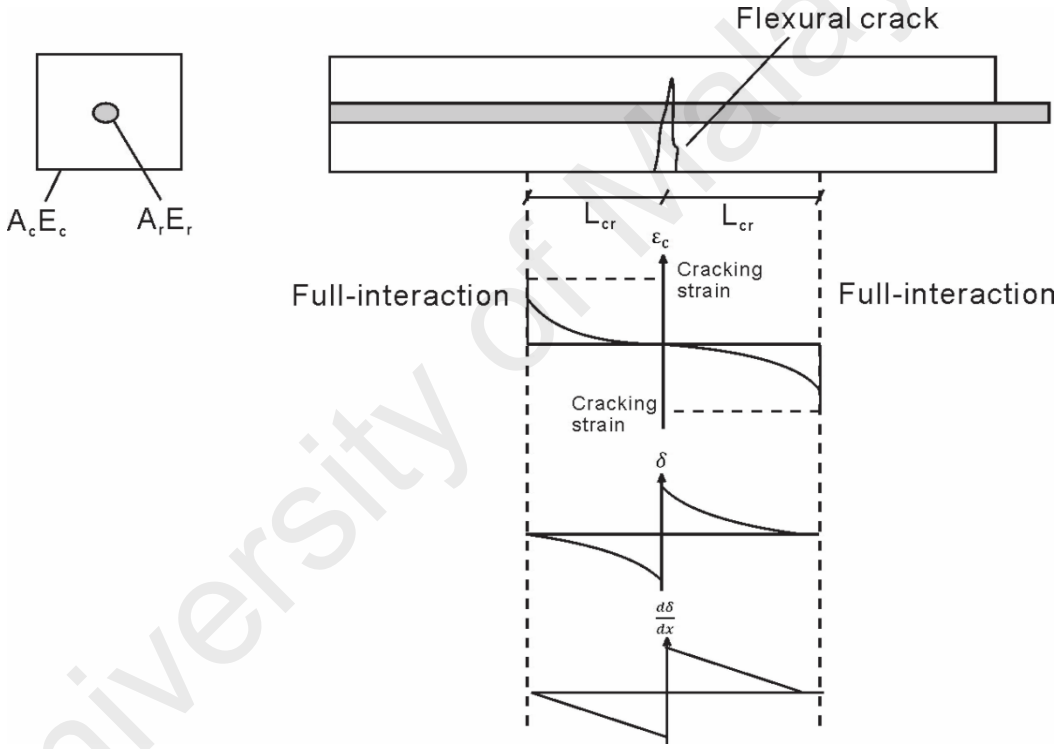

Figure 2.2: Formation of First Flexural Crack.

Assuming a large enough slip occurs at the crack face, the strain in concrete will reach its tensile capacity, as illustrated in Figure 2.2 at L_{cr}. This will cause another set of cracks called the primary cracks to occur, as shown in Figure 2.3. If more load is applied this process will continue and more primary cracks will form along the length of the beam. In cases where a moment gradient is applied to the beam, which is in fact usually the case, it is conservative to consider the distance between the other primary cracks will be L_{cr} as

well. As more load is applied, secondary cracks will also form between primary cracks, and the formation of cracks will continue until the beam fails.

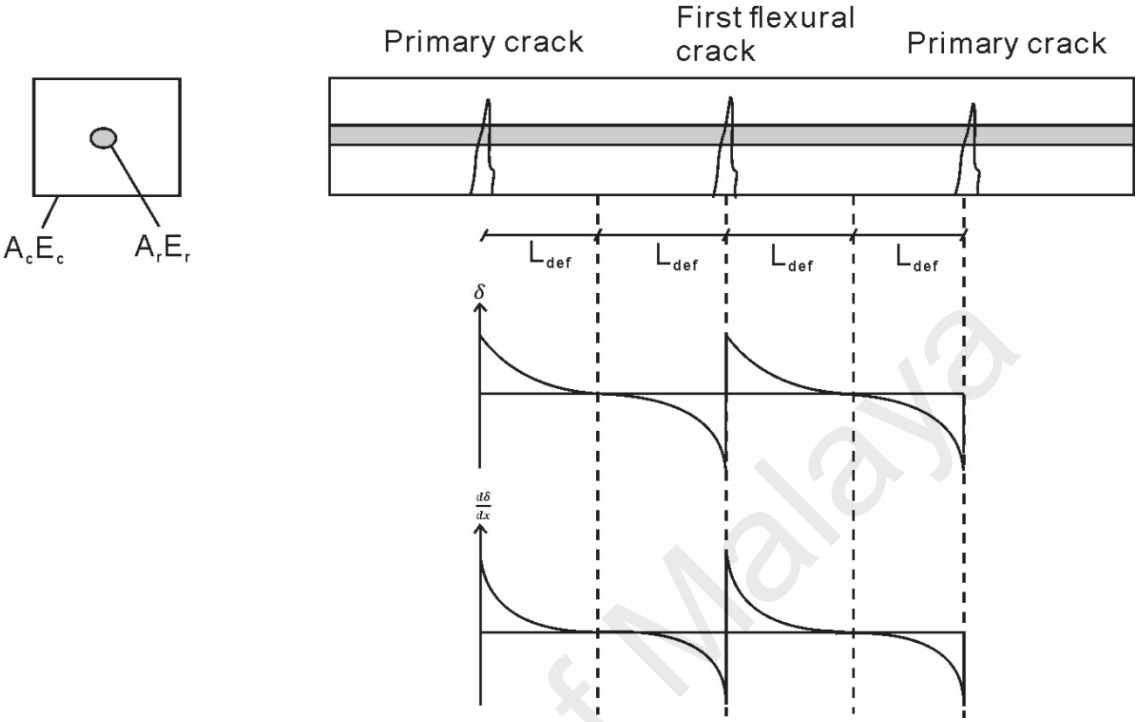

Figure 2.3: Formation of Primary Cracks.

2.2.2 Concrete Softening Mechanism

In order to discuss the concrete softening mechanism, consider a concrete prism specimen subjected to axial compressive stress as shown in Figure 2.4 and Figure 2.5. The resulting stress-strain relationship from the compression of the concrete prism would assume the idealised form as shown in Figure 2.6.

In the beginning the stress-strain curve follows a linear elastic path, as the concrete experience a measurable material strain up to ε_{mat}. This ascending branch of the concrete compressive stress-strain relationship is relatively easily determined and has been quantified empirically. The descending branch of the stress-strain relationship on the other hand is made complicated by the concrete softening behaviour, which causes a gradual drop in the strength of concrete.

The occurrence of the concrete softening can be explained using the established shear friction theory (Walraven et al. 1987; Chen et al. 2014). The concrete reaches the maximum amount of material deformation that it can take at ε_{mat}. Beyond this point further deformation on the concrete cylinder is accommodated by a type of non-material deformation, where concrete wedges will start forming along potential sliding planes and the non-material deformation is obtained through sliding of wedges (Δ_{wedge}).

From shear friction theory, Δ_{wedge} depends on the angle α. The plane of sliding for specimens with L/d≥2 can be assumed to form at its natural angle, where α=26° assuming the specimen's size is large enough. From the value of Δ_{wedge} and α, the vertical component of sliding, Δ_v can be determined. The total strain experienced by the specimen is:

$$\varepsilon_{total} = \varepsilon_{mat} + \varepsilon_{wedge}, \quad \varepsilon_{wedge} = \Delta_v / L_{def} \qquad \text{(Eq. 2.1)}$$

Where,

ε_{mat} = the strain due to material strain.

ε_{wedge} = is the strain due to sliding of wedge.

L_{def} = length of deformation.

Figure 2.4: Concrete Wedge on Prism Specimen (Nurwidayati, 2011).

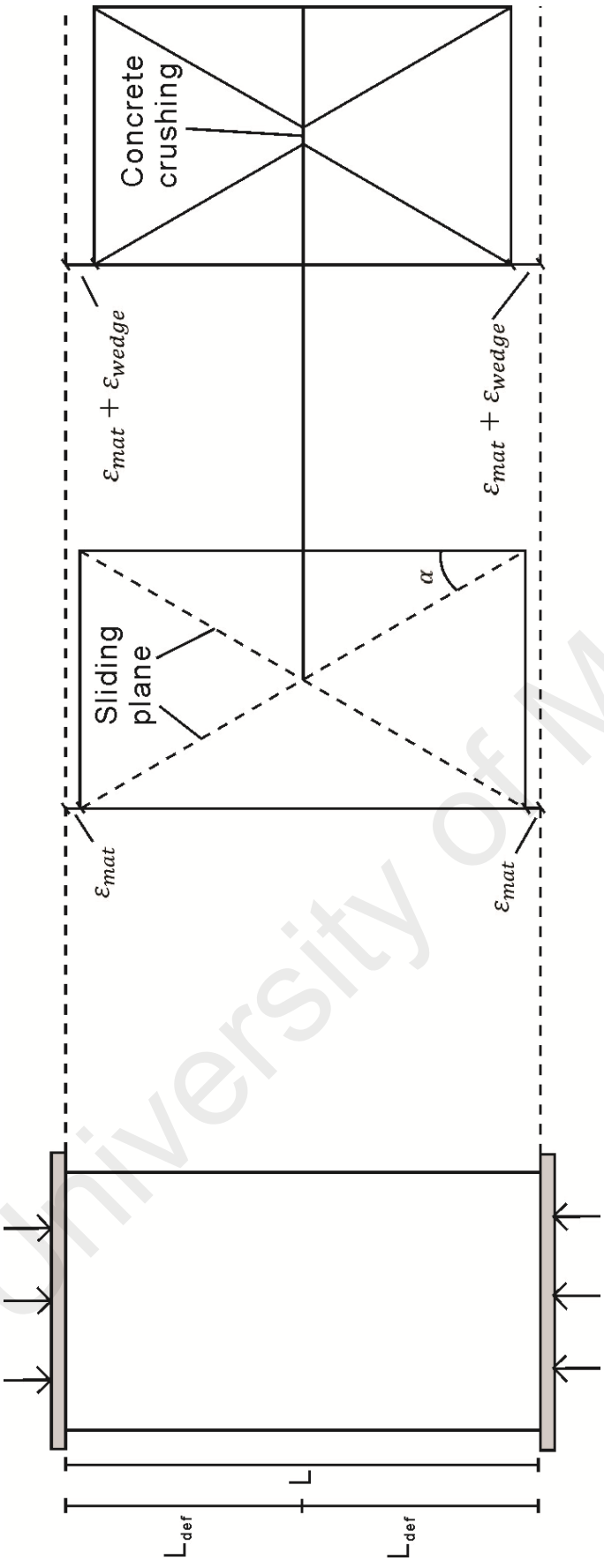

Figure 2.5: Formation of Concrete Wedges.

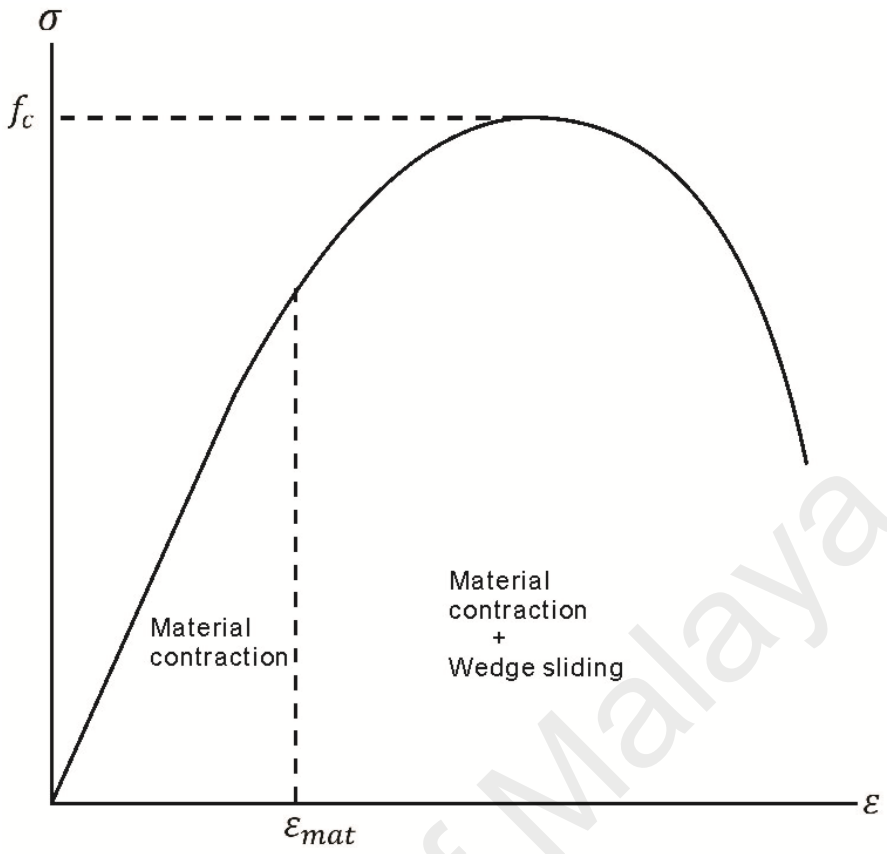

Figure 2.6: Idealised Stress-strain Relationship of Concrete.

2.3 Cyclic Material Models

The behaviour of reinforced concrete materials under cyclic load is well documented from various researchers, and used widely in both moment-curvature and moment-rotation based models. In order to correctly simulate the behaviour of reinforced concrete under cyclic load, these behaviour must be taken into account. The main behaviours that are of interest are:

- The stress-strain relationship of steel reinforcements.
- The stress-strain relationship of concrete.
- The bond stress-slip behaviour of steel reinforcements and the adjacent concrete.

These behaviours as well as available material models for simulating them will be discussed in the following sections. It should be noted here that some parts of these material models would be empirically derived, as although the moment-rotation approach

does not require empiricism to simulate the mechanics behaviour of reinforced concrete, it cannot escape from empiricism in the material models used. Hence it is important to use suitable and reliable material models when using the moment-rotation approach.

2.3.1 Cyclic Stress-Strain Relationship of Steel Reinforcement

There are three key features that are observed of cyclically loaded steel, namely the Baushinger effect, strain softening and isotropic strain hardening. These behaviours are as illustrated in Figure 2.7.

The Baushinger effect refers to the early departure of the stress-strain curve from the linear elastic response line. Strain softening is the degradation of modulus during strain reversals. Isotropic strain hardening is the increase in steel strength beyond its initial yield strength. Note that these characteristics are only apparent during strain reversals caused by cyclic load, and if the yield strain was exceeded.

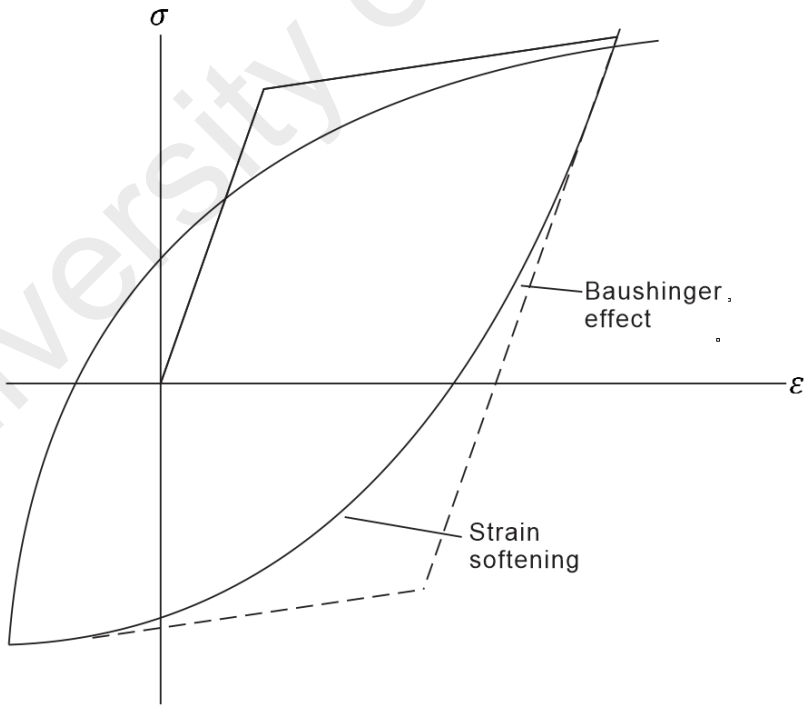

Figure 2.7: Steel stress strain relationship under cyclic loading.

There are a number of models have been developed to simulate the cyclic stress-strain relationship of reinforcing steel. The most widely used models are that of Menegotto and

Pinto (1973) and the model by Filippou et al. (1983). The mathematical expressions for both models are as shown below:

$$\varepsilon^* = \frac{\varepsilon - \varepsilon_r}{\varepsilon_o - \varepsilon_r} \quad \text{(Eq. 2.2)}$$

$$\sigma^* = \frac{\sigma - \sigma_r}{\sigma_o - \sigma_r} \quad \text{(Eq. 2.3)}$$

Where,

σ_o = stress at point where the asymptotes of the branch under consideration meets.

ε_o = strain at point where the asymptotes of the branch under consideration meets.

σ_r = stress at point where the last strain reversal having stress of the same sign took place.

ε_o = strain at point where the last strain reversal having stress of the same sign took place.

σ^* = normalized stress

ε^* = normalized strain

These expressions are also illustrated in Figure 2.8, and represents a curved transition from a straight line with slope E_o to another asymptote, with slope E_1. The values of σ_o, ε_o, σ_r, and ε_r are updated at each strain reversal. There is also another parameter, R, which refers to the parameter that controls the shape of the transitional curve. This allows the representation of the Bauschinger effect. The expression for R is as follows:

$$R = R_o + \frac{a_1 \epsilon}{a_2 + \epsilon} \quad \text{(Eq. 2.4)}$$

Where,

R_o = experimentally derived parameter, assumed value is 20 in most cases.

a_1 = experimentally derived parameter, assumed value is 18.5 in most cases.

a_2 = experimentally derived parameter, assumed value is 0.0015 in most cases.

ϵ = difference between ε_o and ε_r.

From the expression, R is a decreasing function of ϵ which is the strain difference between the current asymptote intersection point (σ_o, ε_o) and the previous load reversal point with maximum or minimum strain, depending on whether the corresponding steel stress at reversal is positive or negative (σ_r, ε_r). The value of ϵ is updated following a strain reversal. The derivation of R remains correct even for cases of partial loading and unloading (Filippou et al. (ref))

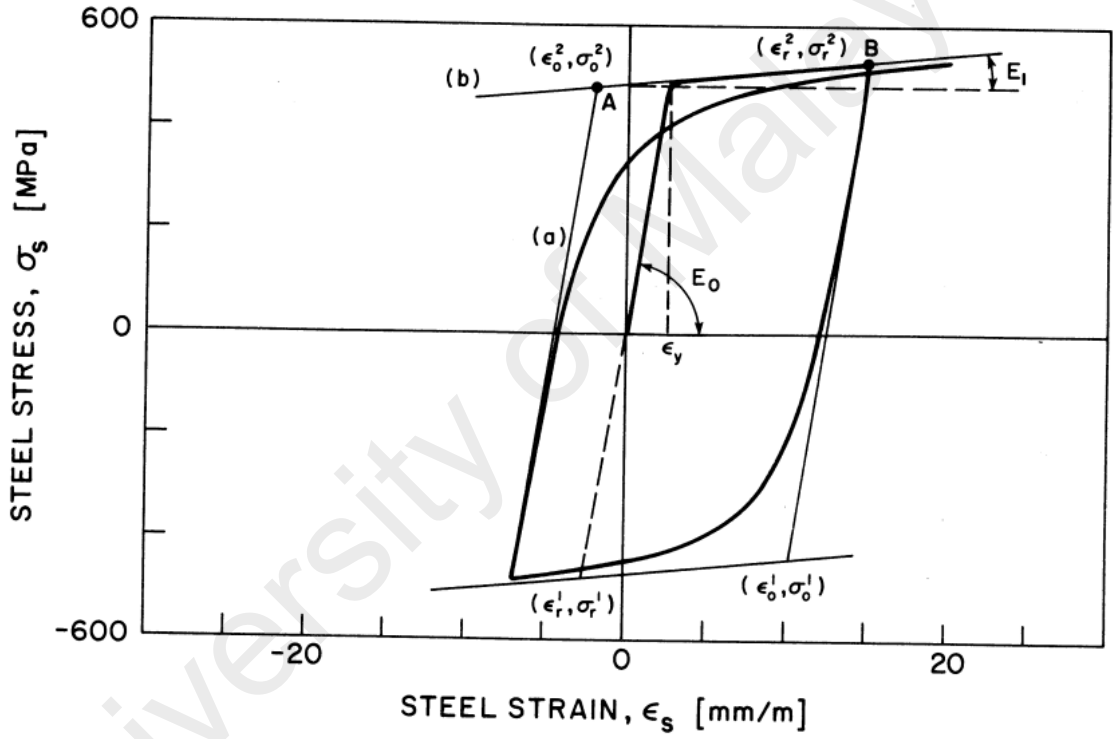

Figure 2.8: Menegotto Pinto Steel Model (Filippou et al., 1983).

2.3.2 Cyclic Model for Stress-Strain Relationship of Concrete

Figure 2.9 shows a typical stress-strain curve for concrete under cyclic loading. When concrete is unloaded, the total concrete strain is gradually reduced as the elastic strain of is recovered. The reduction in strain stops as all recoverable strain is exhausted, and there will be a residual strain, which is an unrecoverable plastic strain. Reloading curve starts at the point of residual strain and follows a linear elastic path until the total strain reaches

the value of strain prior to unloading, beyond which the stress-strain curve once again follows the path of monotonic stress-strain relationship.

Concrete subjected to cyclic loading would show a decreasing strength and stiffness, and this must be accounted for in some way for a concrete stress-strain model to realistically simulate concrete behaviour. The Martinez-Rueda model (Martinez-Rueda and Elnashai, 1997), which is used in this research, uses plastic strain as the primary rule for determining degradation of strength and stiffness. The calculation of plastic strain presented by

Martinez-Rueda is based on the plastic or irrecoverable strain calculation that was presented in the model by Mander et al. (1988), which was in turn based on the model by Popovics et al. (1973).

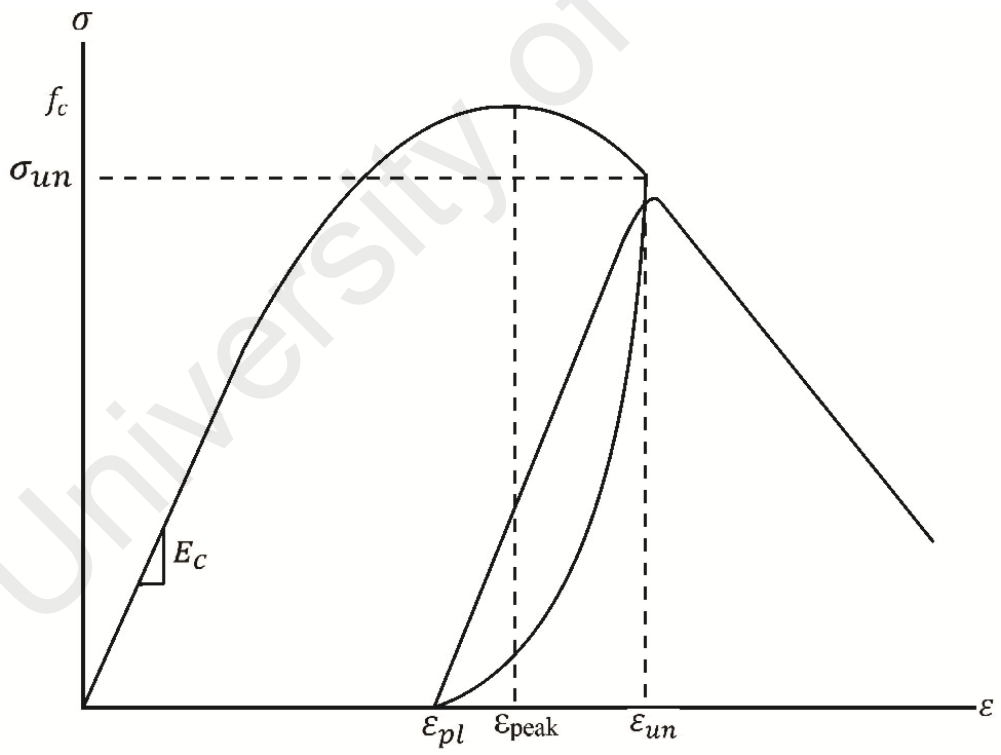

Figure 2.9: Concrete Stress-strain Relationship.

2.3.2.1 Loading Curve

In the Martinez-Rueda model, the loading path is fully based on Popovic's (1973) model, which for case of unconfined concrete can be simplified into:

$$\sigma_c = f_c \frac{\frac{\varepsilon_c}{\varepsilon_{peak}} r}{r-1+(\frac{\varepsilon_c}{\varepsilon_{peak}})^r} \quad \text{(Eq. 2.5)}$$

Where,

σ_c = concrete stress.

f_c = peak strength of the concrete.

ε_c = concrete strain.

ε_{peak} = peak concrete strain.

r = a factor controlling ductility = $\frac{E_c}{E_c - \frac{f_c}{\varepsilon_{peak}}}$

2.3.2.2 Unloading Curve

The low ductility nature of concrete causes plastic strain to occur even before reaching peak strength of the concrete. In order to properly simulate cyclic behaviour of concrete, the plastic strain must be determined and included in the stress-strain relationship. In the Martinez-Rueda model, the plastic strain caused by the load applied to the concrete' is determined as:

$$\varepsilon_{pl} = \varepsilon_{un} - \frac{\sigma_{un}}{E_c}, 0 \leq \varepsilon_{un} \leq \varepsilon_{35} \quad \text{(Eq. 2.6)}$$

$$\varepsilon_{pl} = \varepsilon_{un} - \frac{\varepsilon_{un}+\varepsilon_a}{\sigma_{un}+E_c\varepsilon_a}, \varepsilon_{35} \leq \varepsilon_{un} \leq 2.5\varepsilon_c \quad \text{(Eq. 2.7)}$$

$$\varepsilon_{pl} = \frac{\sigma_{cr}\varepsilon_{un}+\varepsilon_a}{\sigma_{cr}+\sigma_{un}}, \varepsilon_{un} \geq 2.5\varepsilon_c \quad \text{(Eq. 2.8)}$$

Where σ_{un} and ε_{un} are stress and strain at instance of unloading respectively. The unloading path assumes a second degree parabola shape.

2.3.2.3 Reloading Curve

Reloading curves in the Martinez-Rueda model is defined by a linear relationship up to the strain at which the last unloading occurred. The straight line is defined by:

$$\sigma_c = \sigma_{ro} + E_r(\varepsilon_c - \varepsilon_{ro}) \quad \text{(Eq. 2.9)}$$

Where,

$$E_r = \frac{\sigma_{ro} - \sigma_{new}}{\varepsilon_{ro} - \varepsilon_{un}} \quad \text{(Eq. 2.10)}$$

$$\sigma_c = \frac{0.9 f_c \frac{\varepsilon_c}{0.9\varepsilon_{peak}} r}{r - 1 + (\frac{\varepsilon_c}{0.9\varepsilon_{peak}})^r} \quad \text{(Eq. 2.11)}$$

The reloading curve resumes the shape of the old monotonic curve once the strain level reaches past the strain level at last unloading. An illustration of the stress-strain model is given in Figure 2.10.

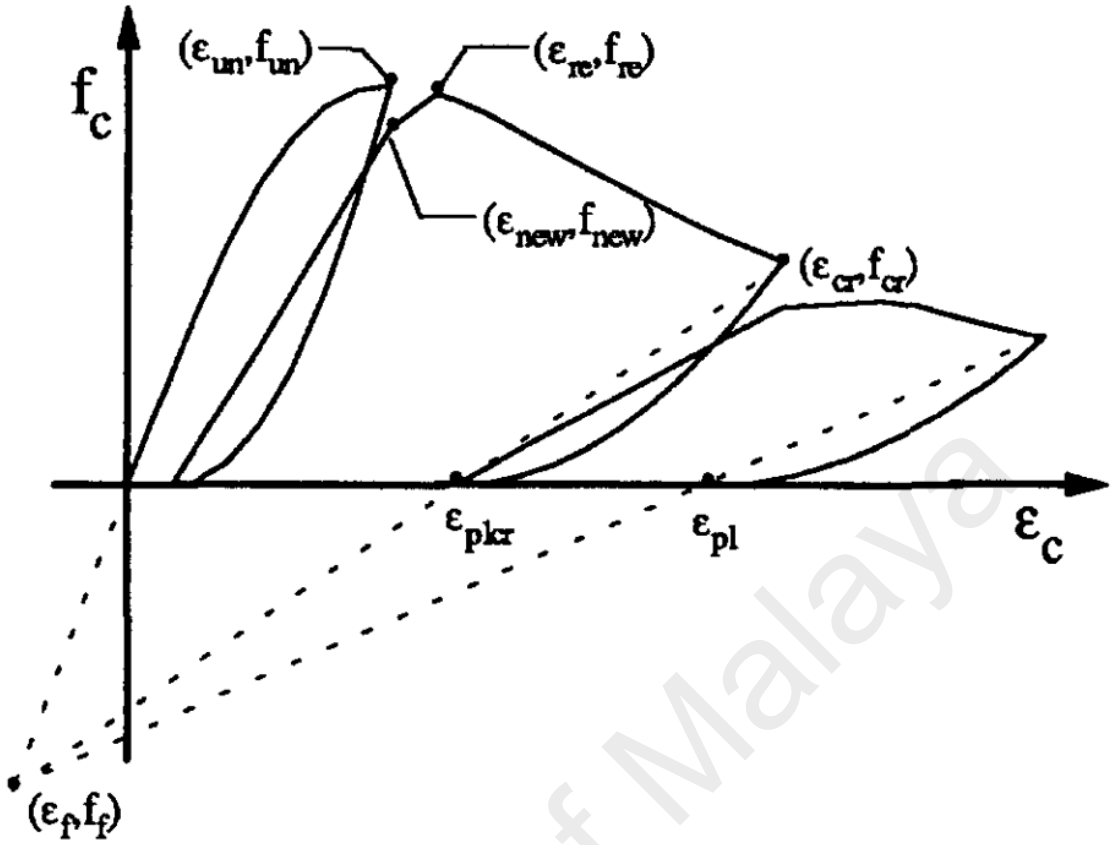

Figure 2.10: Stress-strain curve (Martinez-Rueda and Elnashai, 1997).

2.3.3 Cyclic Model for Bond Stress-Slip Relationship

The most widely used cyclic bond stress-strain model is perhaps the one by Eligehausen et al. (1992), due to its relatively simple usage and its consideration of bond degradation during cyclic loading. The bond stress-slip relationship during cyclic load is as illustrated in Figure 2.11. The author will attempt to give an explanation on the bond stress-slip model is given here, but note that it may not be enough due to the complexity of the model, which require the use of several charts that must be referred to when using it. Hence, the author would suggest that the source material be read for more information.

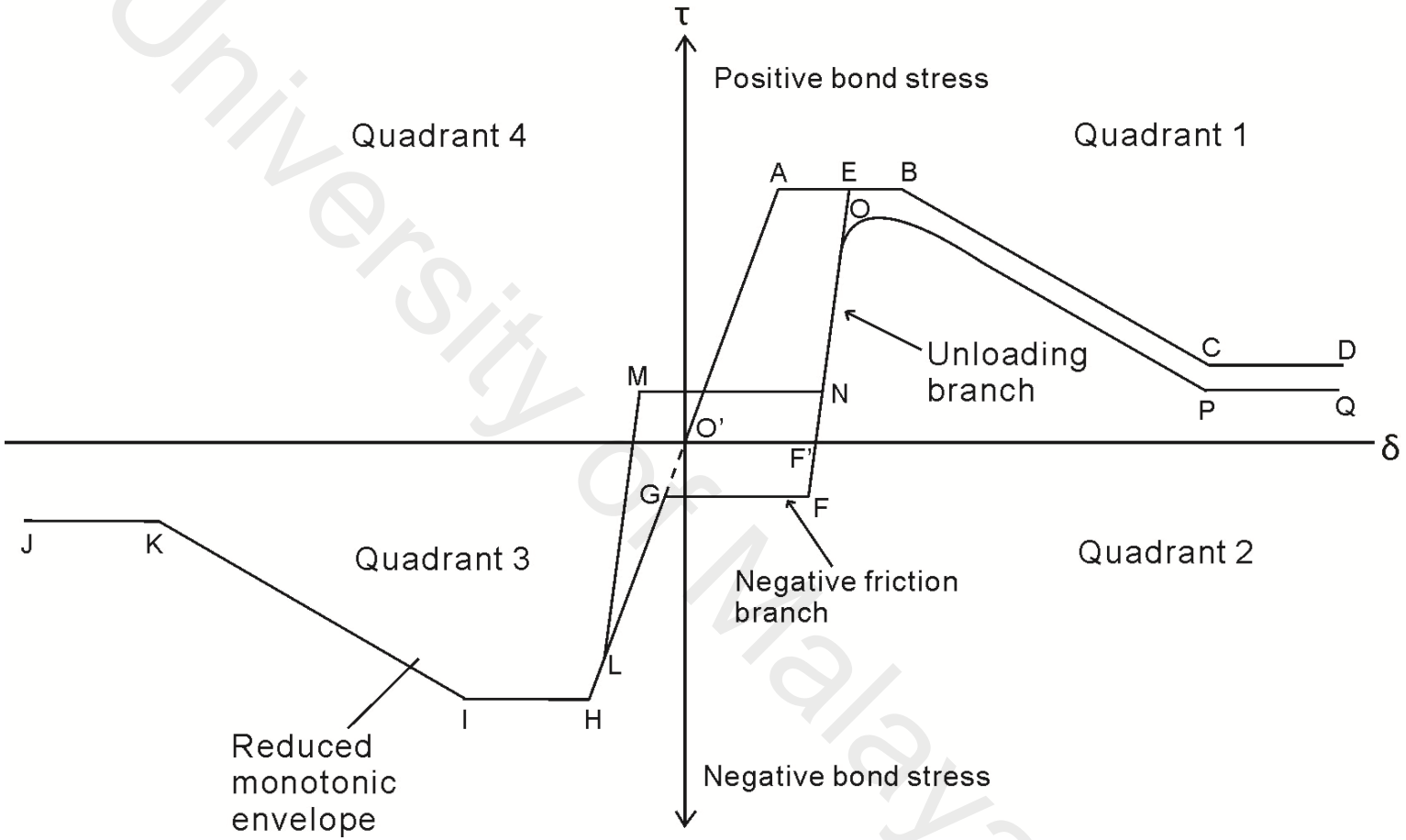

Figure 2.11: Bond Stress-Slip Relationship

2.3.3.1 Loading Curve

On first loading sequence (points O'AB), the bond stress-slip relationship follows the curve that is similar to the much used CEB-FIP model (CEB 1993) for monotonic loading envelope (points O'ABCD). The bond equation for the loading curve is as follows:

$$\tau = \tau_{max}(\frac{s}{s_{max}})^{0.4},\ s < 1 \quad \text{(Eq. 2.12)}$$

$$\tau = \tau_{max},\ 1 < s < 2 \quad \text{(Eq. 2.13)}$$

$$\tau = \frac{\tau_{max}-\tau_3}{(-8)} * (s-10) + \tau_3,\ 2 < s < 10 \quad \text{(Eq. 2.14)}$$

$$\tau = \tau_3,\ s > 10 \quad \text{(Eq. 2.15)}$$

Where,

τ = bond stress.

τ_{max} = maximum bond stress.

s_{max} = slip at maximum bond stress.

τ_3 = residual strength.

As load is applied, internal inclined cracks would begin to appear at the tip of the bar ribs due to high tensile stresses at the concrete surrounding the steel reinforcements. These cracks are referred to as bond cracks. The formation of bond cracks is accompanied by the crushing of concrete keys. Complete crushing and shearing off of the concrete keys will occur when the slip reaches a large enough value. At this stage only friction is resisting the force pulling out the steel reinforcement, thus the bond stress is equal to the frictional resistance.

2.3.3.2 Unloading Curve

As unloading occurs, the bond stress-slip curve follows a stiff downward path (points EF) to account for recoverable elastic deformation. This continues until the bar is slipping in a previously damaged area (points FG), where only the frictional resistance is acting against the slipping of bar. The stiff downward path is assumed to have a stiffness of 180 N/mm^3, while the frictional resistance can be determined using Figure A.1 in Appendix A.

Note that the slipping of bar actually acts in the opposite direction during unloading, thus the frictional resistance has negative value. This has a significant effect to the partial-interaction model, as this causes the load at hinge, P_{r1} to become reversed as well, which means it is under compressive force. This occurs despite the slip at hinge still being of positive value.

After the slip of the steel reinforcement has been reduced to zero (point G), the bar ribs are once again in contact with the surrounding concrete. It can be seen that the frictional resistance contributes very little to the bond stress and most of the bond stress is caused by mechanical interlocking between bar ribs and concrete. The crushing of concrete keys will have an effect during the rest of cyclic loading, and in this model it is taken into account by a damage factor. The damage factor is related to total dissipated energy, and can be determined using Figure A.2 in Appendix A. Further slip in the opposite direction will cause the bond stress-slip curve to assume the shape of the monotonic envelope, albeit with reductions to the magnitude of bond stress (points GHIJK) due to the damage factor explained earlier.

2.3.3.3 Reloading Curve

During reloading, a stiff upward path is encountered (points LM), again to account for recoverable elastic deformation. This continues until the bar reaches previously damaged section (points MN) and only the frictional resistance acts against the force pulling out the steel bar. The frictional resistance this time however has a positive value as slipping of bar occurs in the same direction as during loading. The frictional resistance also experiences reduction in magnitude due to damage incurred during the first loading.

As the steel reinforcement comes into contact with concrete again, the bond stress-slip curve follows another stiff upward path (points NE) to allow for any elastic deformation. At the end of the stiff path the bond stress-slip curve will follow a reduced monotonic envelope (points OPQ), with the amount of reduction calculated using the damage factor. The reduced values of τ_{max} and τ_3 can be determined from Figure A.3 in Appendix A.

CHAPTER 3: METHODOLOGY

Based on the literature review, there are two main mechanisms that governs the behaviour of cracked reinforced concrete beam: tension stiffening and concrete softening. The focus is now on simulating these mechanisms under cyclic loading. The work sequence of the moment-rotation approach used is as shown in Figure 3.1. In brief, the main parts of the moment-rotation approach is as follows:

- A cyclic partial-interaction numerical simulation model will be used to simulate the tension stiffening mechanism and will be used to generate load-slip relationships.
- Size-dependent stress-strain numerical simulation model for concrete will be used to simulate the concrete softening mechanism. It will also be shown how it can be used for cyclically loaded concrete.
- Moment-rotation numerical simulation model, which incorporates the other two models mentioned before will be used to generate a cyclic moment-rotation relationship for beams.

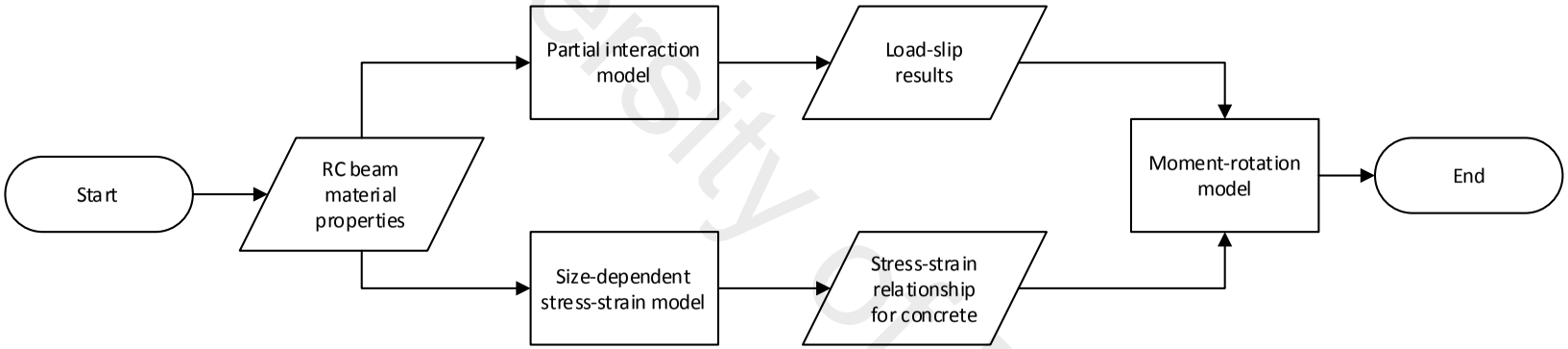

Figure 3.1: Work sequence for moment-rotation approach.

3.1 Partial-Interaction Model

The first step in the proposed moment-rotation model is to quantify the load-slip relationship due to slip of reinforcement using the partial-interaction theory (Haskett et al. 2009; Muhamad et al. 2011b; Visintin et al. 2012b; Oehlers et al. 2013), which also simulates the tension stiffening mechanism (discussed in section 2.2.1). To do so let us initially follow the analysis approach of Visintin et al. (2012b) for monotonic loading. The method will then be extended to allow for cyclic loading. The numerical algorithm that the author use for the model will also be presented.

3.1.1 Fundamental Principles

The partial interaction theory has been used by many researchers to form a numerical model with which the tension stiffening effect was simulated. In the partial interaction theory, the steel reinforcement is pulled out of adjacent concrete when load is applied to the beam, causing it to slip. The amount of slip is the highest at the crack face. The presence of slip is the main focus of the partial interaction theory, as this causes the bond force at the steel-concrete interface to act against the slip of reinforcement.

Consider the tension stiffening region as shown in Figure 3.2. The prism in Figure 3.2 has a cross section where a single reinforcing bar of area A_r and moduli E_r is centrally located in a concrete prism of area A_c and moduli E_c such that when a load P_r is applied no moment is induced.

On initial loading, that is prior to cracking a perfect bond exists between the reinforcement and the concrete such that both the reinforcement and the concrete are uniformly extended. When an initial crack forms there exists an imperfect bond between the reinforcement and the concrete such that the reinforcement slips relative to the concrete and this slip results in a half crack opening Δ_r in Figure 3.2(a). Due to the applied load P_r the reinforcement slips along the length of the prism as in Figure 2.3 which is a

function of the local bond stress-slip (τ/δ) material properties (Eligehausen et al. 1992) as idealised in Figure 2.11.

From the distribution of bond stress in Figure 3.2 (c) and knowing the load developed in the concrete at the crack face is zero the variation in concrete and reinforcement strain can be determined. Hence the slip-strain ($d\delta/dx$) in Figure 3.2 (e), which is the difference between the strain in the reinforcement and the concrete strain, is also known. Applying the boundary condition that full interaction is achieved where the interfacial slip and the slip-strain reach zero at the same point the primary crack spacing, S_{cr} can be determined as it is known that cracks will form when the strain in the concrete reaches the tensile cracking strain, ε_{ct} as shown in Figure 3.2 (f) (Muhammad et al. 2011b; Visintin et al. 2012a; Visintin et al. 2012b).

The crack spacing S_{cr} represents the minimum crack spacing as a subsequent crack can form anywhere in the full interaction region to the right of the region S_{cr} in Figure 3.2 (f). However, if a moment gradient is applied to the beam, which is the usual case, then it is most likely and conservative to take the primary crack spacing as S_{cr} (Visintin et al. 2012b; Chen et al. 2014). As it is highly likely that a member in service will be the member will be initially cracked prior to any cyclic loading let us assume the crack spacing is the same as that be determined from this monotonic load case. If this assumption is not considered appropriate, the model of Visintin et al. (2012b) which simulates the response a prism with the same boundary conditions as Figure 3.2 (d) and Figure 3.2 (e) can be applied to determine the crack spacing.

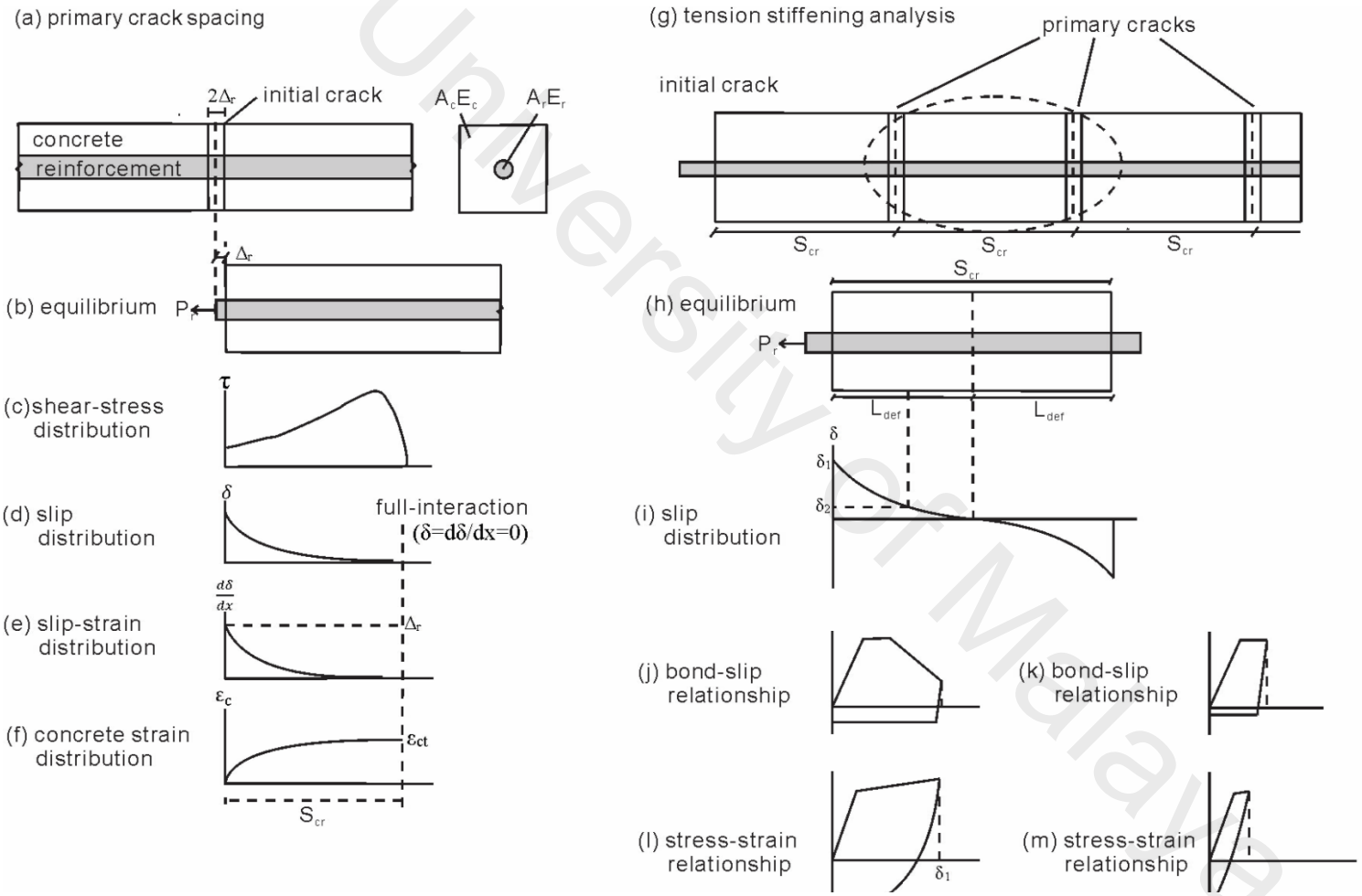

Figure 3.2: Partial-Interaction Tension Stiffening Analyses.

It should be noted here that the length between primary cracks is considered as the hinge length in this moment-rotation model, because once primary cracks have formed along the prism as in Figure 3.2 (g) the loading of each prism is symmetric and hence only a single prism as in Figure 3.2 (h) needs to be considered. The load-slip (P_r/Δ_r) relationship under generalised cyclic loading can be determined following the same mechanism as for the infinitely long prism in Figure 3.2 (c) but in this case a cyclic τ/δ relationship such as that of Eligehausen et al. (1992) must be used to simulate the bond degradation during cyclic load. Bond degradation is caused by the formation of bond cracks and crushing of concrete keys as reinforcement slip from concrete. As the bond degradation depends on the slip history, this causes the prism to have a unique cyclic bond stress-slip relationship at each section along its length. To illustrate this, consider the slip distribution in Figure 3.2 (i) as the slip history of the prism prior to being unloaded. The resulting cyclic bond stress-slip relationship caused by the slip history at two different locations (the crack face and the middle of the half-segment) along the prism is shown in Figure 3.2 (j) and Figure 3.2 (k). As can be seen, the cyclic bond stress-slip curves are markedly different. Note also that the frictional resistance at the crack face is also significantly higher than at the middle of the prism due to the higher amount of bond degradation that occur there.

Similarly, when determining the strain in the reinforcement as in a cyclic stress strain relationship for the steel reinforcement such as the one by Menegotto and Pinto (1973) and Filippou et al. (1983) which has a general shape as in Figure 2.8 must be used. The cyclic stress-strain relationship of steel is also dependent on the slip history experienced during cyclic loading, which means that similar to the cyclic τ/δ relationship, the stress-strain relationship also differs along the prism, as illustrated in Figure 3.2 (l) and Figure 3.2 (m). During unloading process of cyclically loaded steel, if reinforcement was loaded past its yield point, there will be some amount of unrecoverable strain. For further

reduction of strain to occur beyond this point, the reinforcement must be pushed back into the concrete under a compressive reversed load. Note that as reinforcement behaviour dictates most of prism behaviour, this causes load-slip relationship to be under compression while reinforcement slip is still present and also causes a residual load at zero slip. The effect this has on the moment-rotation model will be discussed in detail in later section.

It can be seen that through symmetry, the boundary condition that the slip at the midpoint of the prism at $S_{cr}/2$ must be zero, and this is taken as the boundary condition. Through the application of the partial interaction model above, for any given slip of the reinforcement Δ_r in Figure 3.2 (h) the load developed in the reinforcement P_r is known.

3.1.2 Material Models Used

There are two material models that are essential to the partial-interaction model:

i. Cyclic model for stress-strain of steel. The model by Menegotto and Pinto (1973) will be used.
ii. Cyclic model for bond stress-slip of steel and adjacent concrete. The model by Eligehausen et al. (1992) will be used.

Information on the models can be found in sections 2.3.1 and 2.3.3 of the literature review. Applying these models require several data to be saved every time a load reversal occurs:

i. For the Menegotto-Pinto (1973) steel stress-strain model, the stress and strain at point where load reversal occurs must be recorded. These values are required to calculate R, which is the parameter used to simulate the Baushinger effect.
ii. For the bond stress-slip model by Eligehausen et al. (1992), the slip of steel reinforcement at the point of load reversal must be recorded to determine the damage factor, d.

As mentioned in section 3.1.1 previously, due to partial-interaction, the values of stresses, strains and slips are varied along the length of deformation, L_{def}. This causes each of the prism elements have a different stress-strain shape and damage factor. Therefore it is required to record the values at each prism element when load reversal occur. The example of prism element is shown in Figure 3.4 for more understanding on this matter.

3.1.3 Determining Crack Spacing

A numerical model is presented here for applying the partial-interaction analysis using Matlab. For the partial-interaction analysis, the prism is divided into several small elements. Element size of 0.1mm is found to be able to give a considerably accurate result while not slowing the analysis by too much. For the initial part of the analysis, the number of prism elements is unlimited, which means the analysis is performed on an imaginary, infinitely long prism. This is necessary to determine the hinge length and the length of deformation L_{def}, which will be used in all of the models, namely the partial-interaction, size-dependent concrete stress-strain and moment-rotation models.

Since the stress and strain of concrete in this numerical model is dependent on the concrete area, the prism size is critical to the analysis. In this paper the prism size will be based on the recommended prism size as given by Muhamad et al. (2011a) which stated that the prism depth should be as deep as the bar plus the cover on both sides and the width of the prism is assumed to be the width of the entire beam evenly divided between adjacent bars.

The numerical algorithm used in determining the crack spacing using Matlab is described below. A pseudo code flowchart and an illustrated view of the analysis are also available in Figure 3.3 and Figure 3.4.

1. The tension stiffening prism is divided into small elements of length 0.1mm. The assumption applied here is that the stress and strain acting along the length of individual elements are the same due to its small size.
2. At the crack face, a very small value of slip (δ) is fixed, preferably 0.001mm slip as from the author's work, the primary cracks has been found to form at very low slip value. The amount of load, P_r applied to the reinforcement that is needed to cause this slip is then assumed. Note that force acting on concrete, P_c is assumed to be zero or is negligibly small as the concrete-concrete interface is not touching one another at the crack face.
3. The value of bond stress, τ corresponding to the slip δ is determined using any appropriate bond stress-slip model, such as the model by CEB (1993). Subsequently the bond force, B can be determined.
4. The concrete strain (ε_c) can then be determined by assuming a linear tensile stress–strain relationship where it can be assumed that the concrete remains elastic, because the concrete is subjected only to tensile stresses.
5. A stress-strain model for steel is required to determine the strain of steel (ε_r), where the model is used to determine the appropriate value of modulus. The use of bilinear stress-strain model, with only two values of modulus (elastic modulus and strain hardening modulus) is found to be enough to give accurate results.
6. The difference in the steel strain and concrete strain gives the change in slip, also called the slip-strain ($\frac{d\delta}{dx}$), which is experienced by the steel

reinforcement. By knowing the slip-strain, the slip of the next element can be determined.

7. Using the bond force B calculated earlier, the force in the reinforcement and concrete at the next element can also be determined.
8. The difference in the steel strain and concrete strain is the change in slip, or slip-strain, which is experienced by the steel reinforcement. By knowing the slip-strain, the slip of the next element can be determined.
9. The analysis steps 3 to 8 are repeated with another assumed value of P_r until the slip is reduced to zero. Note however that in calculation it is impossible to reduce slip to zero, so it is assumed here that it is considered close enough to zero if the initial slip is able to be reduced to 1% of its initial value.
10. Once the boundary conditions are satisfied another value of initial slip is fixed and the entire analysis is repeated. To determine L_{def}, the analysis should stop once the full-interaction boundary conditions (slip equal to zero) coincides with the strain in concrete reaching the concrete cracking strain, thereby causing the formation of primary crack. The length of deformation is determined as half the length of crack.

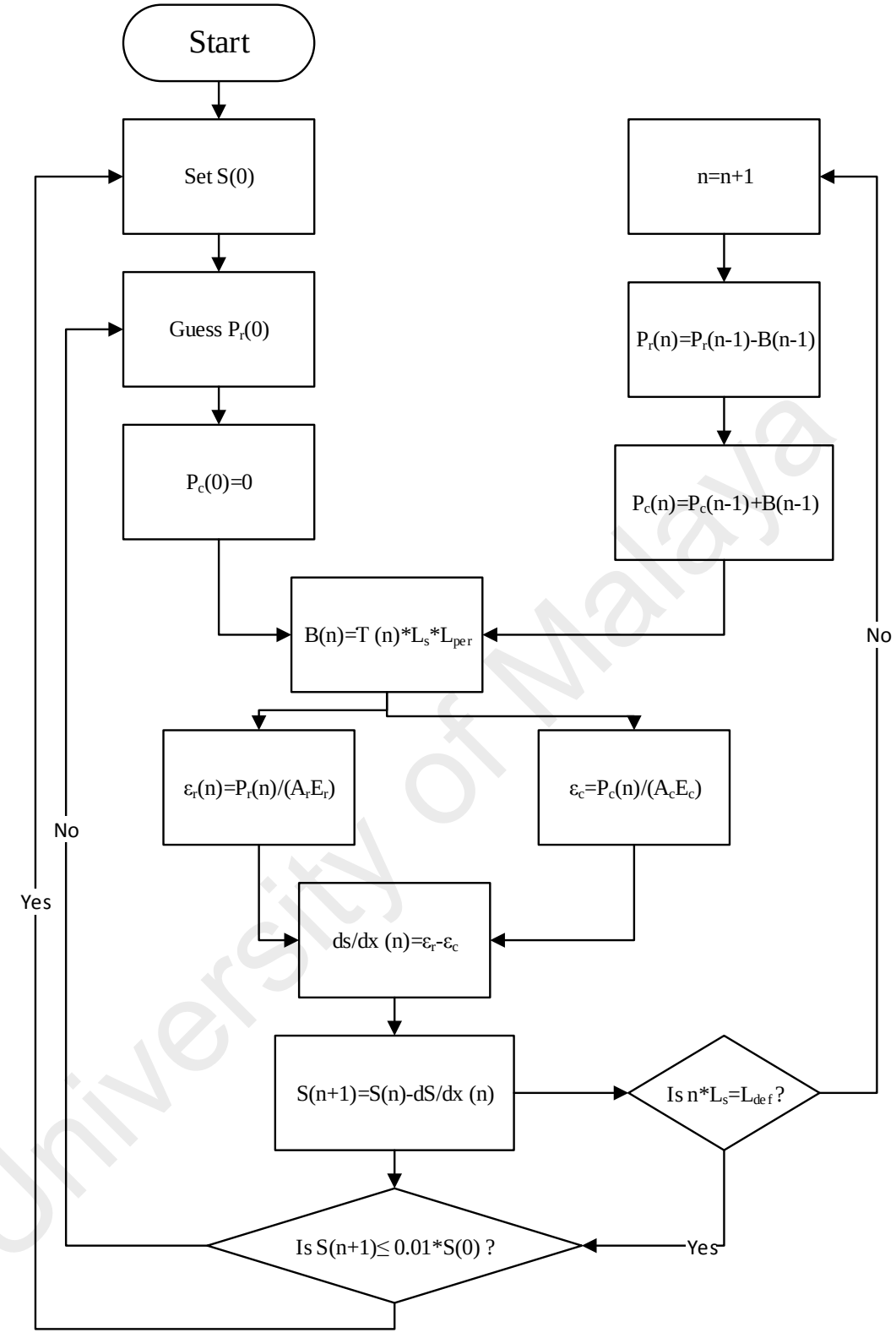

Figure 3.3: Partial-interaction model procedure.

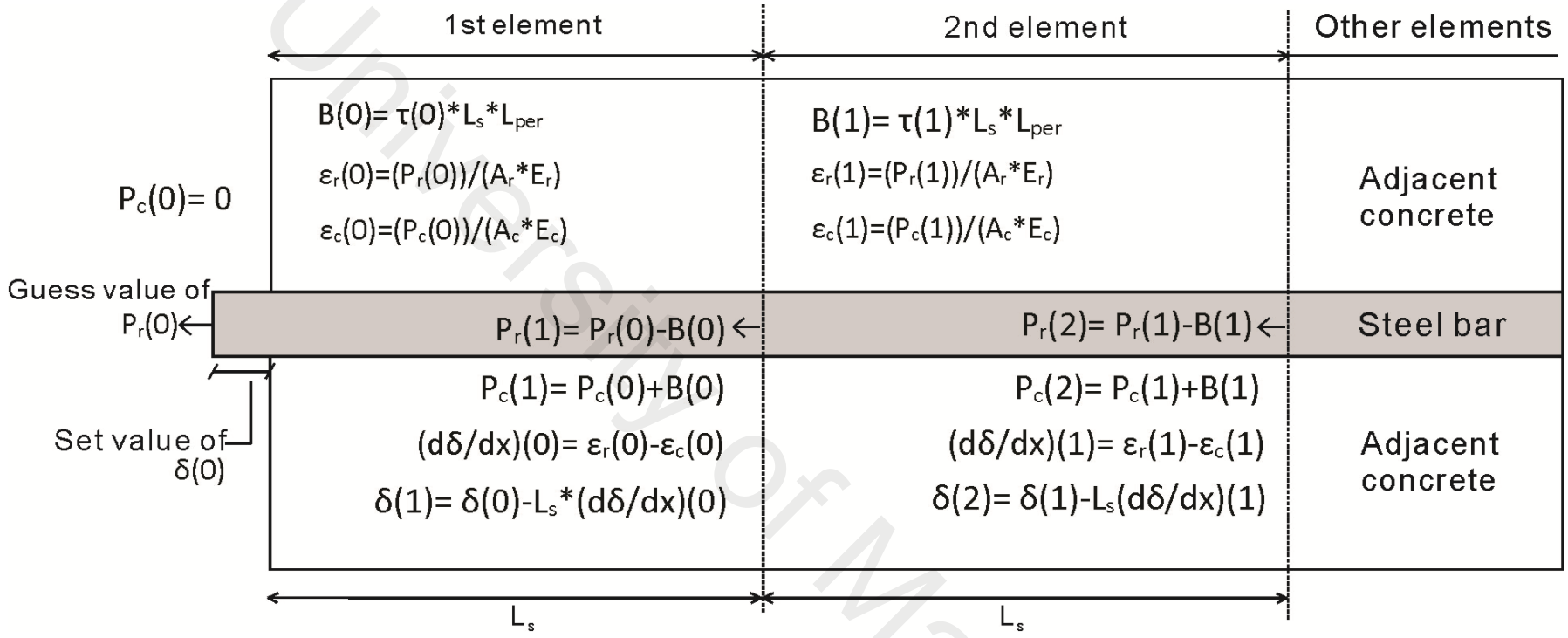

Figure 3.4: Illustration of the Partial Interaction Model

3.1.4 Determining Load-Slip Relationship

Once L_{def} is determined, the analysis is repeated on prism with length L_{def}, in order to obtain a load-slip relationship of the beam section between the primary cracks for the moment-rotation approach. Cyclic material models will also be used, in order to extend the moment-rotation approach to allow for cyclic loading.

The numerical algorithm used in the analysis is as illustrated in Figure 3.3 and Figure 3.4 as shown before. Note that the procedure is nearly identical to the procedure of determining the primary crack spacing (i.e. the hinge length), with some modification to allow for the cyclic material models used.

The partial-interaction analysis procedure, applied using Matlab, is as shown below:

1. At the crack face, a certain value of slip ($\delta(0)$) is fixed. What the value of slip is depends on the beam condition:
   a. If the beam is being loaded for the first time (initial loading) or is being reloaded, the slip can be set to 0.01mm first, then increased gradually as the procedure is repeated to obtain the load-slip relationship.
   b. If the beam is being unloaded, the slip should be set to the last maximum slip experienced by the beam prior to unloading and then decreased gradually to 0.01mm obtain a load-slip relationship.
2. The amount of load, $P_r(\mathrm{n})$ applied to the reinforcement that is needed to cause this slip is then assumed. Note that load applied to concrete, $P_c(\mathrm{n})$ is assumed to be zero or is negligibly small as the concrete-concrete interface are not in contact with one another at the crack face. The value of bond stress, $\tau(\mathrm{n})$ corresponding to the slip $\delta(n)$ is determined using any appropriate bond stress-slip model. If L_{def} has been determined, use a cyclic bond stress-slip model such as the one by Eligehausen et al. (1992).

3. The concrete strain can then be determined by assuming a linear tensile stress–strain relationship where it can be assumed that the concrete remains elastic, because the concrete is subjected only to tensile stresses.
4. A stress-strain model for steel is required to determine the strain of steel, where the model is used to determine the appropriate value of modulus. For cyclic loading, stress-strain models by Menegotto and Pinto (1976) and Filippou et al. (1983) can be used. For cyclic load the equation above cannot be used, as unlike the bilinear monotonic stress-strain relationship, cyclic stress-train relationships have a unique modulus for each value of strain, making it difficult to determine and use the said modulus as in the case of monotonic loading. An easier way is to generate vectors of stress and strain for each prism element and determine the strain of steel by interpolation using the known value of applied stress.
5. The difference in the steel strain and concrete strain is the change in slip, or slip-strain ($\frac{d\delta}{dx}$), which is experienced by the steel reinforcement. By knowing the slip-strain, the slip of the next element can be determined.
6. Using the bond force calculated earlier, the force in the reinforcement and concrete at the next element can also be determined.
7. The analysis steps 2-7 are repeated with another assumed value of $P_r(0)$ until the boundary conditions of full interaction, $\delta(n) = 0.01 * \delta(0)$ is satisfied (Note: In calculation it is impossible to reduce slip to zero, so the stop condition is the initial slip $\delta(0)$ being reduced to 1% of its initial value.)
8. Once the boundary condition is satisfied another value of initial slip, $\delta(0)$ is fixed and the entire analysis is repeated. If the beam is in initial loading or reloading, initial slip is increased. In unloading case the initial slip is reduced instead

3.2 Size-dependent Stress-Strain Model for Concrete

The concrete softening mechanism is defined by the shear friction sliding planes, which forms at some angle (α) in the compression region of a beam. The same shear friction behaviour can also be observed in axially loaded concrete cylinders, which means concrete cylinders can be used to idealise the concrete softening region of beams assuming that the stress-strain relationship a cylinder that has the same length as the hinge length of the beam is determined. It is however neither economical nor convenient to test a cylinder of specific size for every beam in order to simulate the concrete softening, which is why a size-dependent stress-strain relationship (Chen et al. 2014) can instead be used.

Consider a concrete cylinder as in Figure 3.5(a), which is applied an axial load σ_{ax}, then unloaded and reloaded again. The applied cyclic load will yield a stress-strain relationship with a general shape as in Figure 3.5(b). Along the OA region, the deformation experienced by the cylinder occurs through material strain (ε_{mat}), where concrete material contracts as load increases. The maximum material strain a concrete can take is usually low, due to the rigid nature of concrete.

Further deformation along the ABDE region occurs through the mechanism of wedge sliding (Δ_{wedge}). From shear friction theory, Δ_{wedge} depends on the angle α. The plane of sliding for specimens with L/d≥2 can be assumed to form at its natural angle, which is α=26°, assuming the specimen's size is large enough for the wedge to form at that angle. From the value of Δ_{wedge} and α, the vertical component of sliding, Δ_v can be determined. The total strain experienced by the specimen along ABDE is the sum of $\varepsilon_{mat}+\varepsilon_{wedge}$, where ε_{mat} is the strain due to material strain and $\varepsilon_{wedge}=\Delta_v / L_{def}$ is the strain due to sliding of wedge.

The cylinder is unloaded at point B, where a gradual decrease in strain occurs as the elastic material strain of ε_{mat} is recovered. The wedge strain ε_{wedge} on the other hand will

remain as a residual strain at point C, as the deformation is due to concrete crushing and the sliding of wedge Δ_{wedge} and therefore unrecoverable. When the cylinder is reloaded, reloading will start at the point of residual strain of ε_{wedge} at C and will follow a linear elastic path up to D as the concrete takes up the material strain ε_{mat} again. Along DE the stress-strain curve once again follows the path of its monotonic curve.

From this it can be seen that the components of ε_{mat} and ε_{wedge} are present and play a huge role at all stages of cyclic behaviour of concrete. A size-dependent relationship (Chen et al. 2014) can be derived from ε_{mat} and ε_{wedge}, using the assumption that for the same values of σ_{ax} and α, the amount of ε_{wedge} that occur is of equal value in two differently sized concrete specimens. Figure 3.6 shows the comparison of the stress-strain curve obtained from the original specimen size used in tests or model, L_{tm} and the stress strain curve derived for the length L_{def} with the new size-dependent strain determined as:

$$\varepsilon_{def} = \left(\varepsilon_{tm} - \varepsilon_{mat(n)}\right)\left(\frac{L_{tm}}{L_{def}}\right) + \varepsilon_{tm} \qquad \text{(Eq. 3.1)}$$

Where,

ε_{def} = the new size-dependent strain for L_{def}

ε_{tm} = the strain from tests or model

$\varepsilon_{mat(n)}$ = material strain at the n^{th} level, assuming a straight line from the origin

L_{tm} = half the length of specimen used in tests or during the derivation of the stress-strain model.

L_{def} = length of beam segment used in the partial-interaction tension stiffening analysis.

The material model used for the size-dependent concrete stress-strain is the model by Martinez and Elnashai (1997) which was discussed in section 2.3.2 in the literature review.

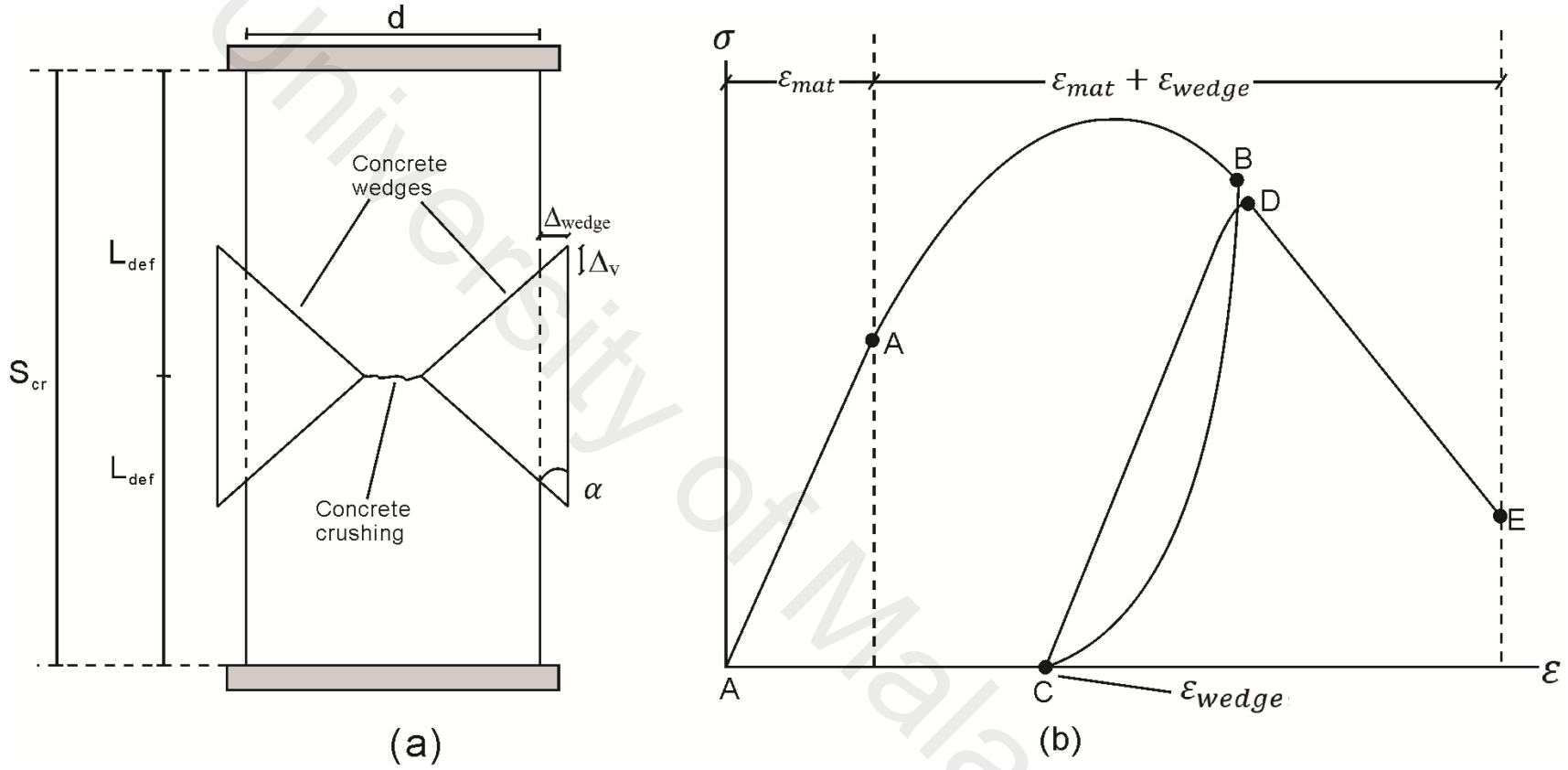

Figure 3.5: Concrete Cylinder Compression Test.

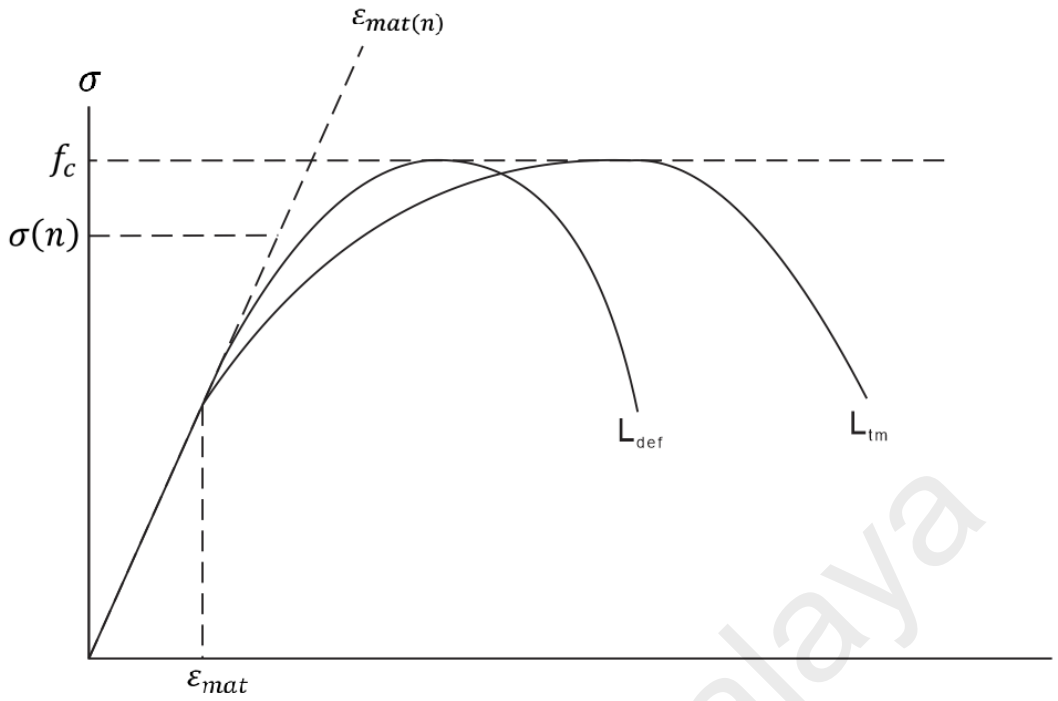

Figure 3.6: Comparison of new stress-strain curve and original curve from tests/model

3.3 Moment-Rotation Model

This section will cover the proposed moment-rotation model. The moment-rotation model is not a standalone model, and in fact uses partial-interaction model and the size-dependent stress-strain model for concrete as components to obtain the force acting on steel reinforcement and concrete for any given amount of rotation. The moment corresponding to these force are then determined, thus giving the moment-rotation relationship. The rotation can be converted to curvature by dividing it with L_{def}, and the moment-curvature relationship allows the load-deflection of a beam to be determined through the double integration method if desired.

The fundamental principles for the cyclic approach to moment-rotation model will first be presented, followed by the procedure for numerical algorithm used by the author for each phase of cyclic loading.

3.3.1 Fundamental Principles

To describe the basic framework for the moment-rotation as developed by Visintin et al. (2012b), let us consider a beam subjected to a monotonic load so that once the methodology is established it can be extended to the cyclic load case. Due to symmetry in the deformation in beam segments between primary cracks, only half of the crack length L_{def} needs to be considered as shown in Figure 3.7 (a). Prior to concrete cracking or softening the distribution of strain in Figure 3.7 (b) the distribution of stress in Figure 3.7 (c) and the distribution of Forces in Figure 3.7 (d) can be determined from the material constitutive relationships. For the now known distribution of forces in Figure 3.7 (d) it is then a matter of adjusting the neutral axis depth d_{NA} until, for a given rotation θ, longitudinal equilibrium is achieved. Importantly prior to strain localisation, that is any concrete cracking or crushing the analysis is identical to that which is commonly applied in a standard Euler Bernoulli moment-curvature model.

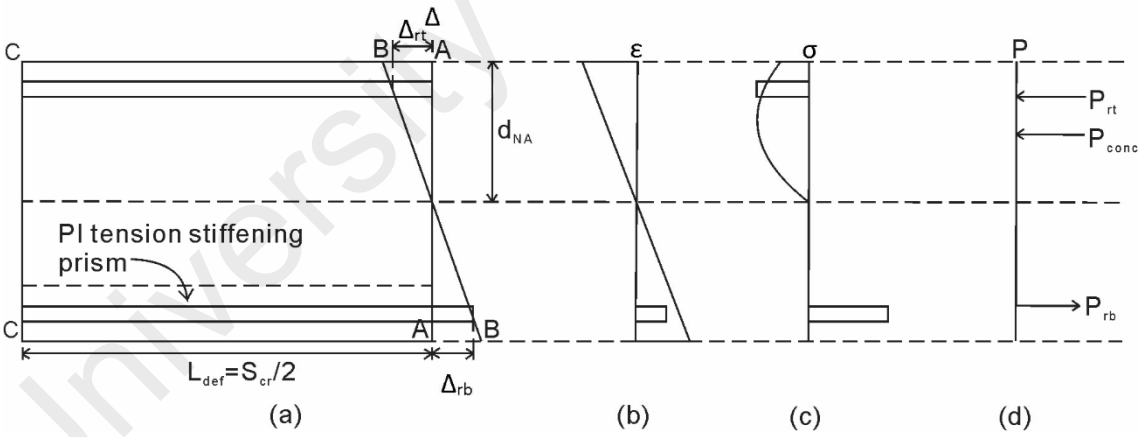

Figure 3.7: The half segment of hinge used for analysis.

Based on the application of the moment-rotation model in terms of monotonic loading was explained just now, the analysis will now be extended to allow for cyclic loading. Analysis of cyclically loaded beam is done in a nearly similar manner, where for a certain amount of rotation the depth of neutral axis is adjusted until equilibrium is achieved. Differences in the cyclic analysis is due to the cyclic stress-strain behaviour of materials

in the beam, namely the concrete and the steel reinforcement. These cyclic behaviour is illustrated in the symmetrical beam segment of Figure 3.8 (a), where it is assumed that the beam was loaded up to a certain point and is currently being unloaded.

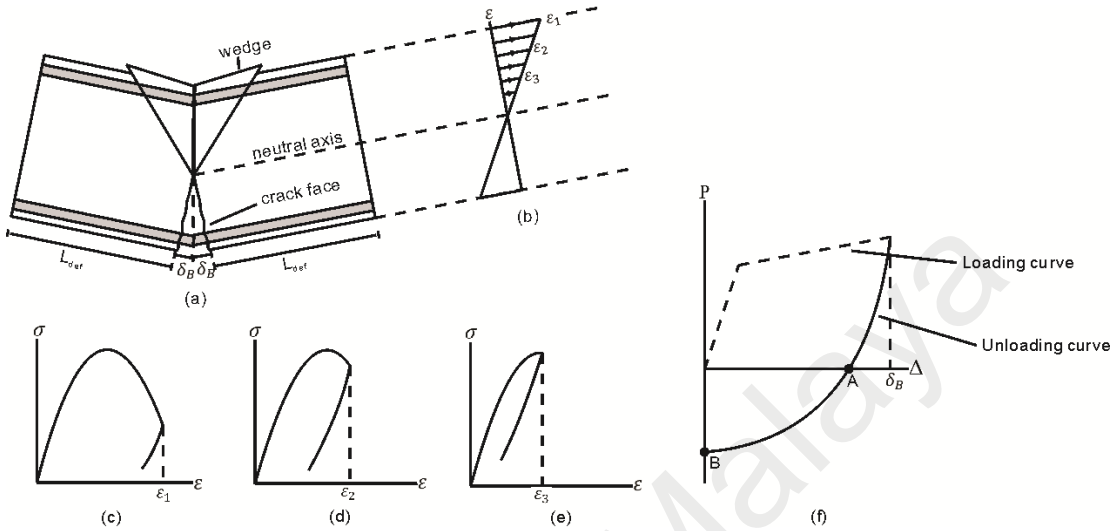

Figure 3.8: Cyclic moment-rotation model.

Concrete layers within the top region of the beam were compressed to different degrees of compression prior to unloading. This causes each concrete layer to have a unique strain history during cyclic loading, as illustrated in Figure 3.8 (b), which leads to each concrete layer having its own unique size-dependent stress-strain curve in Figure 3.8 (c), Figure 3.8 (d) and Figure 3.8 (e). This concept is similar to the application of bond stress-slip and stress-strain of steel described in previous sections. The top reinforcement is still under full-interaction at the early stages of unloading. The force acting on the bottom reinforcement is determined from the unloading curve of P_r/Δ_r relationship obtained using partial-interaction model, which should have a general shape as shown in Figure 3.8 (f). As can be seen for further reduction of slip to occur below point A, a reversed load must be applied. This causes a compressive force on the tensile reinforcement and forces the slipped reinforcement to return into the adjacent concrete. As the reinforcement at the bottom region is under compression, represented by the region AB in Figure 3.8 (f), the top region of the concrete must enter a tensile state for equilibrium to happen, which

causes the top region to crack. As the crack at the top region intercepts the crack at the bottom region, a full depth crack will occur as shown in Figure 3.9. In the full-depth crack situation, any load applied to the beam is taken up by the reinforcements as the concrete-concrete interface along the full-depth crack are not touching one another.

Top reinforcement is now under tension stiffening and the force acting on it can be determined by generating a P_r/Δ_r relationship using the partial-interaction model. Note that the P_r/Δ_r relationship of the top and bottom are not identical, as the general shape of the P_r/Δ_r curve would depend on the size and strength of the top and bottom reinforcements. Another difference is that the P_r/Δ_r curve of the top reinforcement would be for the loading, while P_r/Δ_r curve of the bottom reinforcement would be for unloading, as illustrated in Figure 3.8 (f). Reinforcement slip of the former tensile reinforcement, δ_b will be the fixed value instead of θ. From the known value of δ_b, F_{RB} can be interpolated from the P_r/Δ_r relationship of the bottom reinforcement. Due to equilibrium, $F_{RT}= F_{RB}$ and the slip corresponding to the value of F_{RT} can be interpolated from the P_r/Δ_r relationship of the top reinforcement. The rotation is then determined using the equation as given by Visintin et al. (2012a) which is

$$\theta = \tan^{-1}((\delta_b - \delta_t))/d') \quad \text{(Eq. 3.2)}$$

Where d' is the distance between the top and bottom reinforcements. This procedure is repeated for a reduced value of δ_b.

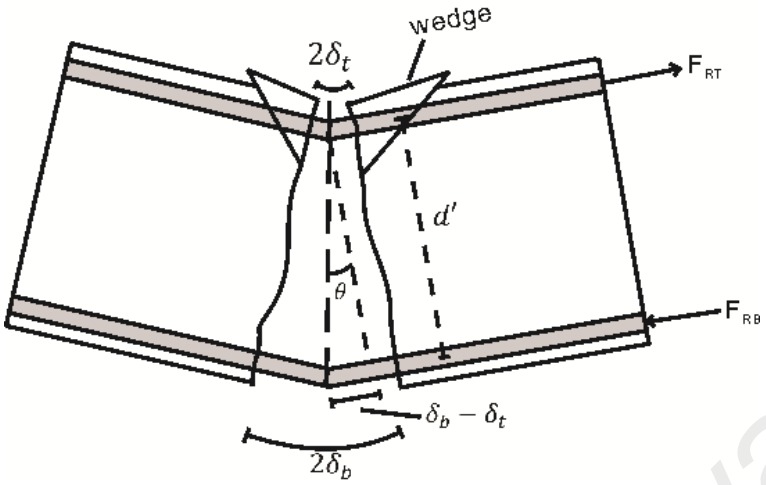

Figure 3.9: Full-Depth Crack on Beam Segment.

The full-depth crack state can be considered to be over once δ_b is reduced to zero, where the crack at the bottom region is now closed. Further application of reversed load in this state would result in the concrete at the bottom region of the beam becoming compressed and forming concrete wedge, while top reinforcement is in a tensile state with tension stiffening. Note that the location of compressed and tensile region are now reversed. This state continues until the applied load is reversed again, where the beam will again enter a full-depth crack and after returns to the normal loading condition as described in the monotonic loading section. It can therefore be seen that moment-rotation model of cyclically loaded beam involves switching between normal loading condition, full-depth crack and reversed loading condition. It should however be noted that in cases where the amount of top reinforcement is half of the bottom reinforcement the beam will not enter reversed loading condition as the top reinforcement would never have enough force to push the bottom reinforcement into the concrete. In this situation further increase in rotation is achieved by slip of top reinforcement, until load reversal.

Another aspect of cyclic loading that must be taken into account is the occurrence of multiple cracks within one wedge length. As concrete is compressed, concrete wedges will form at some point and will become larger as the rotation increases, and the length of wedge that form must be determined to check whether it passes through multiple cracks, as illustrated in Figure 3.10. To do this the depth of the wedge, d_w is first determined, which is simply the summation of each layer of concrete that has strain higher than ε_{mat} (refer Figure 3.6), determined using the size-dependent stress-strain relationship for concrete. The length of wedge, L_w is then calculated as $L_w = d_w \tan^{-1}\theta$, where θ is the natural angle of the wedge, and is usually considered to be 26° (Chen et al. 2014). If the length of wedge passes more than one crack, the entire length is considered to be a constant moment region and the total rotation is thus the summation of all the rotation of the cracks that the wedge passes. This multiple crack analysis was proposed by Visintin et al. (2012b), where it was validated against monotonically loaded specimens. Note that as illustrated in Figure 3.8 (a) and Figure 3.9, the size of wedge that formed will not decrease when beam is unloaded. Therefore if the wedge passes through multiple cracks during loading, then the multiple crack analysis must be used during the unloading phase as well.

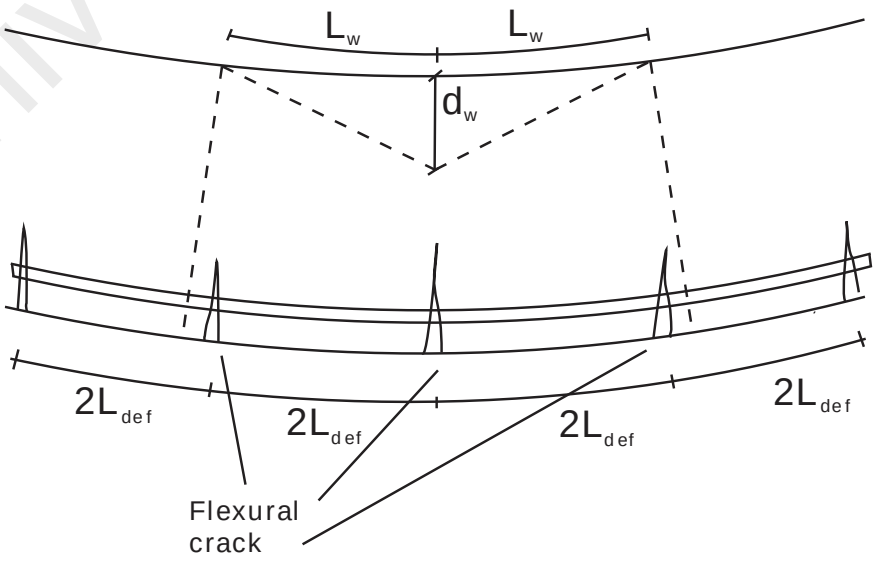

Figure 3.10: Wedge Passing Multiple Cracks.

3.3.2 Determining Moment-Rotation Relationship

While the process of applying the moment-rotation analysis is mostly the same, there are minor differences depending on the condition the beam is in during cyclic loading. From section 3.3.1, it can be concluded that there are four types of beam condition that causes changes in the results:

i. Beam condition prior to cracking.
ii. Beam after flexural cracking.
iii. Beam experiencing full depth crack.
iv. Beam having a reversed load applied.

The procedure for generating the moment-rotation during all four beam condition beam condition is generally the same with some minor changes. Prior to cracking, the load acting on the steel reinforcements is to be determined from the strain caused by the hinge rotation, θ as the reinforcement is in full interaction with the surrounding concrete.

When the beam experiences flexural cracking, force acting on the reinforcement is determined from the load-slip relationship generated using the partial-interaction model. Note that the analysis of the beam during unloading is the same as this analysis, with the only change being the load-slip relationship used is now from an unloading analysis.

In full depth crack the requirement of using load-slip to determine the force acting on the reinforcement is also applied to both the tensile and compression bar. In reversed load condition, the crack in the former tensile region of the beam is closed, and load-slip relationship is used on only the former compression bar (now under tension).

The procedure for generating the moment-rotation is as shown below, with the analysis done using Matlab. Pseudo code flowchart (Figure 3.11) and illustration (Figure 3.12) of the model are also provided.

1. A small value of rotation, θ if fixed at the loaded end. The depth of neutral axis from top fibre, d_c is assumed to be at the middle of the beam.
2. The deformation at top and bottom fibre are determined.
3. The beam is then divided into 0.1mm slices and deformation at each slice is then interpolated using the known value of top deformation, bottom deformation, depth of neutral axis and assuming a linear deformation profile.
4. The strains experienced by each slice are determined.
5. The stresses and forces acting on the segments are determined from the calculated strain values by using any appropriate material models for steel and concrete. If the concrete strain ε_t exceeds the concrete cracking strain, the force acting on the steel reinforcement is determined from the load-slip relationship generated using the partial-interaction tension stiffening model.
6. The procedure is repeated with different location of neutral axis until the total summation of forces acting on the beam is less than 100N (or any suitable tolerance value).
7. Once equilibrium (or until a very low value of summed force, such as F_{sum}<100N) is achieved, the resulting moment is calculated and another value of rotation is fixed, and the procedure is repeated until any value of rotation (θ) to obtain a moment-rotation relationship.

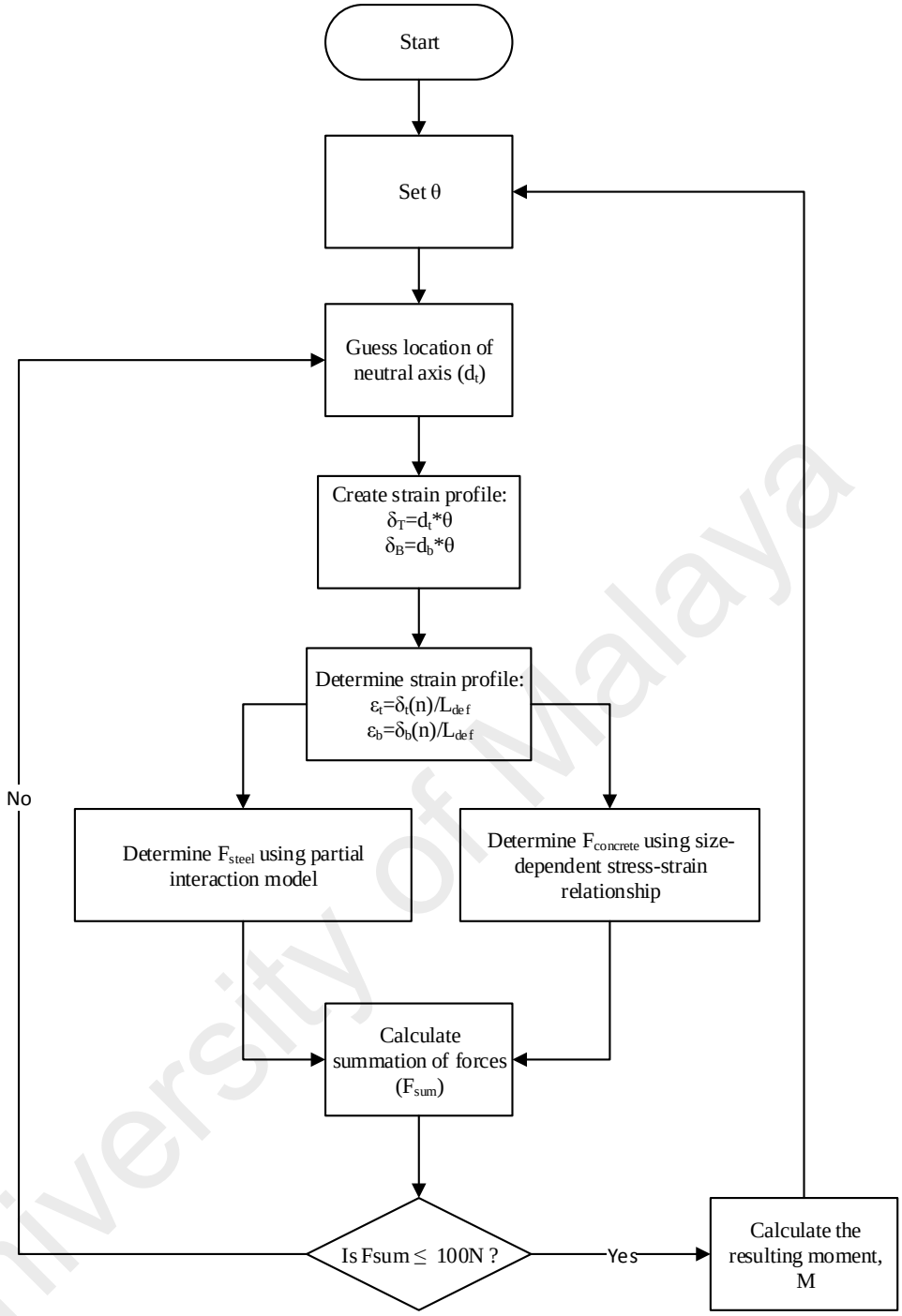

Figure 3.11: Moment-rotation model procedure.

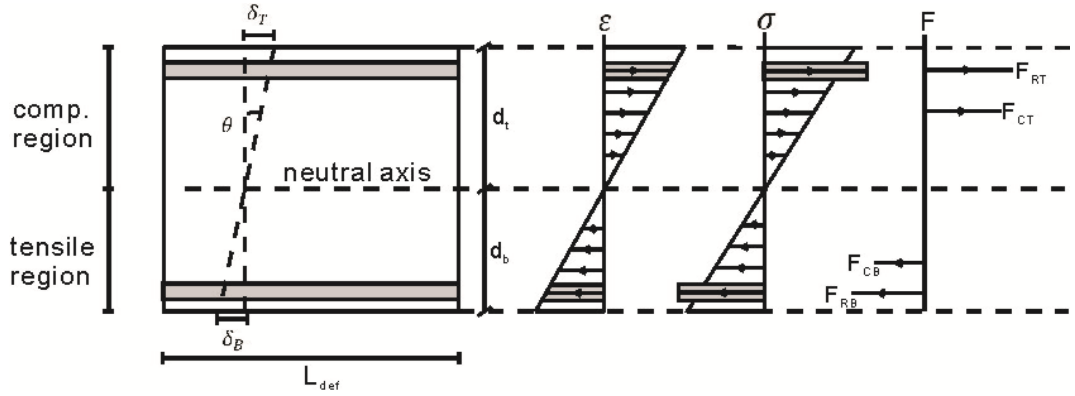

Figure 3.12: Analysis Prior To Cracking.

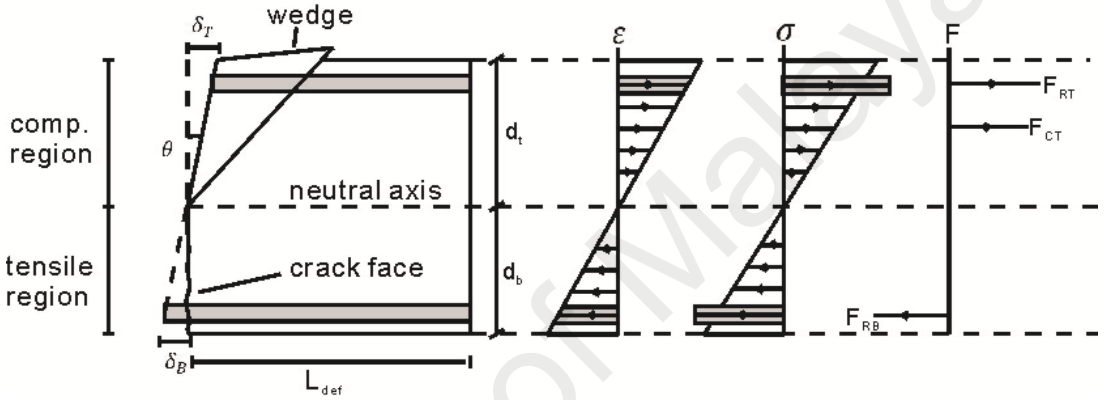

Figure 3.13: Analysis with Cracked Concrete.

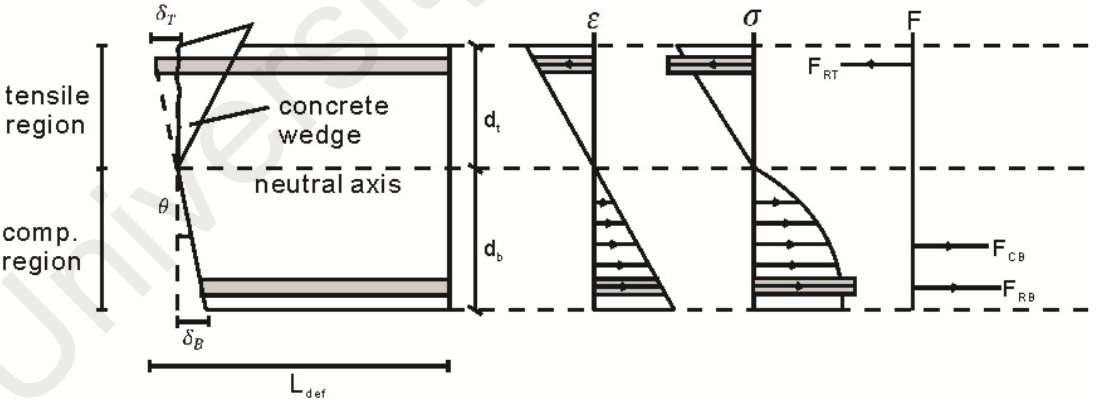

Figure 3.14: Analysis with Reversed Load.

3.4 Validation of Proposed Moment-Rotation Model

Although it is usually more prudent to validate the proposed cyclic moment-rotation analysis against experimental results done by author, University of Malaya unfortunately lacks the necessary equipment to do the testing. As such the model described previously was validated against several experimental results from published works of other researchers. Also note that the current moment-rotation model cannot capture the effect of shear, thus the experimental results presented are only beam specimens that fails by flexural deformation while tested under cyclic load. Due to lack of available published experimental result that is free of shear effect, only four comparisons can be provided in this study, and it should be noted that shear is still present in these four beams.

Note however that as the published data does not provide moment-rotation results, the beams were assumed to form a single hinge at the support during cyclic loading, and then the published load-deflection results were converted to moment-rotation based on this assumption. Thus the compared moment-rotation is for rotation at the support section of the cantilever beams. Any major difference in simulated and experimental moment-rotation curves is therefore attributed to the fact that there were more than one hinge forming during the cyclic test, thus converting the experimental load-deflection to moment-rotation based on the assumption of single hinge forming caused some regrettable error that the author apologizes for.

The specimens are cantilever reinforced concrete beams, with properties as shown below. The specimens with code BJ are specimens from the published results of Brown and Jirsa (1971), while specimens with code MA are specimens from the published results of Ma et al. (1976).

A summary of the beam specimen is given in Table 3.1. The beams are all cantilever beams, to allow the beams to be tested under reversed cyclic loading. Steel reinforcement

is provided at the top and bottom of the beams. Table 3.2 shows the material properties of the beams. The beam section details are given in Figure 3.15 and Figure 3.16 for MA and BJ specimens respectively. Finally, the published load-deflection results of each beam are given in Figure 3.17, Figure 3.18, Figure 3.19 and Figure 3.20.

Table 3.1: Summary of beam specimen (Brown and Jirsa, 1971 and Ma et al., 1976).

Reference	**MA1**	**MA2**	**BJ1**	**BJ2**
Type	Cantilever beam	Cantilever beam	Cantilever beam	Cantilever beam
Beam dimension (mm)	229 x 407	229 x 407	254 x 457	254 x 457
Beam length (mm)	1587.5	1587.5	1520	1520
Amount of tensile bar	4	4	2	2
Amount of compression bar	3	3	2	2
Size of tensile bar (mm)	19.05	19.05	25.4	25.4
Size of compression bar (mm)	15.88	15.88	25.4	25.4

Table 3.2: Material properties (Brown and Jirsa, 1971 and Ma et al., 1976).

Beam	**MA1**	**MA2**	**BJ1**	**BJ2**
Concrete strength (MPa)	34.96	30.2	33.09	33.09
Concrete elastic modulus (MPa)	28282	26269	27036	27036
Steel reinforcement yield strength (MPa)	451.61	451.61	317.16	317.16

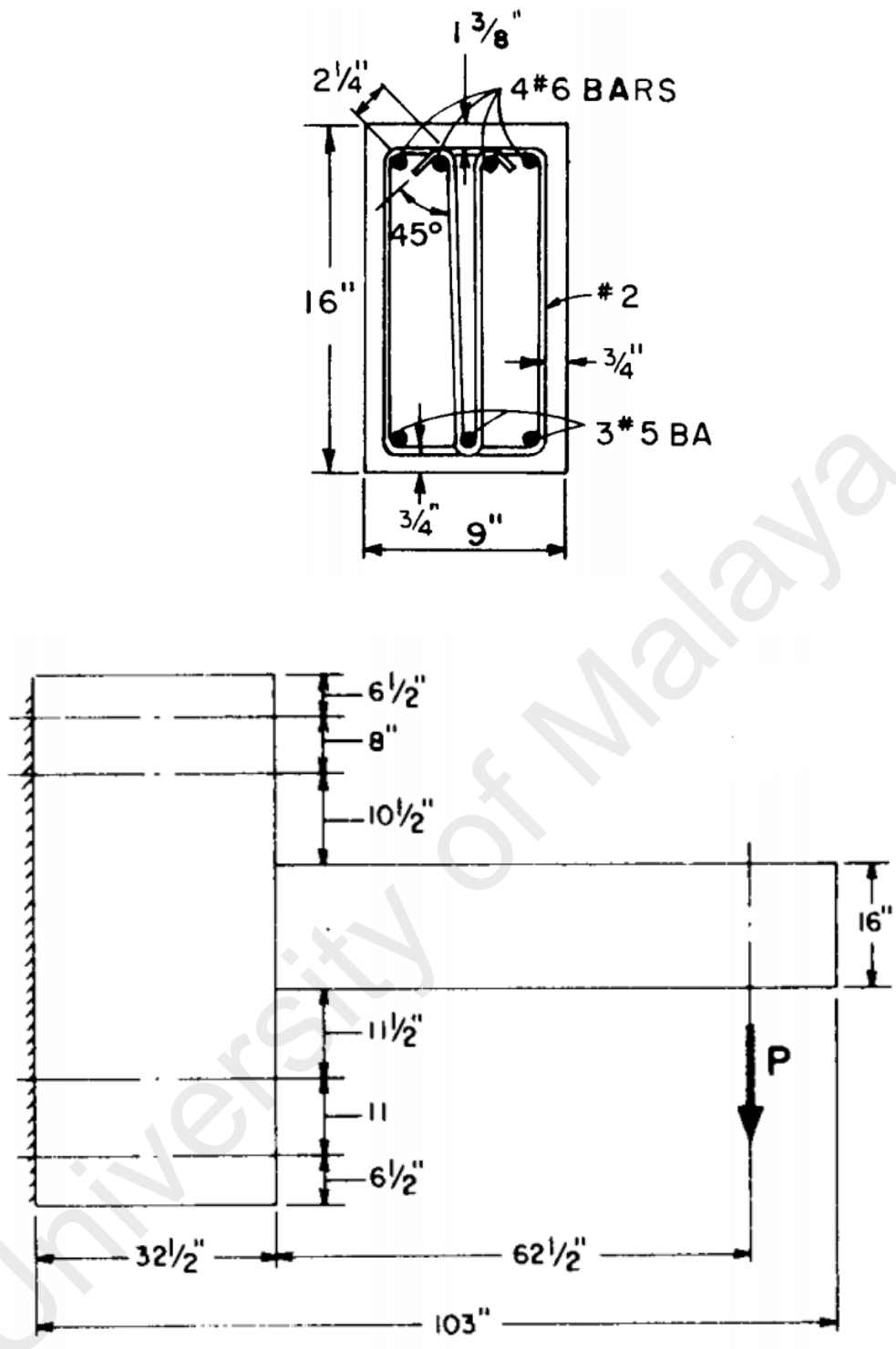

Figure 3.15: Beam Details for MA1 and MA2 (Ma et al., 1976).

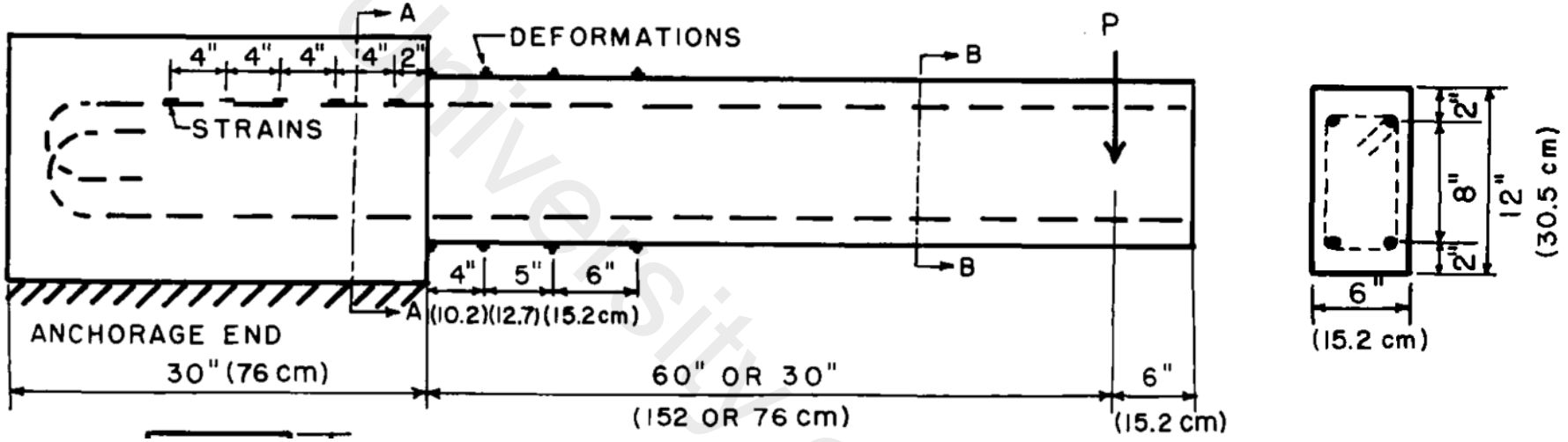

Figure 3.16: Beam Details for BJ1 and BJ2 (Brown and Jirsa 1971).

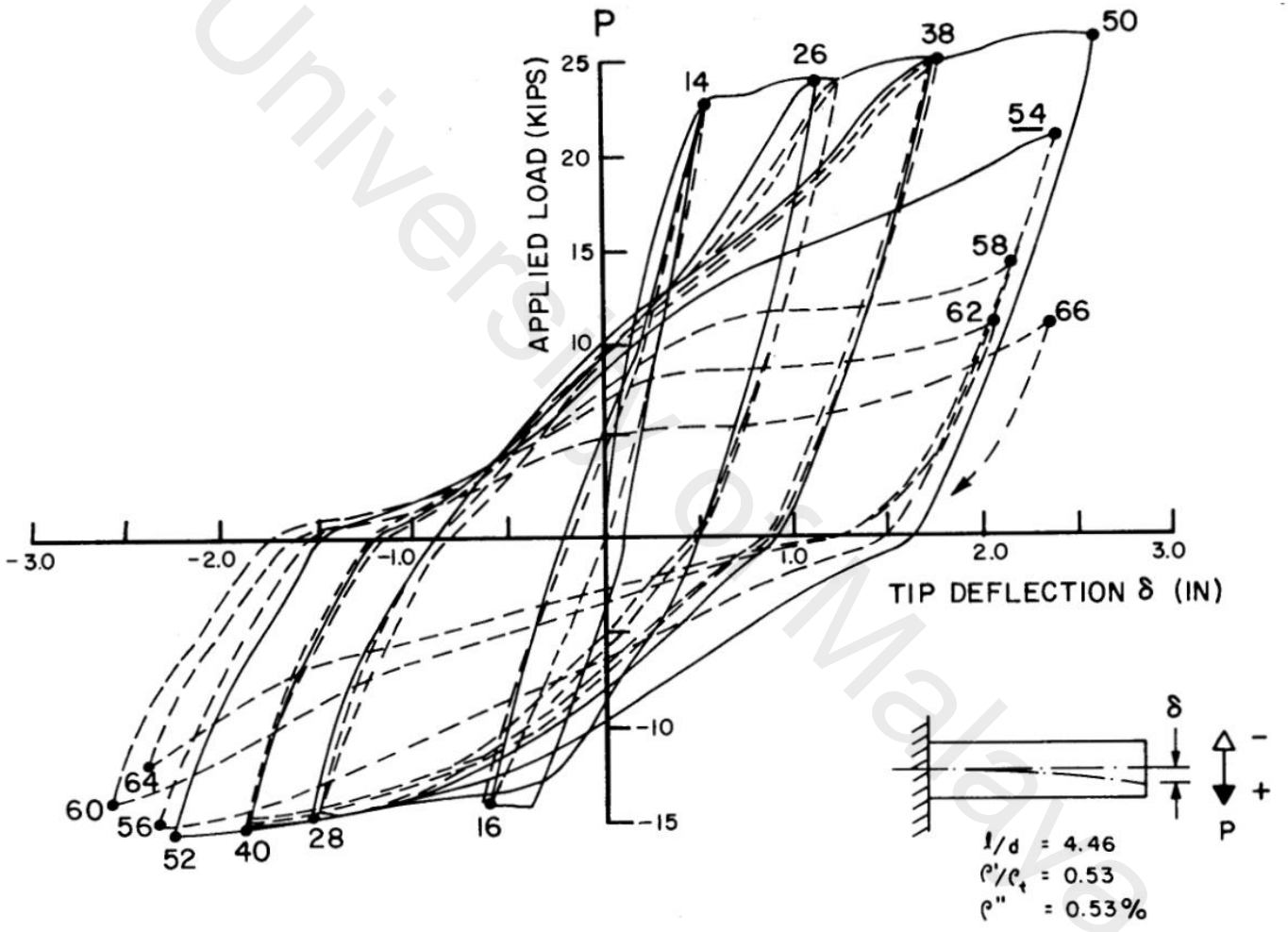

Figure 3.17: Load-Deflection Results for Beam MA1 (Ma et al., 1976).

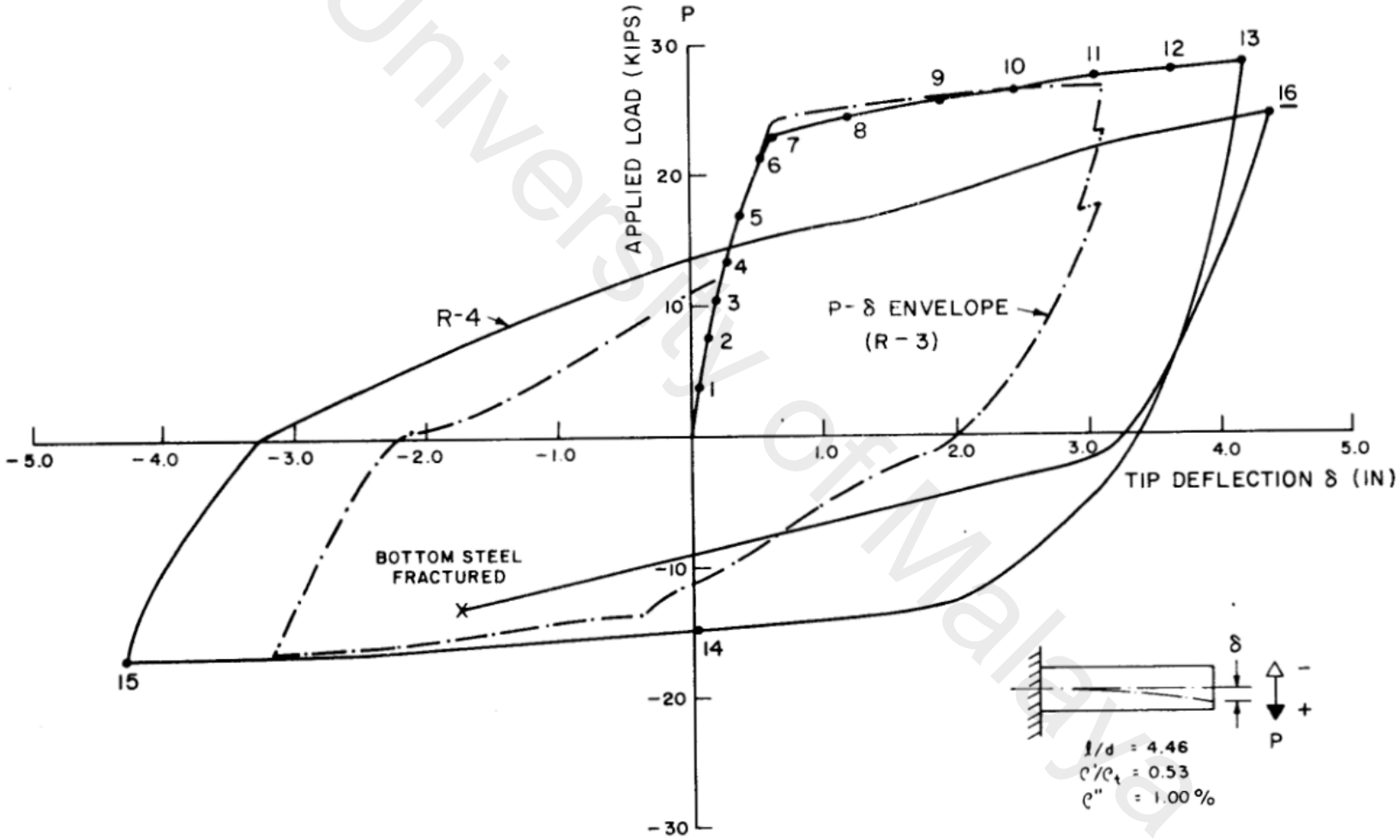

Figure 3.18: Load-Deflection Results for Beam MA2 (Ma et al., 1976)

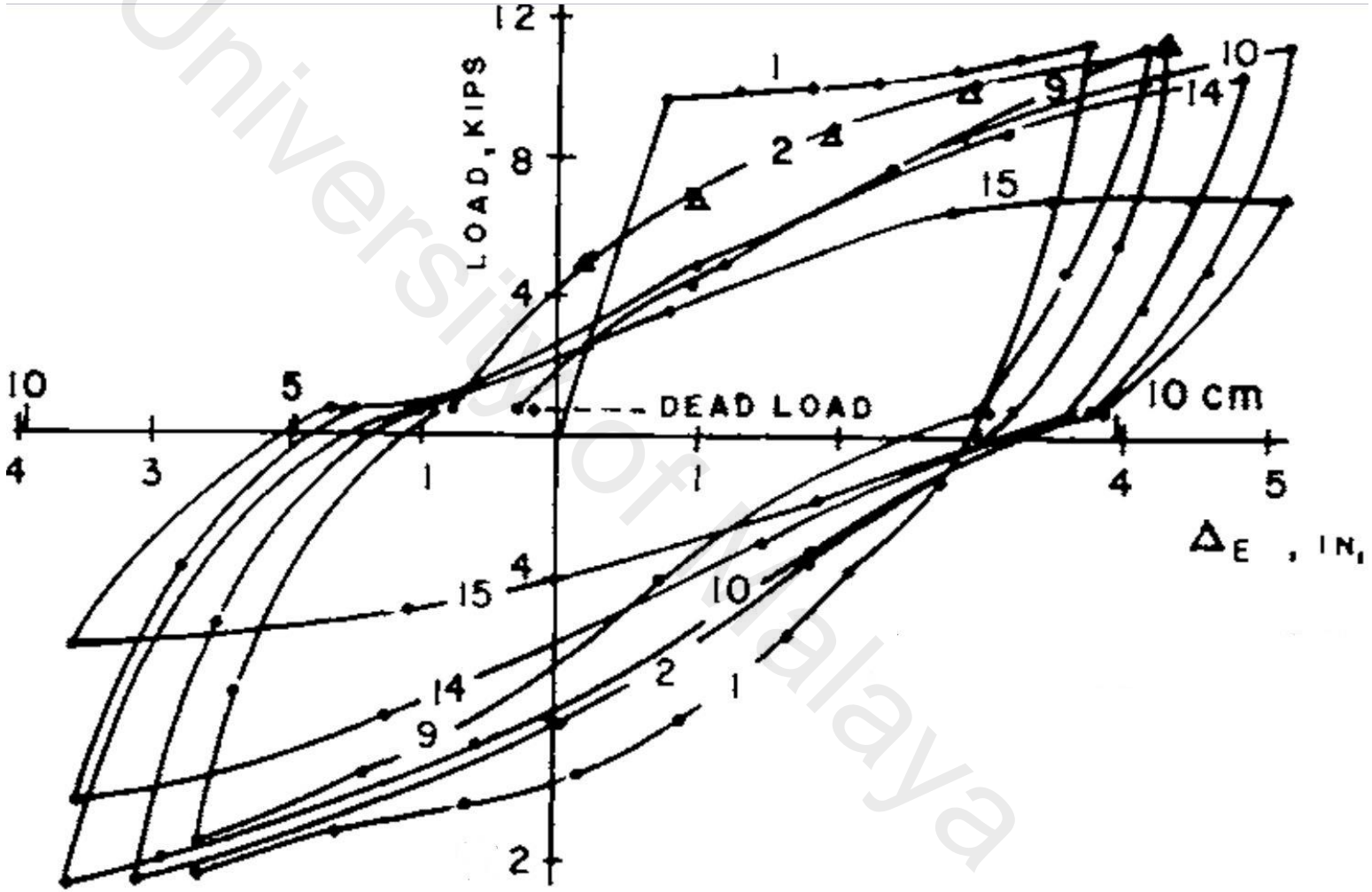

Figure 3.19: Load-Deflection Results for Beam BJ1 (Brown and Jirsa, 1971)

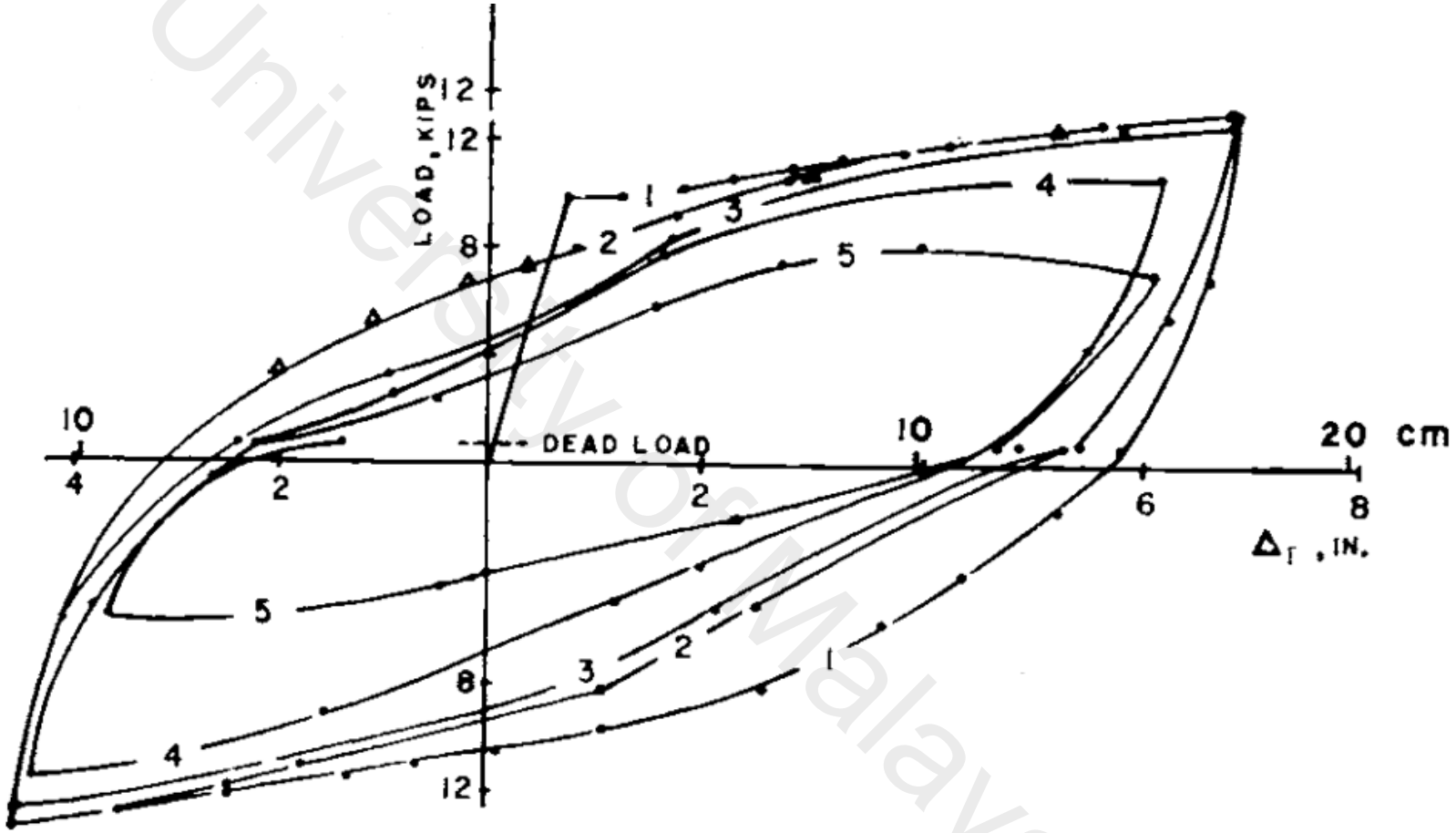

Figure 3.20: Load-Deflection Results for Beam BJ2 (Brown and Jirsa, 1971)

As mentioned previously, the moment-rotation of the beams were obtained through the assumption of single hinge forming at the support of the cantilever beams. The process of converting the load-deflection to moment-rotation was done using Matlab, with the process as shown below:

1. Obtain the loads and deflections of the beams and save each as Matlab data file.
2. Based on the values of load, determine the moment acting on the beams:

   $$Moment = Load \times Beam\ length \quad \text{(Eq. 3.3)}$$

3. Determine the rotation:

   $$\theta = \tan^{-1}\left(\frac{Deflection}{Beam\ length}\right) \quad \text{(Eq. 3.4)}$$

It should be noted that the process is relatively simple and does not really need Matlab as the operations can also be done in an Excel sheet. The obtained moment-rotation results are as shown in Figure 3.21, Figure 3.22, Figure 3.23 and Figure 3.24. Comparison of simulated and experimental moment-rotation will be given in section 4.1 of chapter 4, along with discussions on the result.

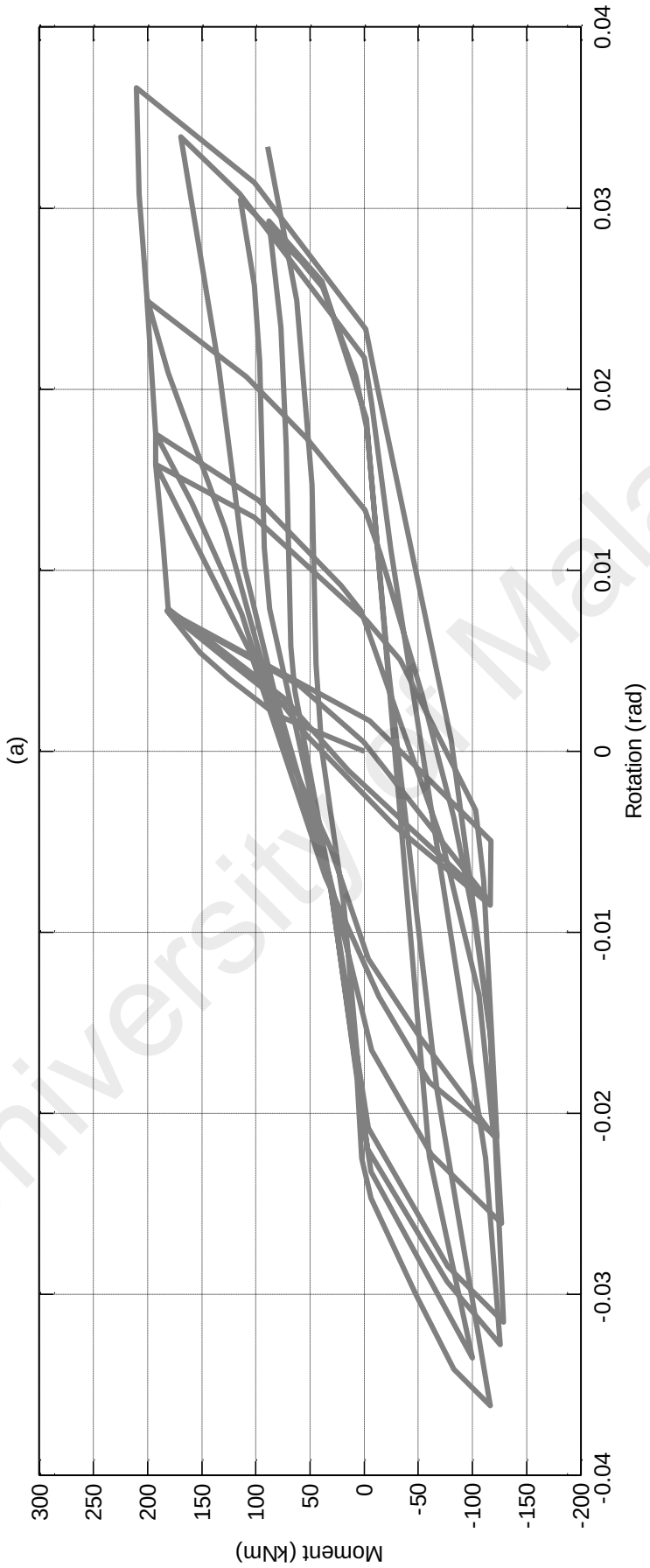

Figure 3.21: Moment-Rotation of Beam MA1.

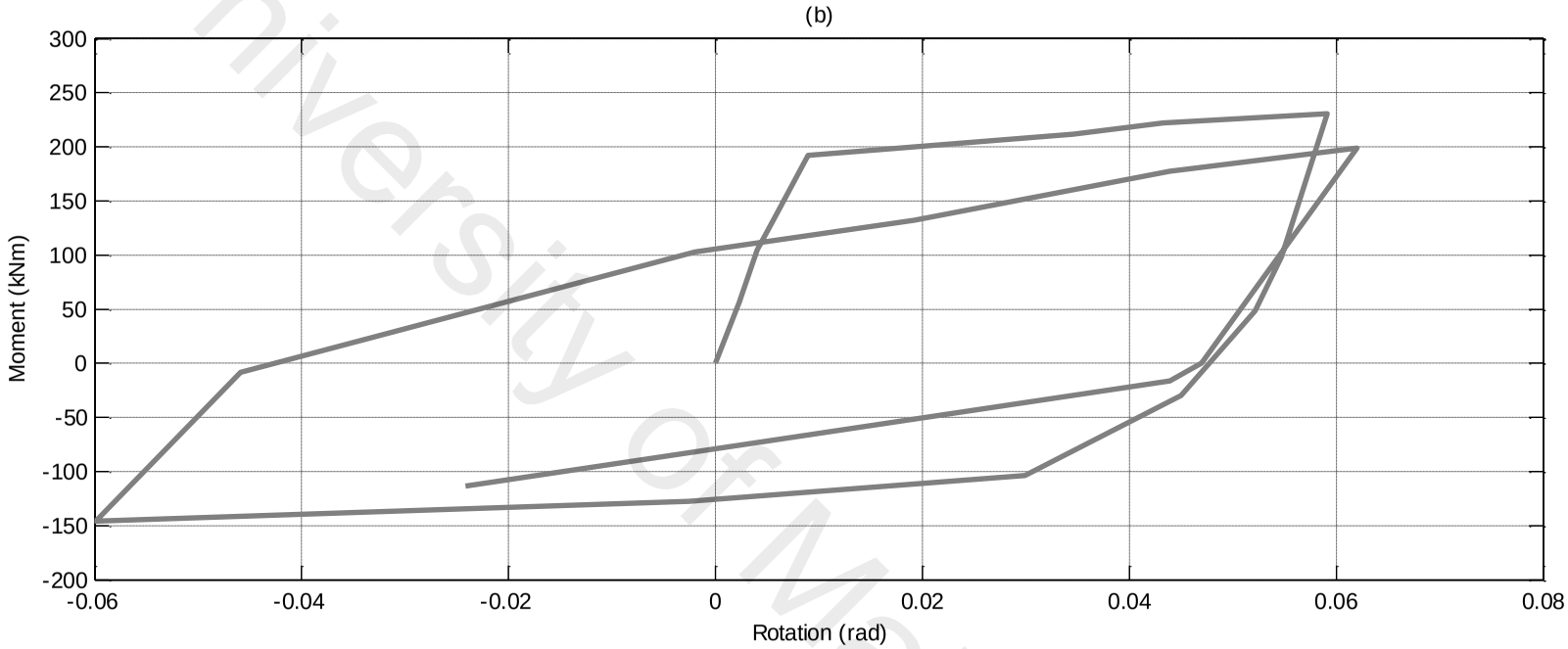

Figure 3.22: Moment-Rotation of Beam MA2.

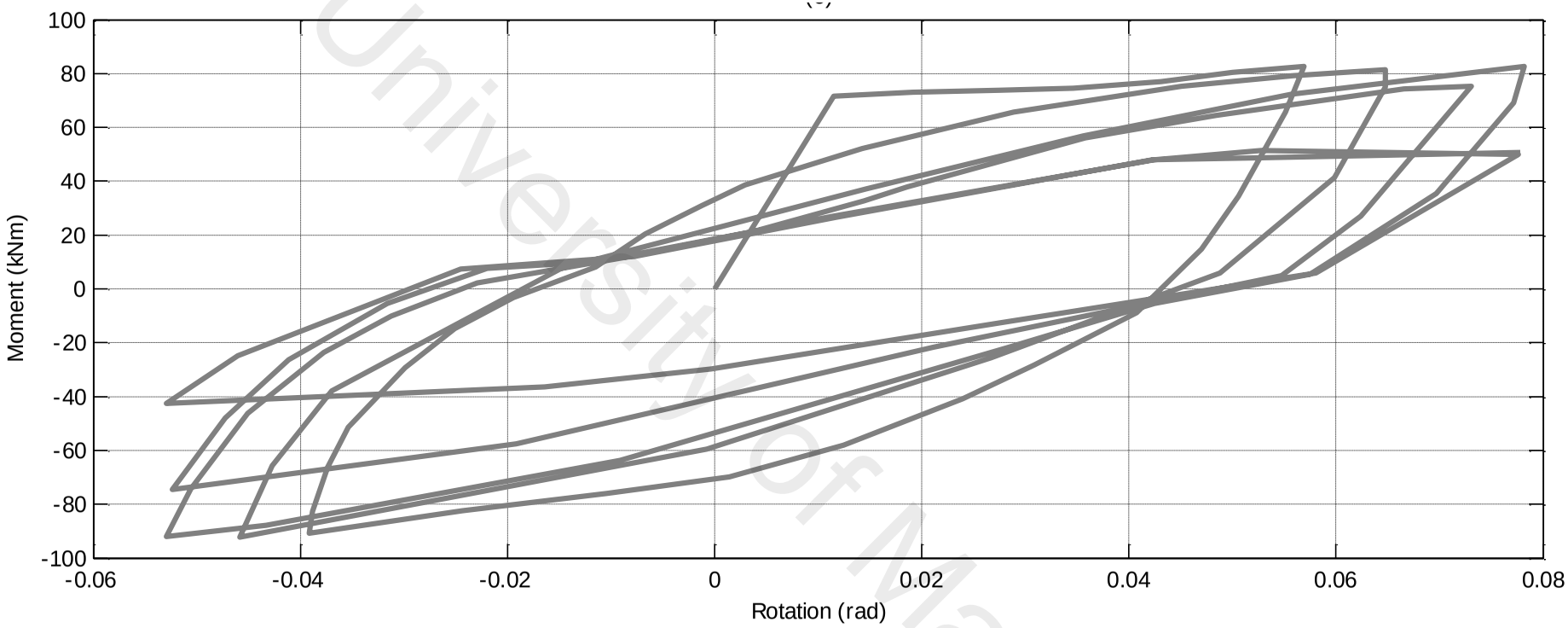

Figure 3.23: Moment-Rotation of Beam BJ1.

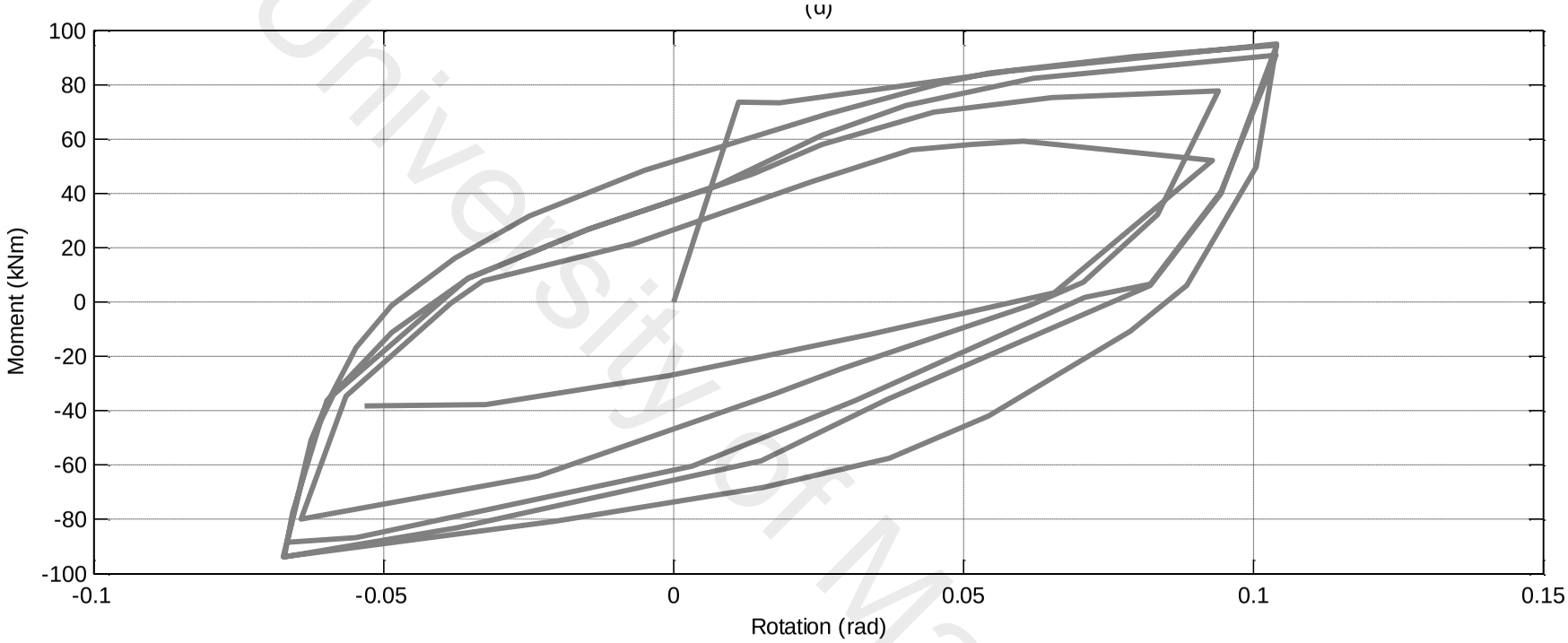

Figure 3.24: Moment-Rotation of Beam BJ2.

CHAPTER 4: RESULTS AND DISCUSSION

4.1 Comparison of Experimental and Simulated Moment-Rotation

The comparison between the experimental and simulated moment-rotation results will be presented first prior to discussion of other simulated results, as this will act as a validation of the proposed moment-rotation model. The comparisons are as presented in Figure 4.1, Figure 4.2, Figure 4.3 and Figure 4.4. In general all the graphs show good accuracy in terms of predicting peak values during cyclic load. However the simulated results do show a decrease in accuracy as rotation increases, as can be seen in Figure 4.1 and Figure 4.3. The accuracy of the simulated curve is also found to be a lot higher when the rotation is already large to begin with, as can be seen in Figure 4.2 and Figure 4.4.

The difference between simulated and experimental results is also found to be more pronounced during full-depth crack. As the steel reinforcement behaviour is dominant at that stage of cyclic loading, this may point to inaccuracies in the steel stress-strain as a bilinear model was used in order to simplify the partial-interaction tension stiffening mechanism and save time.

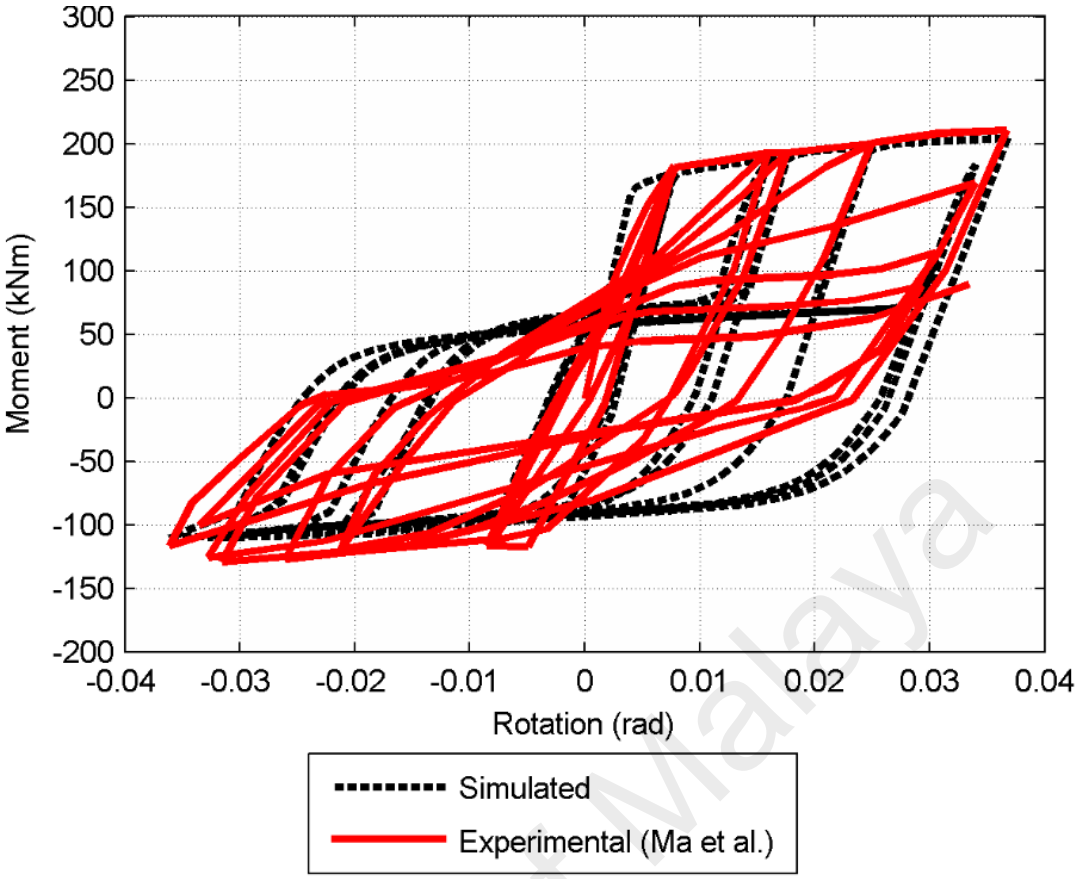

Figure 4.1: Comparison of Simulated and Experimental Curves for Beam MA1.

The simulated moment-rotation of beam MA1 in Figure 4.1 manages to predict the maximum and minimum moments with acceptable accuracy, with average accuracy of -3.43% for the maximum moments and an average accuracy of -12.71% for the minimum moments. The simulated curve follows the shape of the experimental curve well for the first five cycles, but at higher cycles the simulated curve tends to give a higher moment values during full-depth cracks. This is attributed to the slight presence of shear during the experimental testing. Shear effect in cyclically loaded RC connection is characterised by reduction of strength during full-depth crack, resulting in a pinching of the curve towards the origin.

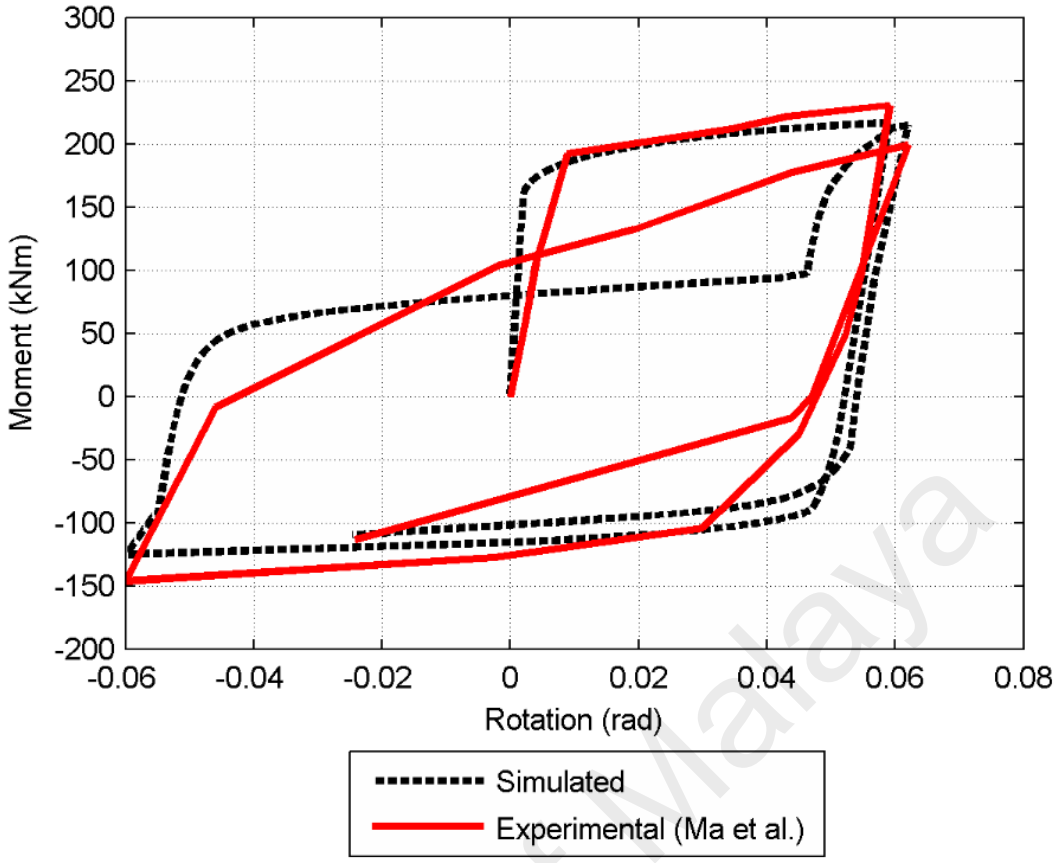

Figure 4.2: Comparison of Simulated and Experimental Curves for Beam MA2.

The moment-rotation response of beam MA2 in Figure 4.2 involves only two large cycles. The simulated maximum moments have an average accuracy of 1.51% while the minimum moments have an average accuracy of -8.16%. It can be seen from the figure that the simulated curve shows a sharp increase in moment during crack closing at the second cycle, as currently the cyclic moment-rotation approach presented in this research have a sudden change between full-depth crack and crack closing. However, as more understanding of the mechanics behind crack opening and closing is achieved it is believed that one day this problem can be solved.

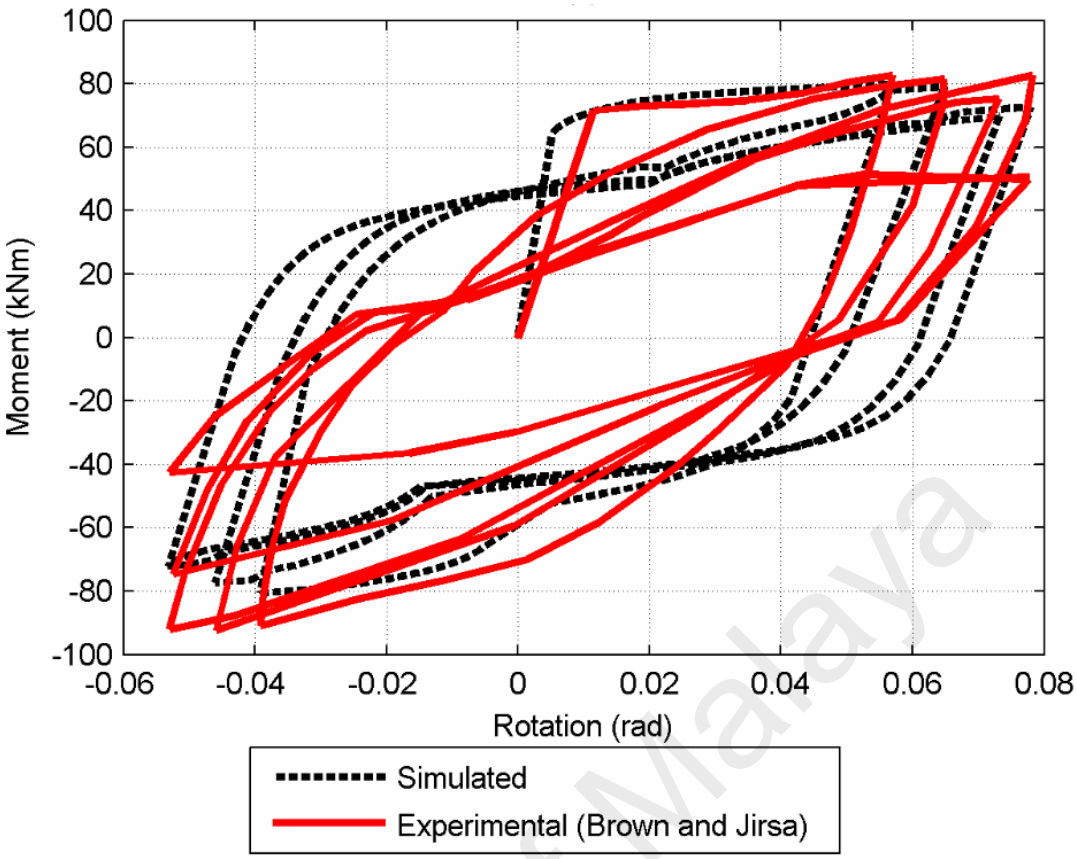

Figure 4.3: Comparison of Simulated and Experimental Curves for Beam BJ1.

The simulated response of beam BJ1 in Figure 4.3 shows the same problem as beam MA1, where the accuracy of the full-depth crack condition is greatly reduced at higher cycles of load. Again it is believed to be the effect of shear causing some pinching towards the origin. The maximum moments are predicted decently with average accuracy of -7.23%, while the minimum moments have an average accuracy of -16.55%. Transition between full-depth crack to crack closing is less pronounced here compared to beam MA1 and MA2. This is due to beam BJ1 having the same amount of tensile and compression reinforcement.

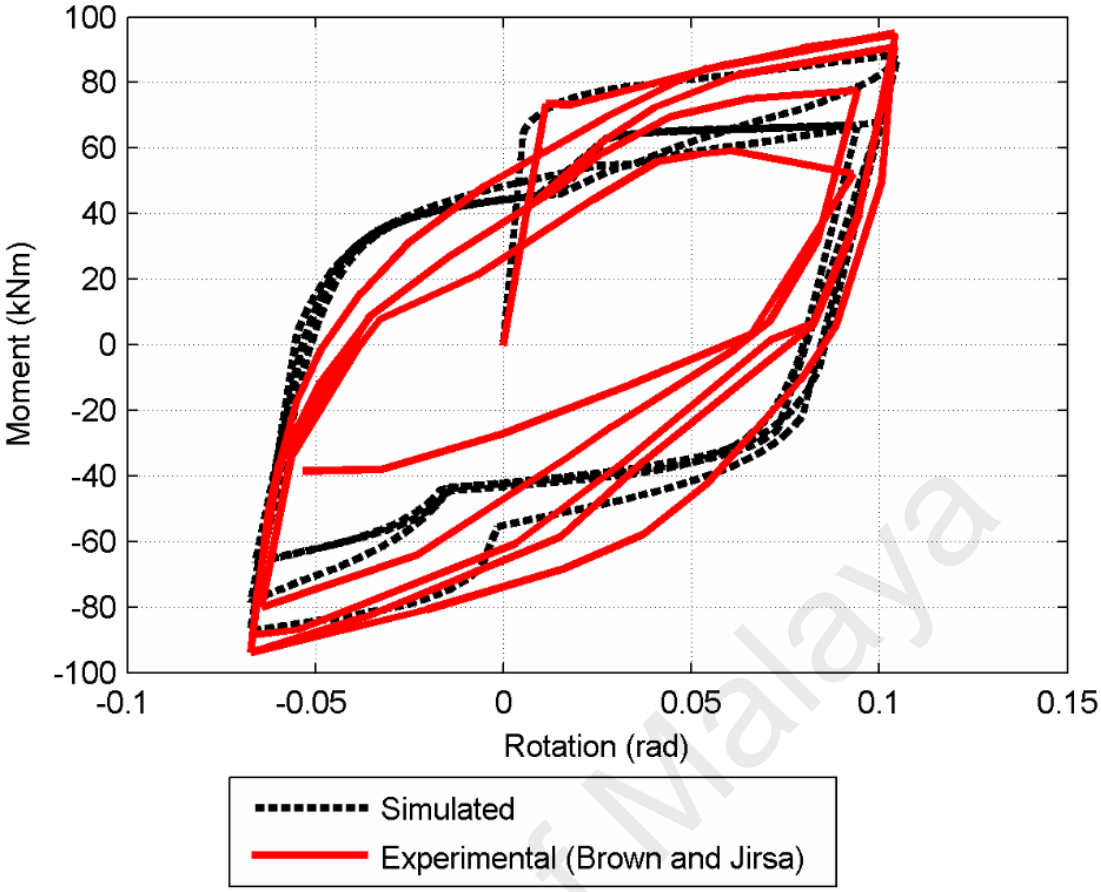

Figure 4.4: Comparison of Simulated and Experimental Curves for Beam BJ2.

The simulated response of beam BJ2 in Figure 4.4 shows good agreement with the experimental curve. Again transition between full-depth crack and crack closing is less pronounced here, due to the amount of tensile and compressive reinforcements being identical. The maximum and minimum moments were predicted with acceptable accuracy, with an average accuracy of 6.11% for the maximum moments and an average accuracy of -5.83% for the minimum moments.

Based on the four comparisons made, it can be seen that the moment-rotation approach tends to give a conservative estimate of RC beam strength, with nearly all of the predicted maximum and minimum moments being less than the actual maximum and minimum moments.

4.2 Observation on Cyclic Tension Stiffening Behaviour between Flexural Cracks

As the model has been validated, the simulated results can be used to further understand the behaviour of reinforced concrete beam under cyclic loading. This research will focus on the studying the tension stiffening behaviour within beam regions located between flexural cracks, when under cyclic load. There is a lack of discussion on cyclic tension stiffening behaviour in the literature, likely due to the difficulty in conducting a pull-out test under cyclic condition. Cyclic tension stiffening behaviour has also not been studied using finite element method. While the author is unsure of the reason, it may be that simulation of tension stiffening in finite element relies mostly on empirical method, which means it cannot be used to study the cyclic tension stiffening behaviour reliably. As the mechanic based model used in this research does not rely on empirical method, its cyclic tension stiffening results is more easily attained compared to experimental study and more reliable than current finite element methods.

Based on the validated simulation results, the cyclic tension stiffening behaviour can be divided into several distinct phases:

i. Initial loading (along O-A-B in Figure 4.5).
ii. Unloading phase I (along B-C).
iii. Unloading phase II (along C-D).
iv. Reloading phase (along D-E).

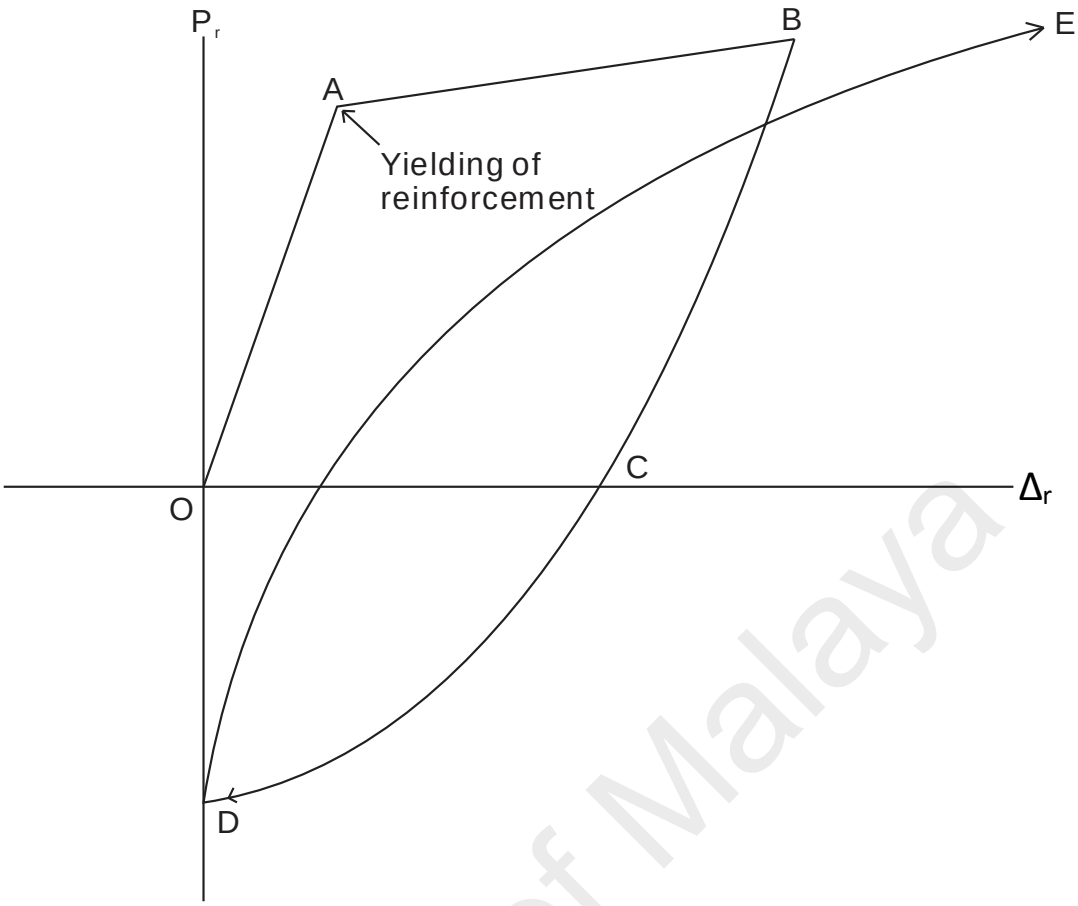

Figure 4.5: Cyclic load-slip relationship.

4.2.1 Initial loading phase

Figure 4.5 shows the general shape of the load-slip relationship with tension stiffening during cyclic loading. At initial loading along path OAB in Figure 4.6 (a), load reversals has yet to take place. The material properties and relationships of the beam during this stage is the same as a monotonically loaded beam, where the bond stress-slip relationship is as defined by path O'ABCD in Figure 2.11.

Upon unloading from point B in Figure 4.5, the load-slip relationship is strongly dependent on the load history of the local bond stress-slip properties as well as the stress-strain relationship of the reinforcement. This dependency is a result of the inconsistencies in the signs of the bond stress-slip and stress-strain relationships which arise due to cyclic

loading, where it is possible to have an increase in shear stress associated with a reduction in slip, that is, the negative friction branch (line FG) as illustrated in Figure 2.11.

Moreover, it is possible for reinforcement to develop a compressive stress with an extending strain, for example along path CD in the second quadrant of Figure 4.6. Due to this, to show the influence of the cyclic bond stress-slip and stress-strain material properties, it is thought to be appropriate to discuss the mechanics of tension stiffening during unloading in two distinct phases, namely the Unloading Phase I and Unloading Phase II, as defined by the reinforcement stress-strain behaviour.

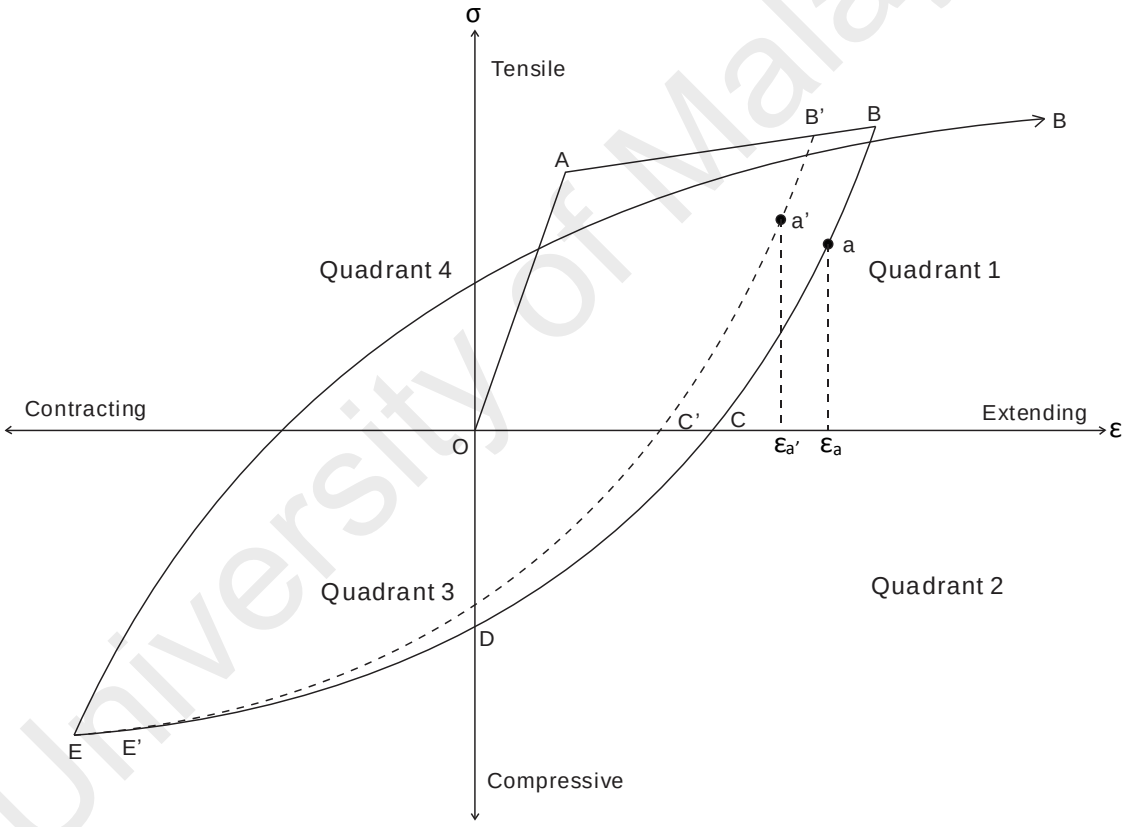

Figure 4.6: Cyclic stress strain relationship of reinforcing steel.

4.2.2 Unloading phase I

The first phase of unloading takes place along path BC in Figure 4.5, and is characterised by a reduction in the slip of the reinforcement bar at the crack face

corresponding to a reduction in the applied tensile load. The response of the bar can be divided into two distinct zones (Zone 1 and Zone 2), as shown in Figure 4.7 (a).

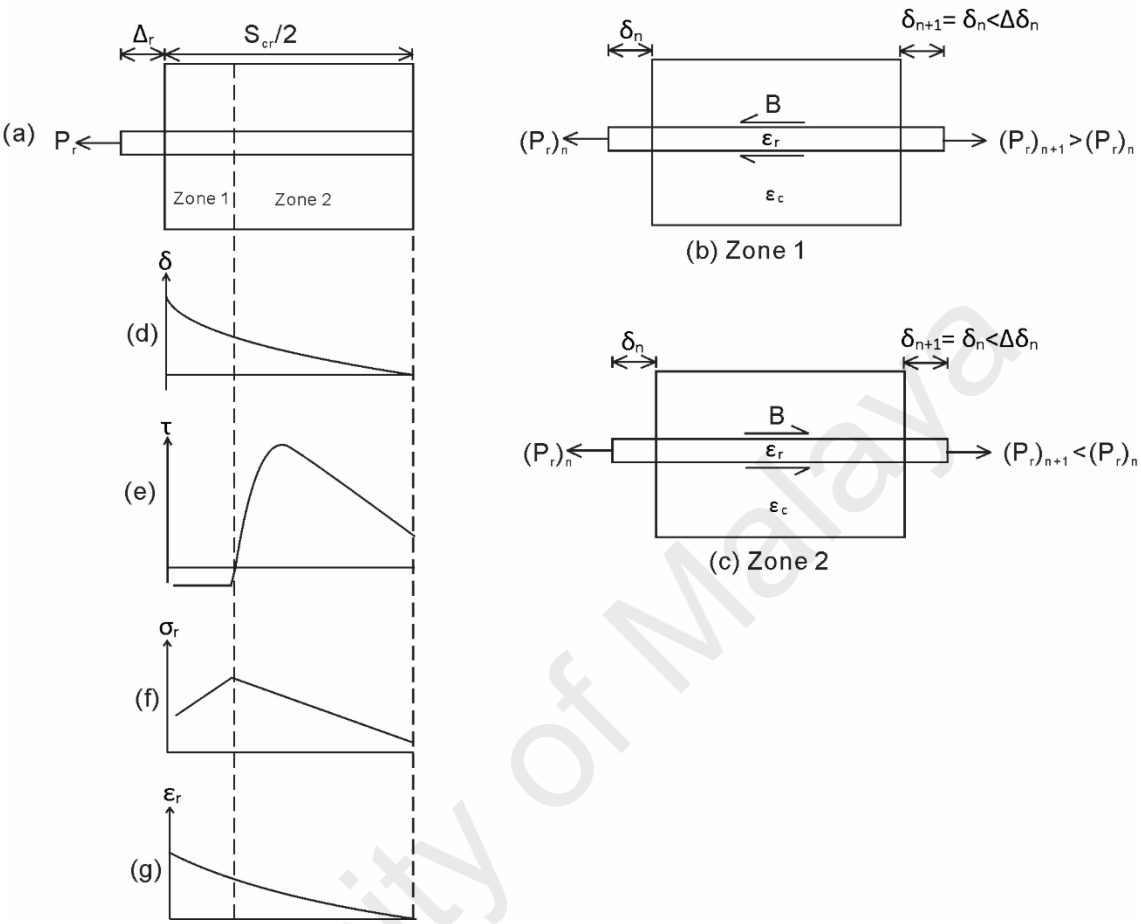

Figure 4.7: Tension stiffening during unloading phase I.

Consider an element from Zone 1 in Figure 4.7 (a) shown in Figure 4.7 (b). The bar is subjected to a tensile load, but with a force which is reduced from that experienced during initial loading. Assuming the bar had previously yielded so that unloading takes place along branch BC in Figure 4.5, a tensile load occurs with an extending strain. The reduction in slip in Zone 1 of Figure 4.7 (d) is such that the bond stress in Figure 4.7 (e) is located on the friction branch FG, in the second quadrant in Figure 2.11. Thus from equilibrium across the element in Figure 4.7 (b), the bond force acts to increase the load in the bar from the left hand side to the right hand side and, therefore, the stress in the bar in Figure 4.7 (f) increases in Zone 1. Although an increase in reinforcement stress occurs, the reinforcement strain as shown in Figure 4.7 (g) reduces. This behaviour occurs as each

element of length dx in the partial interaction prism in Figure 4.7(b) is assigned a different stress strain relationship, which degrades according to the cyclic properties of the reinforcement in Figure 4.6, which as illustrated depends on its individual load history. For example, consider an increase in stress between 2 elements in zone 1 where the stress-strain relationship of the first element is defined by curve B-C in Figure 4.6 and for the second element by B'C'. It can be seen in Figure 4.6 that increasing the stress from *a* on path B-C to *a'* on path B'C' results in a reduction in strain. Importantly, as the strain in the reinforcement is an extending strain, the slip strain $d\delta/dx=\varepsilon_r-\varepsilon_c$ is an extending strain and therefore the change in slip across the element $\delta\Delta=(d\delta/dx)dx$ results in a reduction in slip.

The behaviour characterised in Zone 1 in Figure 4.7 by an increasing bar stress but a reducing bar slip continues until the bond stress is no longer in Quadrant 2 of Figure 2.11. This may occur either if the change in slip of an element is small enough such that path F'E in Figure 2.11 is followed, or, if the slip at a given element is greater than that achieved during previous loading, in which case path F'OPQ in Figure 2.11 is followed. The transition from Zone 1 to Zone 2 which occurs when the bond stress in Figure 4.7 (e) changes sign can be seen by a reversal of the direction of the bond force B when comparing Figure 4.7 (b) and Figure 4.7 (c). Elements in Zone 2, such as that shown in Fig. 4.7 (c) are characterised by the bar being pulled with a tensile force and an extending strain and the bond stress resisting the pulling out of the bar such that across each element the bar force reduces.

4.2.3 Unloading phase II

The second phase of unloading, that is, along branch CD in Figure 4.5 is characterised by the requirement that the bar be pushed in order to further reduce the slip. In this phase, the response of the bar is again divided into two distinct zones (Zone 3 and Zone 4) as in Figure 4.8.

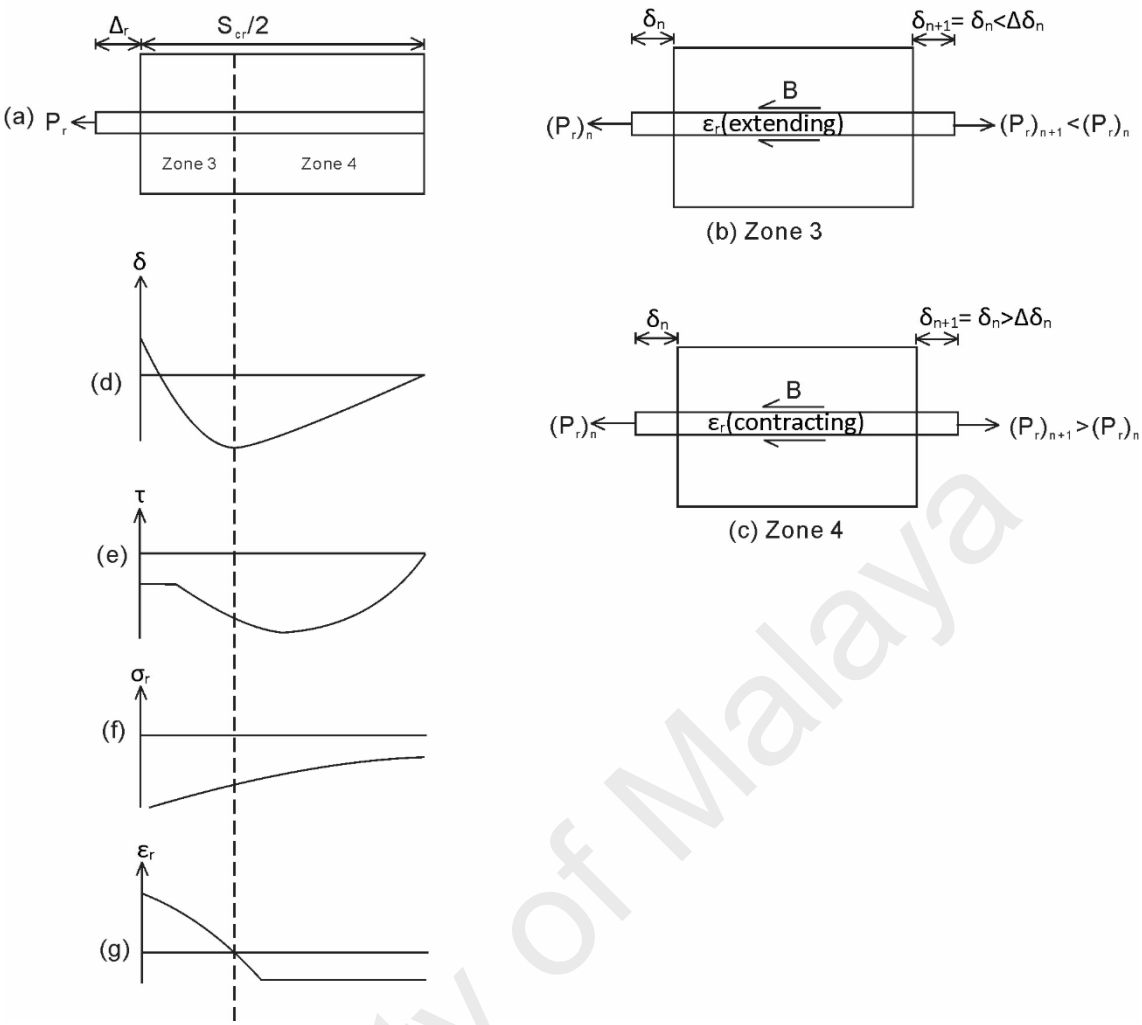

Figure 4.8: Tension stiffening prism during unloading phase II.

An element from Zone 3 in Figure 4.8 (a) is shown in Figure 4.8 (b). In this zone, the bar is subjected to a compressive load and due to strain hardening an extending strain, that is, the stress-strain behaviour of the element is described by the second quadrant of the reinforcement stress-strain relationship in Fig. 4.6.

Similar to phase I of unloading, in Zone 3 in Figure 4.8 (b) the reduction in slip due to unloading causes the bond stress to lie in the second or third quadrant of the τ/δ relationship in Figure 2.11. However in Zone 3 as shown in Figure 4.8 (b), equilibrium of the forces over the elements causes a reduction in the bar force and therefore stress in Figure 4.8 (f). Importantly, as reinforcement has previously strain hardened, in Zone 3 the compressive stress is associated with an extending strain and thus the slip reduces

along each element as described for Zone 1. The reduction in slip shown in Figure 4.8(d) continues until the end of the strain hardening region, that is, at the point where a compressive stress is now associated with a contracting strain.

An element from Zone 4 is shown in Figure 4.8(c). The element is subjected to a compressive stress, a contracting strain and a bond stress in the second or third quadrant of Figure 2.11. By equilibrium in Figure 4.8(c), the bond force acts to reduce the bar force and therefore stress in the reinforcement towards zero. Moreover, in Zone 4, as the strain in the reinforcement is a contracting strain the slip strain $d\delta/dx = \varepsilon_r - \varepsilon_c$ has a contracting sense and therefore acts over an element length dx to increase the slip $\Delta\delta = (d\delta/dx)dx$ towards zero. As shown in Figure 4.8(d), this leads to convergence on the boundary condition that the slip is zero at $S_{cr}/2$.

It should also be noted here that the reversal of slips in Zones 3 and 4 may result in the bar being pushed locally to a slip not previously achieved. That is slip may result in bond stresses along the negative loading path GHIJK in Figure 2.11 which implies that damage to the concrete other than due to friction is taking place and this can cause significant reductions in the bond stress transferred for any given slip.

4.2.4 Reloading phase

During reloading along path DE in Figure 4.5, the mechanics behind each unloading phase already described also applies. A detailed description of the reloading behaviour is therefore not provided here. However it should be noted that the P_r/Δ_r relationship in Figure 4.5 can be obtained by seeking the same distributions of slip, bond stress and reinforcement stress and strain as shown in Figure 4.7 and Figure 4.8.

4.2.5 Sample distributions according to phases

The distributions of slip (Figure 4.9), bond stress (Figure 4.10), and steel stress (Figure 4.11) and steel strain (Figure 4.12) obtained from the partial-interaction model is presented here to show the transition of loading, unloading phase I and unloading phase II as discussed in previous sections. Note however that it is impossible to show all of the distribution results here, as the results are too numerous and difficult to comprehend due to endless overlapping of distribution curves. Instead the distribution shown here are only a few sample distributions taken from the partial interaction result of beam MA-1 during its first cycle of cyclic load.

The slip distribution in Figure 4.9 shows that slip gradually reduces for unloading phase I and II. In order to fully close the flexural crack and enter reversed loading, the compressive force applied causes the steel reinforcement to slip in the opposite direction, as shown in unloading phase II with slip close to zero.

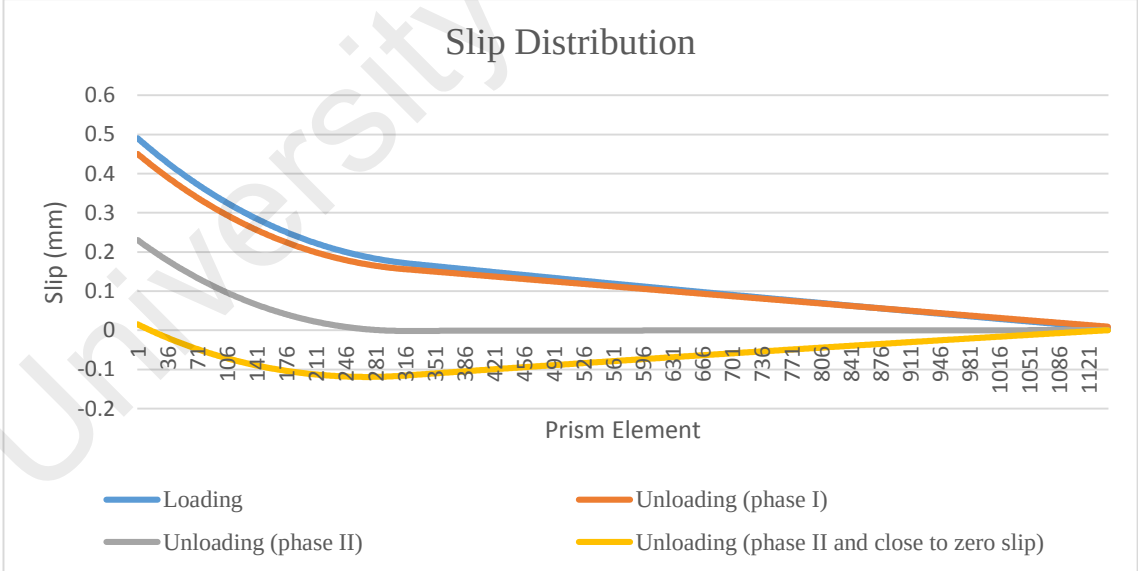

Figure 4.9: Slip distributions of beam MA-1

Figure 4.10 shows the bond stress distribution. The bond stress reduces rapidly during unloading, with half of the prism elements already in frictional resistance region in unloading phase I. As compressive force is applied on the steel reinforcement, the bond stress will all enter into previously damaged region and only frictional resistance will remain. Further compression will cause the bond stress to become negative, thus allowing the negative slip as shown in Figure 4.9 to occur.

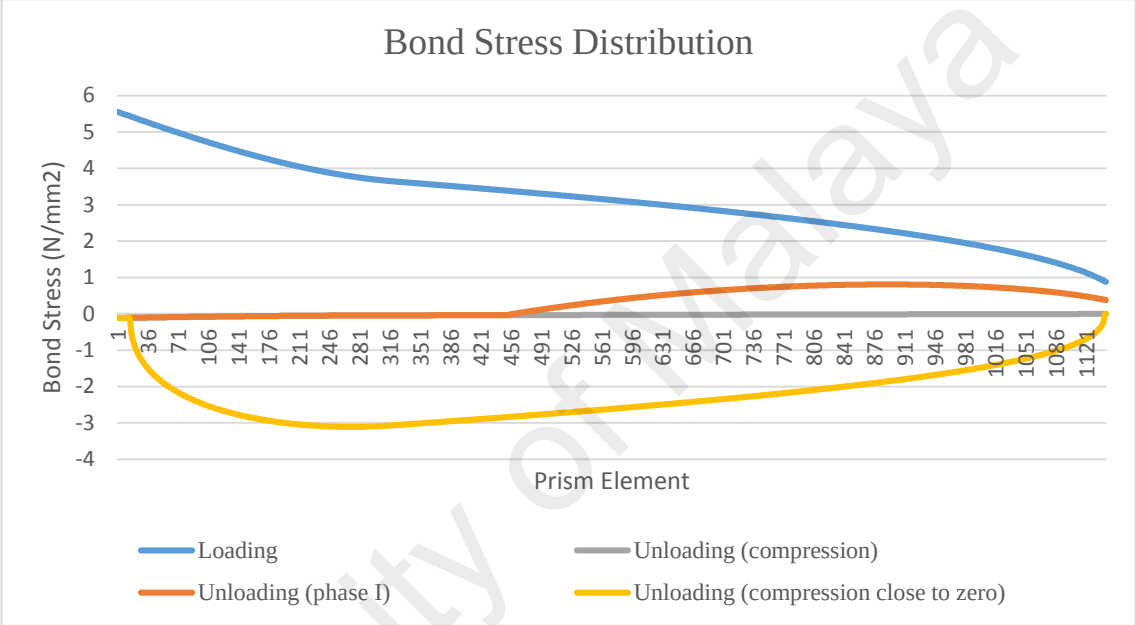

Figure 4.10: Bond stress distributions of beam MA-1.

Figure 4.11 and 4.12 shows the stress and strain distribution of the steel reinforcement during unloading. In the beginning the stress and strain reduces gradually during unloading. However once compressive force is applied, the stress and strain will gradually become negative as the slip of steel reinforcement is pushed back into the concrete to close the flexural crack. For unloading phase II close to zero slip, it can be seen that the steel strain can be positive while experiencing a negative stress. This is due to the stress-strain relationship for steel during unloading, as discussed in section 2.3.1 previously.

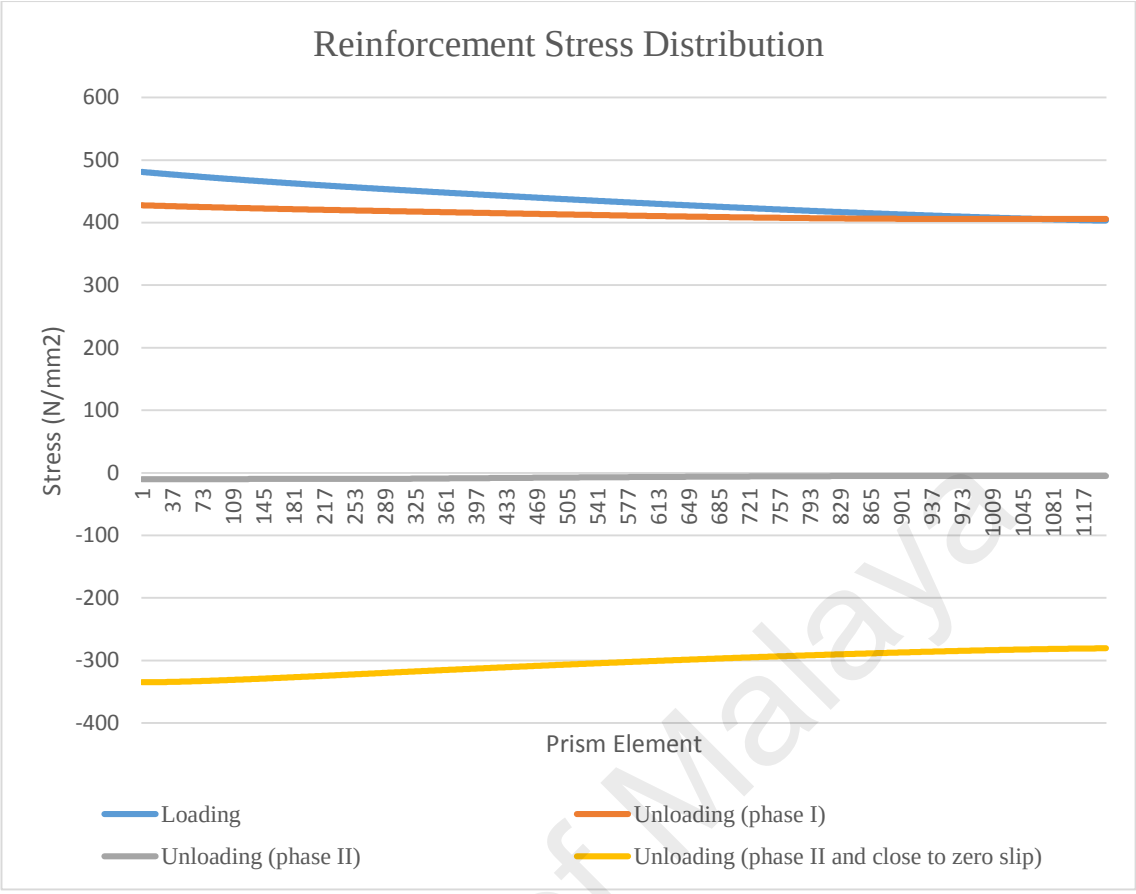

Figure 4.11: Steel reinforcement stress distributions of beam MA-1.

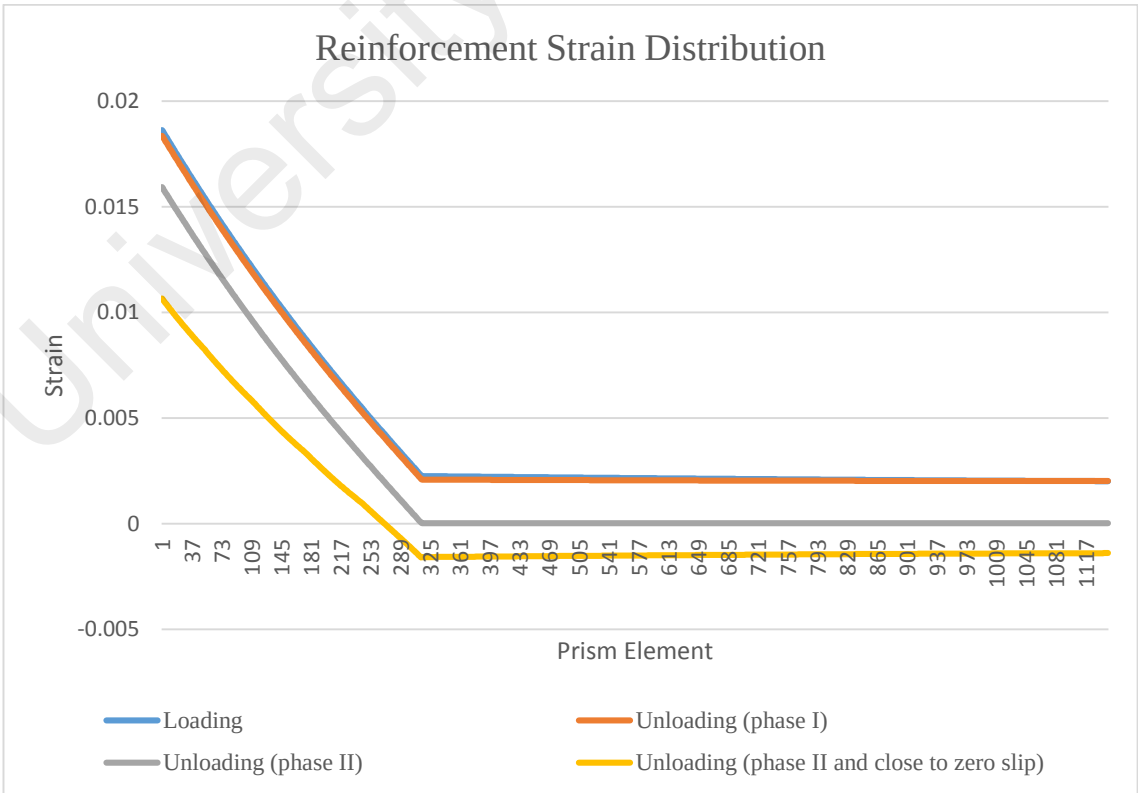

Figure 4.12: Steel reinforcement strain distributions of beam MA-1.

4.3 Simulated Load-Slip Relationship

Using the partial-interaction model, the simulated cyclic load-slip results of the cyclically loaded beams is as shown in Figure 4.13 and 4.14, where the former shows the load-slip of tensile bars and the latter shows the load-slip of compression bars.

The simulated load-slip results, as shown in Figure 4.13 tends to follow the stress-strain property of steel reinforcement. Here it can be seen that due to the bilinear stress-strain model for steel that is used, the resulting load-slip shows a linear curve up to yielding of steel reinforcement, beyond which the load-slip curves loses most of its' rigidity due to the strain hardening of steel bars. Note however that the overall rigidity is still higher than the rigidity of only steel reinforcement due to the effect of tension stiffening, as discussed in section 2.2.1 previously. One other interesting thing to note is the sudden loss of rigidity during the early stages of load reversals in all of the curves. This is caused by the bond stress-slip relationship rather than the material stress-strain relationship, as during the early stages of unloading the steel bar passes through previously damaged sections of concrete, causing a steep decrease in the amount of bond stress exerted on the steel until only frictional resistance acts against the sliding of steel reinforcement, as discussed in section 2.3.3.1 previously.

The simulated load-slip curves of compression bars in Figure 4.14 is more or less the same as the tensile bars. Thus the discussions made on the tensile load-slip curves also applies to the compression bar load-slip and will not be repeated. Note that although the general shape of the compression bar load-slip curves are the same as tensile bars, the amount of slip incurred during loading is usually larger as the amount of compression reinforcement provided in beams are usually half of that which is provided as tensile reinforcement

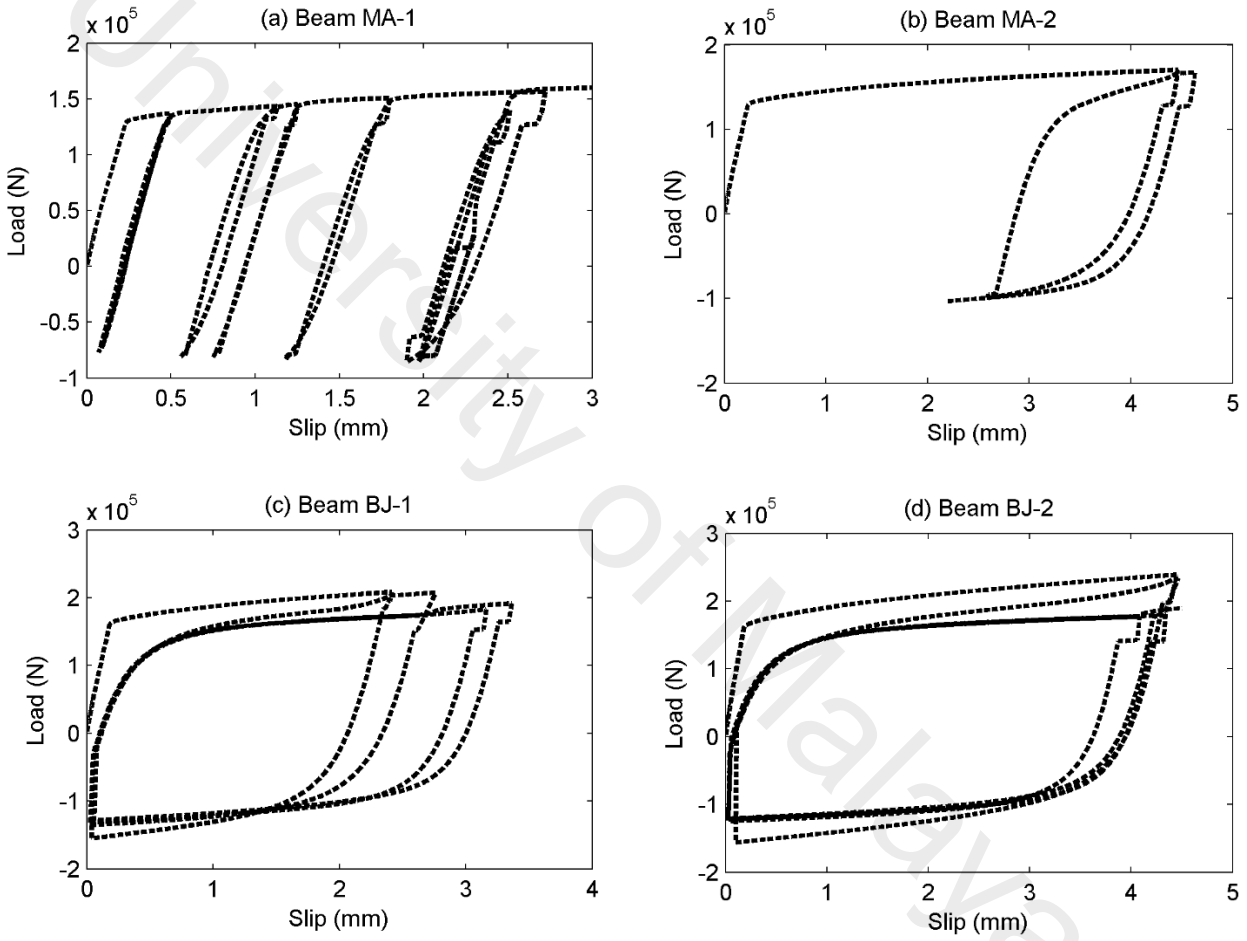

Figure 4.13: Simulated Load-Slip Results for Tensile Bars.

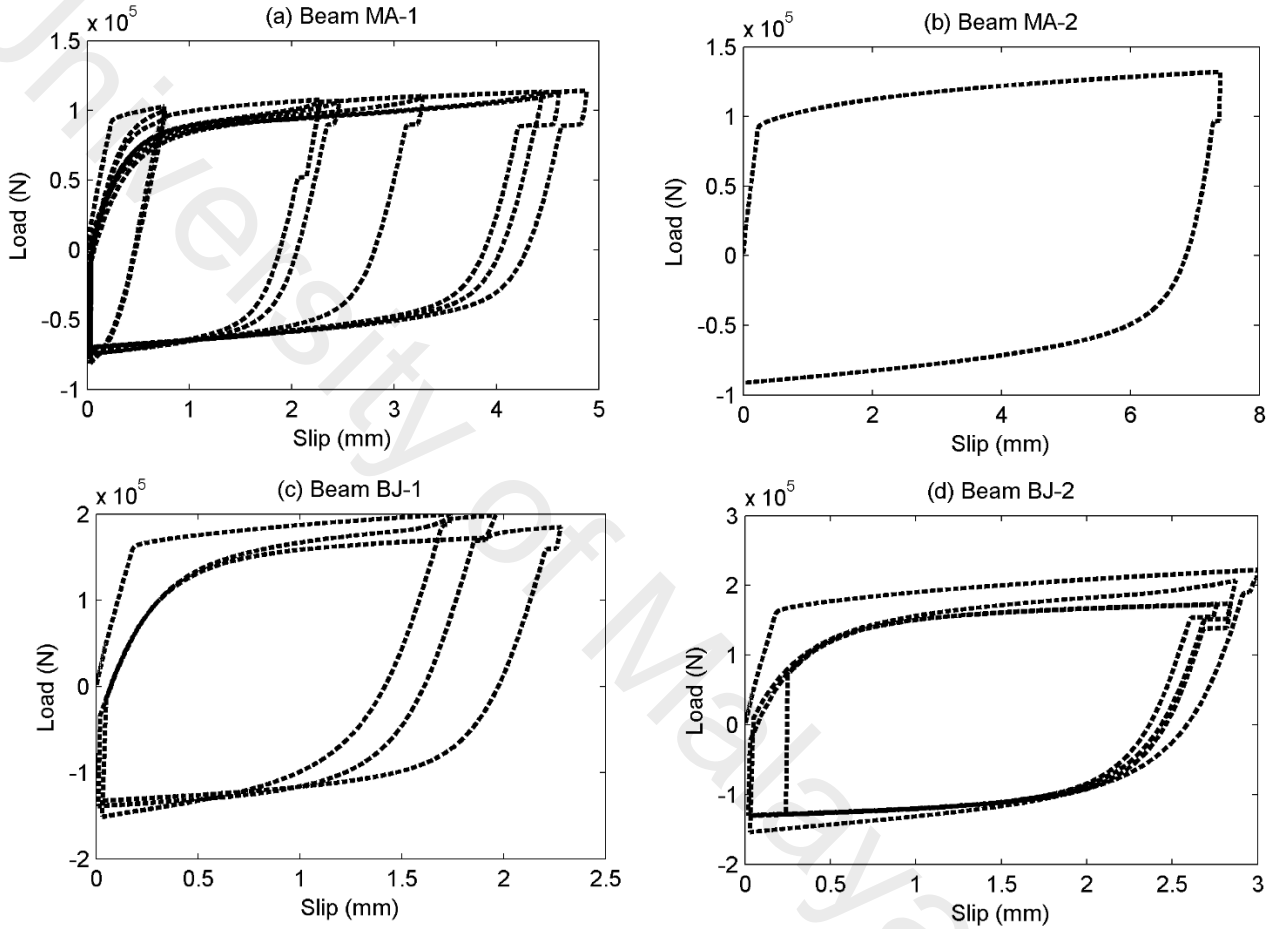

Figure 4.14: Simulated Load-Slip Results for Compression Bars.

CHAPTER 5: CONCLUSIONS

Based on the objectives of this research, these conclusions can be made:

i. A numerical cyclic partial-interaction model was proposed, which incorporates various cyclic material models. The model was then used to obtain the load-slip relationship of steel reinforcement and its adjacent concrete under cyclic loading condition.

ii. The method to create a size-dependent stress-strain relationship for concrete from existing stress-strain model, as proposed by Chen et al. (2014), was shown to be applicable for cyclically loaded concrete. The cyclic stress-strain model for concrete presented by Popovics (1973) was then made size-dependent using the method shown by Chen et al. (2014).

iii. The partial-interaction model and size-dependent stress-strain model for concrete was used as components in the proposed cyclic moment-rotation model. The model was then validated with experimental results by Ma et al. (1971) and Brown and Jirsa (1976). The simulated and experimental moment-rotation results were found to agree fairly well.

Further research is needed to try include the effect of shear during cyclic loading in the moment-rotation model. The model should also be validated for beams using uncommon concrete materials such as fiber and palm oil fuel ash.

REFERENCES

Bischoff P. H. (2005). Reevaluation of deflection prediction for concrete beams reinforced with steel and fiber-reinforced polymer bars. *Journal of Structural Engineering*, 131(5):752-67.

Bouc, R. (1967). 'Forced vibration of mechanical systems with hysteresis. *Proc., 4th Conference on Non-linear Oscillations*.

Brown, R., & Jirsa, J. (1971). Reinforced concrete beams under load reversals. *ACI Journal Proceedings*, (68), 380–390.

CEB (1993). *CEB-FIP Model Code 1990: Design Code*. Thomas Telford, London, UK.

Chen, Y., Visintin, P., Oehlers, D., & Alengaram, U. (2014). Size-Dependent Stress-Strain Model for Unconfined Concrete. *Journal of Structural Engineering*, 140(4).

Clough R. W. (1966). Effect of Stiffness Degredation on Earthquake Ductility Requirements. *Structural Engineering and Structural Mechanics Department of Civil Engineering Report No. 66–16.*

Coleman, J. & Spacone, E. (2001). Localization Issues in Force-Based Frame Elements. *Journal of Structural Engineering*, 127(11), 1257–1265.

Daniell, J. E., Oehlers, D. J., Griffith, M. C., Mohamed Ali, M. S., & Ozbakkaloglu, T. (2008). The softening rotation of reinforced concrete members. *Engineering Structures*, 30(11), 3159–3166.

Eligehausen R., Popov E. P., Bertero V. V. (1992). Local bond stress-slip relationship of deformed bars under generalized excitations. *Earthquake Engineering Research Centre*, UCB/EERC83/23.

Fields K., Bischoff P.H. (2004). Tension stiffening and cracking of high-strength reinforced concrete tension members. *ACI Structural Journal*, 101(4):447–56

Filippou F. C., Popov E. P., Bertero V. V. (1983). Effects of bond deterioration on hysteretic behavior of reinforced concrete joints. *Earthquake Engineering Research Centre*, UCB/EERC-83/19.

Haskett M. Oehlers D. J., Mohamed Ali M. S. (2010a). Design for Moment Redistribution in RC Beams Retrofitted with Steel Plates. *Advances in Structural Engineering*. Vol. 13 No. 2 April 2010 pp.379-392.

Haskett, M., Oehlers, D. J., & Mohamed Ali, M. S. (2008). Local and global bond characteristics of steel reinforcing bars. *Engineering Structures*, 30(2), 376–

Haskett, M., Oehlers, D. J., Mohamed Ali, M. S., & Sharma, S. K. (2011). Evaluating the shear-friction resistance across sliding planes in concrete. *Engineering Structures*, 33(4), 1357–1364.

Haskett, M., Oehlers, D., Ali, M., & Wu, C. (2010b). Analysis of Moment Redistribution in Fiber-Reinforced Polymer Plated RC Beams. *Journal of Composites for Construction*, 14(4), 424–433.

Haskett, M., Oehlers, D., Mohamed Ali, M., & Wu, C. (2009). Yield Penetration Hinge Rotation in Reinforced Concrete Beams. *Journal of Structural Engineering*, 135(2), 130–138.

Knight, D., Visintin, P., Oehlers, D. J., & Mohamed Ali, M. S. (2014). Simulation of RC beams with mechanically fastened FRP strips. *Composite Structures*, *114*, 99–106.

Lucas, W., Oehlers, D., & Ali, M. (2011). Formulation of a Shear Resistance Mechanism for Inclined Cracks in RC Beams. *Journal of Structural Engineering*, 137(12), 1480–1488.

Ma S. M., Bertero V. V., Popov E. P. (1976). Experimental and analytical studies on the hysteretic behavior of reinforced concrete rectangular and T-beams. *Earthquake Engineering Research Centre*, UCB/EERC76/2.

Massicotte, B., Elwi, A., & MacGregor, J. (1990). Tension-Stiffening Model for Planar Reinforced Concrete Members. *Journal of Structural Engineering*, 116(11), 3039–3058.

Menegotto, M., & Pinto, P. E. (1973). Method of analysis for cyclically loaded reinforced concrete plane frames including changes in geometry and non-elastic behavior of elements under combined normal force and bending. *IABSE Symposium, Resistance and Ultimate Deformability of Structures Acted on by Well-Defined Repeated Loads*, Lisbon, Spain.

Mostaghel, N. (1999). ‘‘Analytical description of pinching, degrading hysteretic systems.’’ *Journal of Engineering Mechanics*, ASCE, 125(2), 216–224.

Muhamad, R., Mohamed Ali, M. S., Oehlers, D., & Hamid Sheikh, A. (2011b). Load-slip relationship of tension reinforcement in reinforced concrete members. *Engineering Structures*, 33(4), 1098–1106.

Muhamad, R., Oehlers, D., & Ali, M. M. (2011a). Discrete rotation deflection of RC beams at serviceability. *Proc ICE Struct Buildings*, 164, 1–14.

Nurwidayati, R. (2011). An empirical approach to simulate the concrete softening mechanism in RC members. PhD thesis, University of Adelaide, Adelaide, Australia.

Oehlers, D. J., Visintin, P., Haskett, M., & Sebastian, W. M. (2013). Flexural ductility fundamental mechanisms governing all RC members in particular FRP RC. *Construction and Building Materials*, 49, 985–997.

Panagiotakos T. B., Fardis M. N. (2001). Deformations of reinforced concrete members at yielding and ultimate. *ACI Structural Journal*, 98(2):135–48.

Park, Y. J., Reinhorn, A. M., & Kunnath, S. K. (1987). ''IDARC: Inelastic damage analysis of reinforced concrete frame—shear-wall structures.'' *Technical Report NCEER-87-0008*, State University of New York at Buffalo, Buffalo, N.Y.

Popovics S. (1973). A numerical approach to the complete stress–strain curve of concrete. *Cement and Concrete Research*, 3(5), 583–99.

Sivaselvan M. V., Reinhorn A. M. (2000). Hysteretic models for deteriorating inelastic structures. *Journal of Engineering Mechanics*, 126:633–640.

Takeda T., Sozen M. A., Nielson N. N. (1970). Reinforced concrete response to simulated earthquakes. *ASCE Journal of the Structural Division*, 96(12), 2557–2573

Visintin, P., Oehlers, D. J., Wu, C. W., & Griffith, M. C. (2012a). The reinforcement contribution to the cyclic behaviour of reinforced concrete beam hinges. *Earthquake Engineering & Structural Dynamics*, 41(12), 1591-1608.

Visintin, P., Oehlers, D. J., Wu, C., & Haskett, M. (2012b). A mechanics solution for hinges in RC beams with multiple cracks. *Engineering Structures*, 36, 61–69.

Walraven, J., Frenay, J., & Pruijssers, A. (1987). Influence of Concrete Strength and Load History on the Shear Friction Capacity of Concrete Members. *Journal Prestressed Concrete Institute*, 32(1), 66-84.